# Binocular combination of light in canonical and non-canonical pathways

Federico Gabriele Segala

Doctor of Philosophy

University of York

Psychology

November 2023

# Abstract

Humans possess two forward-facing eyes allowing combination of individual images to form a cyclopean representation of the world. Image quality is determined by the amount of light hitting the retina, regulated by the pupils. The anatomical pathways behind binocular combination and that regulate pupil size are well understood. Many studies have investigated how the brain combines information across the eyes: for spatial patterns, visual areas implement 'ocularity invariance', which equalises monocular and binocular responses. However, not much is known about the computational processes that regulate binocular combination of the pupil response. This was the main aim of this thesis: to investigate and understand the rules of binocular combination in the cortical pathways (the visual cortex) and the subcortical pathways that govern the pupil diameter.

In Chapter 2, a novel combination of EEG, pupillometry, psychophysics, and computational modelling was used to investigate if this invariance is implemented for luminance flickering stimuli. The results show violations of ocularity invariance in the cortex, with strong facilitation of binocular signals, and in the subcortical pathways governing pupil diameter, where non-linear combination was observed. In Chapter 3, these findings were expanded using fMRI to investigate where, within the visual cortex, this facilitation happens. Facilitation was observed mainly in V1 but not as strong as for EEG (likely due to the different nature of EEG and fMRI recordings). Finally, in Chapter 4, silent substitution and pupillometry were used to investigate binocular combination while targeting the intrinsically-photoreceptive retinal ganglion cells, the L-M and the S-(L+M) pathways. The results showed non-linear combination in all pathways but with differences in interocular suppression levels.

The studies undertaken in this thesis contribute to the wider understanding of binocular combination of light signals and provide methodological developments (simultaneous EEG and pupillometry) that can benefit researchers interested in binocular combination disorders (e.g. amblyopia).

# Contents

# List of Figures

11

15

# List of Tables

# Acknowledgements

There are a lot of people that I would like to thank for the support and guidance that they have given me during the three years of my PhD. First of all, I would like to thank greatly Daniel Baker, my primary supervisor, for giving me this amazing opportunity to pursue this research project, for introducing me to the wonderful world of R (especially R markdown, which saved me so many days of thesis formatting!), and for introducing me to the world of academia. I am grateful for his availability (his door was always open, both literally and figuratively) and his patience when I was constantly dropping by his office to ask questions or ask for advice. His enthusiasm for research and vision was very contagious and influential and has encouraged me to continue a career in academia. I feel like I should also apologise for taking over his office while I was running my experiments: I think at some point people around the department started thinking that his office had become mine because of all the time I spent in there!

A big thank you also goes to Aurelio Bruno, my secondary supervisor, whose help, suggestions and words of encouragement were always appropriate and whose presence was very helpful during the Covid period: having someone else whom I could speak Italian with once in a while was a great way to distract myself and feel like I was home!

I would also like to thank my thesis advisory panel, Professor Anthony Morland, Professor Alex Wade, Dr Daniel Kaiser, and Dr Tom Hartley, who replaced Daniel when he left, for the important advice and insightful comments that they have suggested throughout my research. Also, my endless gratitude goes to Dr Joel Martin, whose help was essential to set up the experiments from the last chapter of this thesis and for his detailed explanations on silent substitution, and Dr Lauren Welbourne, who was of great company during the endless fMRI scanning hours in YNiC and for her great help with the MRI data analysis.

An enormous thank you goes to my office mates. I started my PhD during the Covid pandemic and I got assigned to a (very large) empty office, which I really enjoyed having all to myself. When people moved in at the start of my second year, I was not particularly excited as I felt like I was losing my space. Little did I know how much my life changed (for the better) the moment these guys moved in. So, Bee, Kirri, Lydia, Anna, Erin: thank you very much for the company, the support, the stupidity and the laughs we all shared together. Thank you for the fun shenanigans nights. Thank you for putting up with my obsession with Inter (which, despite what everyone thinks, is very healthy) and football. Thank you for volunteering for all my experiments. I will cherish these precious memories forever.

I am grateful to my friends back home, even though they are not back home any more but they have spread around the world. Thank you Adriano for our weekly comments and discussions on the new chapter

of One Piece and for always making time to see me whenever I go back home. Thank you Emanuele for always trying to watch Inter matches with me via WhatsApp despite you travelling around all the time and thank you for trying to change your flights to the UK to come and visit me once in a while: I promise I will visit you in Dubai at one point.

I would like to thank mamma and papà and the rest of my family, especially nonna Emma, for giving me the necessary emotional and mental support to pursue and finish my PhD: without them, I would not be where I am today. I want to dedicate this thesis to a very special person who, despite not being actually family, was always like a second mother to me: my godmother Enrica. She would have shown endless support and belief in me, and I know she would have been very proud of me for what I have accomplished.

Finally, and most importantly, I want to thank the person that changed my life the most during my PhD. Thank you Rana, you have been a great source of inspiration and support, and a great motivator. I am looking forward to spending the rest of my life with you. I love you.

# Author's Declaration

I, Federico Gabriele Segala, declare that this thesis is a presentation of original work, carried out under the supervision of Professor Daniel Baker and Dr Aurelio Bruno, and I am the sole author. This work has not previously been presented for a degree or other qualification at this University or elsewhere. All sources are acknowledged as references. All the studies contained in this thesis were conducted in accordance with the ethical standards of the Department of Psychology at the University of York and the York Neuroimaging Centre. The research carried out in Chapters 3 and 4 was supported by a Biotechnology and Biological Sciences Research Council grant awarded to Professor Daniel Baker and Professor Alex Wade. Data in Chapters 3 and 4 was collected in collaboration with Dr Joel Martin and Dr Lauren Welbourne. The work presented in Chapter 2 has been published in the form of the following article:

> Segala FG, Bruno A, Martin JT, Aung MT, Wade AR, Baker DH. 2023. Different rules for binocular combination of luminance flicker in cortical and subcortical pathways. eLife 12. doi: 10.7554/elife.87048

> **Federico Segala**: Methodology, software, formal analysis, investigation, data curation, writing - original draft, writing - review & editing, visualization. **Aurelio Bruno**: Conceptualization, writing - review & editing, supervision, project administration, funding acquisition. **Joel Martin**: Software, resources, writing - review & editing. **Myat Aung**: Software, resources, writing - review & editing. **Alex Wade**: Conceptualization, methodology, resources, writing - review & editing, supervision, project administration, funding acquisition. **Daniel Baker**: Conceptualization, methodology, software, formal analysis, investigation, resources, data curation, writing - original draft, writing - review & editing, visualization, supervision, project administration, funding acquisition.

Data used in this thesis has been presented in the following conferences in the form of posters or oral presentations:

> Talk: Segala, F. G., Martin, J. T., Bruno, A., Wade, A. R., & Baker, D. H. (2023). Binocular combination of the pupil response depends on photoreceptor pathway. Optica 2023 Fall Vision Meeting, Seattle (WA), USA.

> Talk: Welbourne, L. E., Martin, J. T., Segala, F. G., Wade, A. R. & Baker, D. H. (2023).

Measuring binocular combination of luminance and chromatic stimuli using fMRI. Optica 2023 Fall Vision Meeting, Seattle (WA), USA.

Talk: Segala, F. G., Bruno, A., Wade, A. R. & Baker, D. H. (2022). Binocular response to light: contrast matching of luminance flicker. The 44th European Conference on Visual Perception (ECVP) 2022, Nijmegen, The Netherlands. (2022). Perception, 51(1_suppl), 1–207. https: //doi.org/10.1177/03010066221141167

Poster: Segala, F. G., Bruno, A., Wade, A. R. & Baker, D. H. (2021). Binocular response to light: a novel pupillometric and electrophysiological approach. 43rd European Conference on Visual Perception (ECVP) 2021 Online. (2021). Perception, 50(1_suppl), 1–244. https: //doi.org/10.1177/03010066211059887

# Primary Supervisor's Statement

I am listed as a co-author on the paper that comprises Chapter 2 of this thesis:

Segala, F.G., Bruno, A., Aung, M.T., Wade, A.R. & Baker, D.H. (2023). Different rules for binocular combination of luminance flicker in cortical and subcortical pathways, eLife, 12: RP87048.

In this paper, the work was primarily that of Federico Segala. Federico collected and analysed all of the data, wrote the first draft of the paper and did the majority of the editing and revising of the manuscript. I assisted with implementation of the computational model, provided advice, guidance and editing in my capacity as supervisor.

Collection of the data in Chapters 3 and 4 was conducted in collaboration with other members of the lab. However I am satisfied that Federico's contribution to the data collection and analysis was substantial, and meets the University's criteria for inclusion in a thesis.

Professor Daniel H. Baker

30/10/2023

# Secondary Supervisor's Statement

I am listed as a co-author on the paper that comprises Chapter 2 of this thesis:

Segala, F.G., Bruno, A., Aung, M.T., Wade, A.R. & Baker, D.H. (2023). Different rules for binocular combination of luminance flicker in cortical and subcortical pathways, eLife, 12: RP87048.

In this paper, I confirm that the work was primarily that of Federico Segala. He collected and analysed all the data, wrote the first draft of the paper and did the majority of the editing and revising of the manuscript. I assisted with guidance and editing in my capacity as secondary supervisor.
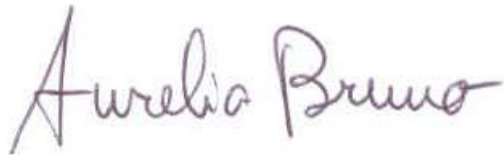
Dr Aurelio Bruno

31/10/2023

# 1 Chapter 1: Introduction

## 1.1 Overview

Binocular vision is characterised by the two eyes that are arranged to be forward facing and to have overlapping visual fields in humans and many other animal species. This allows binocular combination of the individual images from each eye to create a cyclopean image of the surrounding environment, from which the viewer can obtain useful and meaningful information. This configuration provides various advantages, such as precise depth perception and a three-dimensional view of the world, which would not be possible with only monocular vision.

The anatomical pathway supporting this binocular combination has been thoroughly studied and is well understood: light enters the eyes through the pupils and signals are sent from the left and right retinae, remaining anatomically isolated while passing through the lateral geniculate nucleus (LGN) until they reach the primary visual cortex (V1), where they are binocularly combined (Purves et al., 2008). To explain this combination process, various models have been developed, which involve a combination of interocular suppression and binocular summation (Ding and Sperling, 2006).

Most of contemporary vision research focuses on the retina and how it has a key role in visual response, by converting light into a neural signal that will be transmitted to the visual areas. However, there is an eye component that is often underestimated in its role to determine the quality of the visual information: the pupil. Pupils are black holes placed in the centre of both eyes and they allow light to strike the retina (Mathôt, 2018). Their size determines how much light will reach the retina and is usually determined by the ambient levels of light: in brightness, the pupils will constrict and, in darkness, they will dilate. This is known as the pupillary light response (sometimes it is also referred to as the pupillary light reflex). The subcortical anatomical pathways that regulate this response are well understood, however, not much is known about the computational processes behind it.

This chapter will first provide a summary of the key findings about binocular combination of signals. It will then focus on the pupils and the pupillary light response. This will be followed by an overview of the techniques that can be used to study binocular combination in the visual cortex and in the subcortical pathways that govern the diameter of the pupils. Finally, it will offer an overview of the structure of this thesis, detailing the information contained in each chapter.

## 1.2 Binocular combination

Binocular viewing provides a higher visual sensitivity compared to monocular viewing. This superiority has been studied over the past century with experiments often focussing on detection thresholds for contrast sensitivity (Blake and Wilson, 2011). Studies have manipulated contrast levels, spatial frequencies and temporal frequencies of the stimuli presented to each eye, which allowed conclusions to be drawn on the neural processes behind this combination.

This superiority is known as binocular summation and is defined by the ratio (the binocular summation ratio, BSR) of binocular to monocular contrast sensitivity (Campbell and Green, 1965). The BSR was initially defined to be on average $\sqrt{2}$ ($\approx 1.4$) by Campbell and Green (1965), which means that, for a monocular stimulus to elicit the same response as a stimulus presented binocularly, it would need to have a contrast 1.4 times higher. Campbell and Green proposed that this ratio could be explained by a linear summation of monocular signals whose variances were uncorrelated. The magnitude of the BSR allowed them to discard previous proposed models that were not based on physiological summation but on probability summation. The probability summation model was proposed by Pirenne (1943) and it was based on the idea that improvement in binocular performance compared to monocular performance was to be expected because a simultaneous presentation to both eyes provided two opportunities to make a detection, and it was this additional opportunity that provided a superior binocular performance. By offering a description based on the detection of physiological signals, Campbell and Green were able to offer a more general explanation of binocular summation.

Based on the $\sqrt{2}$ ratio, Legge (1984) developed an influential model that used quadratic summation to describe binocular combination. This model states that monocular signals are squared before being summed together and the output is the square root of the summed value, giving the following equation:

$$B = \sqrt{R^2 + L^2}, \tag{1}$$

with B being the binocular response and R and L being the left and right eye contrasts. This equation gives the expected ratio of $\sqrt{2}$, i.e. when R and L are equal to 1.

Although Campbell and Green's and Legge's accounts have been widely accepted, subsequent research has shown that their explanations are not fully adequate to account for binocular summation. Both of these accounts constitute single channel models and evidence from a subsequent study by Anderson and Movshon (1989) showed that this type of model was unable to account for contrast detection in the presence of noise.

Moreover, other studies have found summation ratios that exceed the value of $\sqrt{2}$. For example, a recent meta-analysis has found that the ratio could vary greatly between $\sqrt{2}$ and 2, depending on factors such as the spatial and temporal frequencies of the stimulus and the difference in sensitivity between the two eyes (Baker et al., 2018).
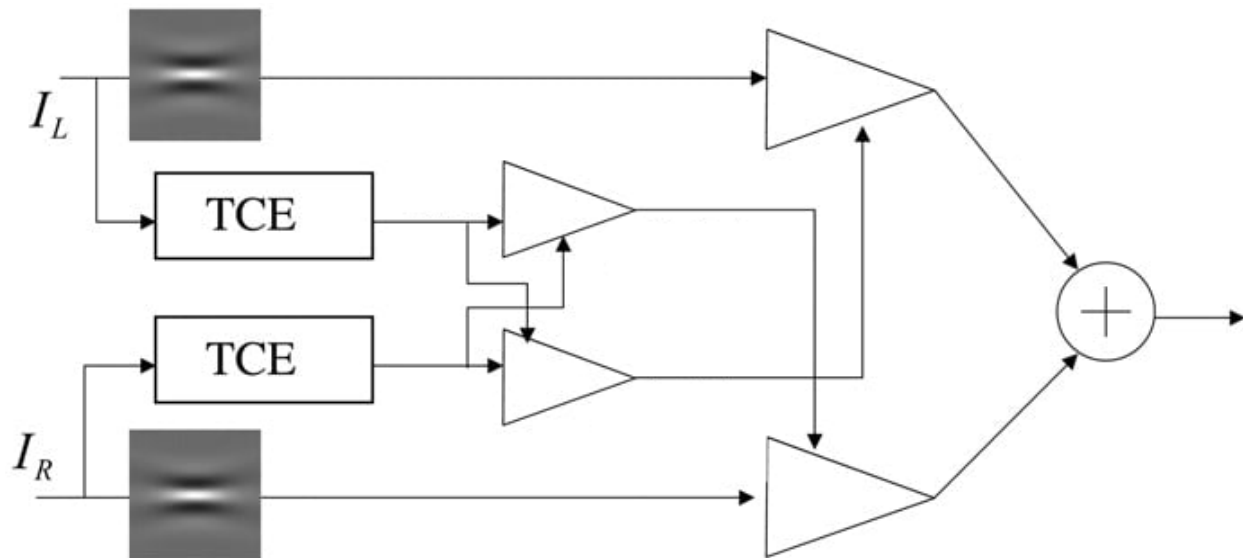


Figure 1.1: Multistage model developed by Ding and Sperling (2006). First, the channels exert gain control on each other and then they exert gain control on each other's total weighted contrast energy.

At high spatial contrast, an adequate model needs to include dynamic contrast gain control, a process in which neurons reduce each other's signal by mutual inhibition to keep themselves within their optimal operating range (Heeger, 1992). In the context of binocular combination, gain control theory allows to develop a computational model that combines binocular summation and interocular suppression. Based on this idea, Ding and Sperling (2006) developed a multistage model consisting of two pairs of contrast gain control mechanisms, with each pair inhibiting each other (figure 1.1). The left and right eye channels initially receive an image. In the earlier stage, each channel exerts gain control on the other. Then, it exerts gain control on the other channel's gain control. Finally, the outputs are summed binocularly to determine the binocular signal's magnitude. Similarly, another two-stage gain control model was developed by Meese et al. (2006) (figure 1.2). In the first stage, gain control is applied to the two monocular channels with suppression from the opposite eye. Then at the second stage, contrast gain control is applied after binocular summation. This model seems to be strong as it can account for contrast matching, detection and discrimination (Baker et al., 2007).

Alternative models have also been proposed and developed. For example, based on observations that differences in temporal and spatial properties of monocular signals produce a less apparent summation,

monocular sensitivity levels were tested when one eye remains unstimulated (Denny et al., 1991). They found that sensitivity was suppressed by the unstimulated eye (they defined this as tonic interocular suppression) and that, when this suppression was removed, there was an improvement in monocular sensitivity. They suggested that the removal of this interocular suppression could be as likely an explanation as binocular summation for the improved binocular performance.
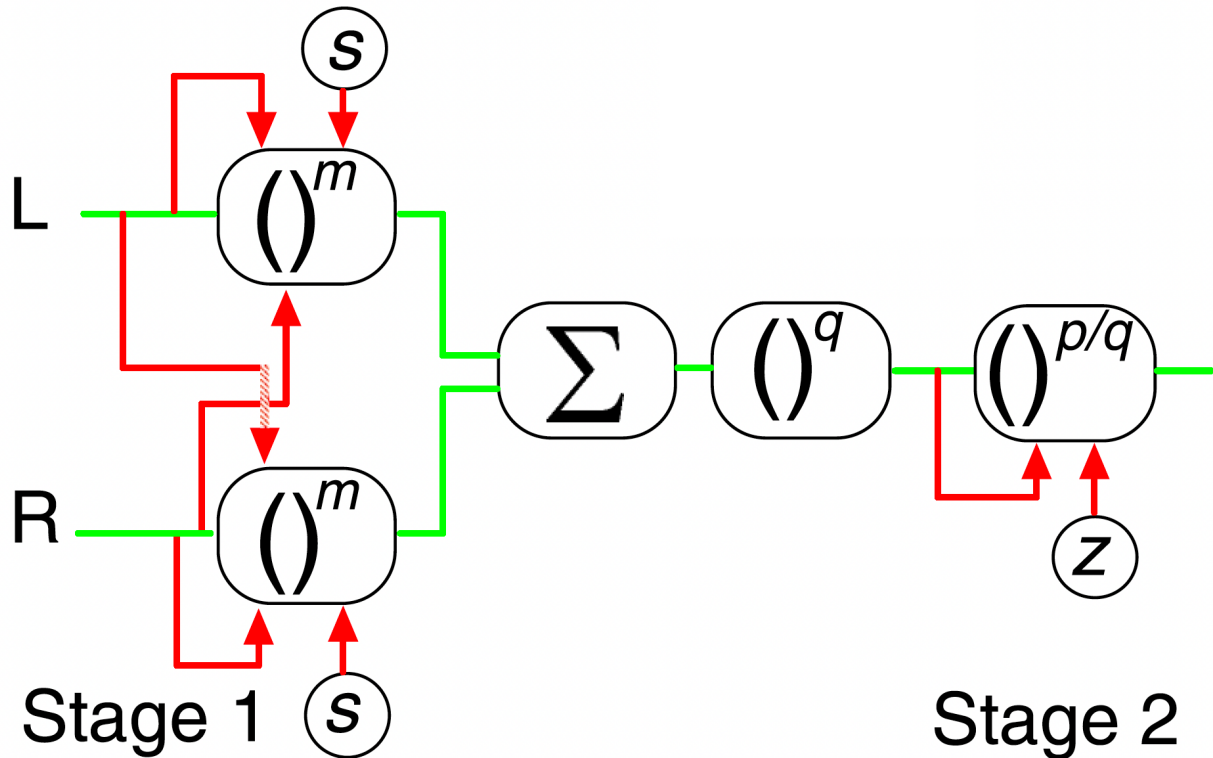


Figure 1.2: Two-stage model of binocular contrast gain control developed by Meese and colleagues (2006). L and R refer to the left and the right eye. The green and the red pathways are excitatory and inhibitory respectively. The red arrows indicate divisive suppression. $\Sigma$ indicates summation.

## 1.3   Pupils and the light response

As stated in the overview, pupils are openings found in the centre of eyes that appear to be black and allow light to enter the eyes by exposing the lenses. Their diameter can vary from roughly 2 to 8 mm depending on light conditions (Spector, 1990). Their size is controlled by muscles that are found in the iris, the coloured area around the pupil (Angée et al., 2021): the iris sphincter muscle, a circular muscle that encircles the pupil and reduces the pupil's size when it contracts (figure 1.3a), therefore controlling the

constriction of the pupil; the iris dilator muscle, consisting of radially-oriented fibres that connect the exterior of the iris to its interior and increases the pupil's size when it contracts (figure 1.3b), therefore controlling the dilation of the pupils. Thanks to these muscles, it is possible to optimise the quality of visual information that we receive from the eyes (Binda et al., 2013). When there are low levels of light, for example, pupil dilation allows the eye to capture more photons and therefore increases the sensitivity.

Iris sphincter muscle

Iris dilator muscle



a.

b.
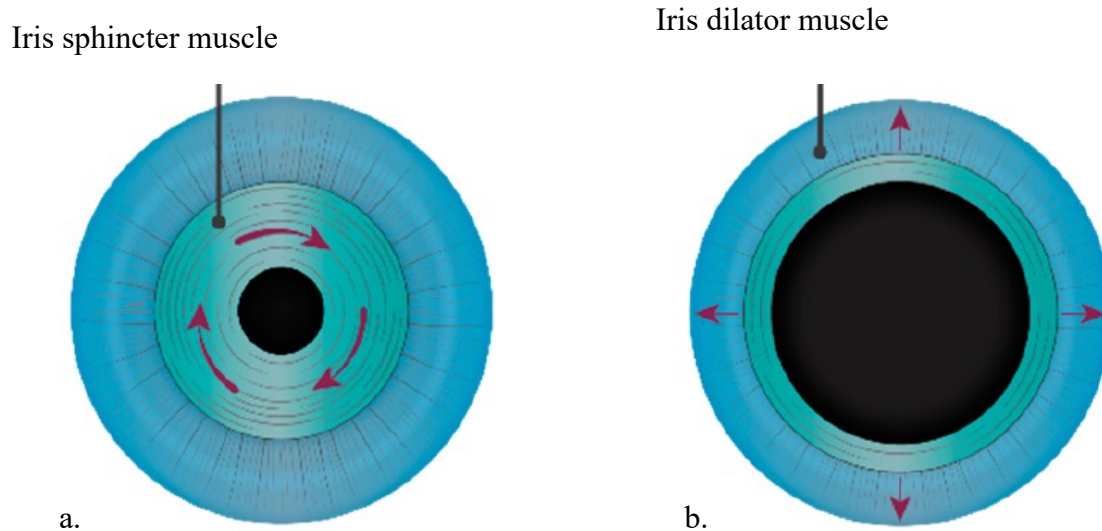
Figure 1.3: The puillary light response (adapted from Angée et al, 2021). Panel (a) shows the constriction of the pupil during which the iris sphincter muscle contracts and makes the pupil smaller. Panel (b) shows the dilation of the pupil during which the iris dilator muscle contracts and makes the pupil larger.

Constriction and dilation are controlled by two distinct pathways: the parasympathetic constriction pathway and sympathetic dilation pathway (Wang and Munoz, 2015). The fact that the former is part of the parasympathetic nervous system, which is involved in homeostasis, explains why pupils are relatively constricted when at rest. The latter, on the other hand, is part of the sympathetic nervous system, which is involved in wakefulness. This could explain why during increased cognitive activity, it is possible to observe pupil dilation. As described by McDougal and Gamlin (2008), the constriction pathway connects the retina to the iris sphincter muscle. When light falls on the retina, a monocular signal is sent to the Pretectal Olivary nucleus (PON) in both hemispheres. From there, a binocular input from both PON is received by both left and right Edinger-Westphal nuclei (EWN). Following this, a signal is sent to the ciliary ganglions that will finally stimulate the sphincter muscle. The dilation pathway connects the hypothalamus and the locus coeruleus (LC) to the iris dilator muscle (McDougal and Gamlin, 2008). When stimulated, they send a signal to the superior cervical ganglion through the intermedio-lateral columns, which then projects to the dilator muscle. While these two pathways are segregated from each other, they still interact: a study by Koss

(1986) has shown evidence of inhibition of pupilloconstriction neurons in the EWN by neurons originating from the LC. This could also mean that the LC is causing pupil dilation not only by activating the dilation pathway but also by actively inhibiting the constriction pathway.

Originally, it was thought that these changes in size only happened in response to light, but it has been shown that they happen in response to three kinds of stimuli: constriction to light (pupillary light response or reflex, PLR), constriction to near fixation (pupillary near response, PNR) and dilation when there is increased cognitive activity (psychosensory pupillary response, PPR) (Mathôt, 2018). These responses are mostly spontaneous, meaning that a similar stimulus will always cause a similar response (e.g. when there is light, pupils will always constrict). However, in some cases, these responses can be considered voluntary: for example, shifting attention to a brighter region of an image will cause more constriction than if the light is not attended (Binda and Murray, 2015). Here, we will focus mainly on the PLR.

The PLR is the constriction and dilation of the pupil in response to changes in ambient light levels: the pupil will constrict to increased brightness and will dilate to decreased brightness. This response can be deconstructed in four major components: the latency period, the maximum constriction, the pupil escape and the return to the original state. The first component is the latency period and is very short (lasts a few tenths of a second). In this period, the pupil does not yet respond despite the light being already present. This period can vary based on the stimulus intensity: for a higher intensity, the latency will be shorter (Ellis, 1981), which will also cause the PLR to be higher and quicker. The second component is the constriction, during which the pupil will shrink very rapidly to its minimum size. This too is dependent on the intensity of the stimulus, with a higher intensity causing an increase of the constriction amplitude and velocity (Ellis, 1981). The third component is the pupil escape, during which the pupil will slightly dilate depending on the brightness (and sometimes also on the colour, Mathôt, 2018) of the light. The last component is the dilation and the return to the original size, which happen when the light stimulus is turned off. This is a slow process that can take minutes to happen due to an effect known as the post-illumination pupil response (Markwell et al., 2010). This is a particular effect where the pupil dilates after light offset and stabilises at a smaller diameter than at the start for a prolonged period before returning to its original size.

This difference in timing between constriction and dilation can be explained by the different retinal photoreceptors that drive the PLR: rods (which are very sensitive and mediate vision at low luminance), cones (which are colour sensitive) and the intrinsically photosensitive retinal ganglion cells (ipRGCs, these cells govern non-image forming vision and are crucial to control the circadian rhythm and sleep, Panda et al., 2002; Provencio et al., 2000; Ruby et al., 2002). While the first two photoreceptor classes have been known for a very long time, the ipRGCs have been discovered relatively more recently, being first identified

in rodents (Provencio et al., 2000). The idea of a third photoreceptor class existing was first developed in the nineties, when it was observed that blind individuals with degenerated photoreceptors still showed decreased melatonin production to light (Czeisler et al., 1995; Lockley et al., 1997), and that rats with the same deficiency also maintained light entrainment and their pupillary light reflex (Freedman et al., 1999; Yoshimura and Ebihara, 1996). This suggested that another class of photoreceptors must exist for these functions to be maintained, leading to the identification of the ipRGCs. While these cells were first shown to be involved in regulating the circadian cycle, they were later also shown to form a major input to the PON, suggesting that they play a key role in the PLR (Dacey et al., 2003; Gamlin et al., 2007; Lucas et al., 2003).

The three photoreceptor classes control different phases of the PLR. The initial rapid constriction is driven by the rods and the cones, while ipRGCs are not involved due to their slow onset. To give some context, previous studies have recorded the temporal responses for these photoreceptor classes. Cones and rods have shown responses after 30 to 40 ms and after approximately 150 ms respectively (Dacey et al., 2005), while ipRGC have shown a much longer latency, with a minimum of 1.78 s (McDougal and Gamlin, 2010). When it comes to the PLR, with a higher light intensity, some studies have recorded a minimum latency of 230 ms for ipRGCs (Bergamin and Kardon, 2003). On the other hand, the slower and longer response of the ipRGCs is what allows them to maintain constriction (Gamlin et al., 2007) and what regulates the post-illumination pupillary response (Markwell et al., 2010).

Historically, the PLR has always been considered a simple reflex response to light. However, there are some recent studies that have shown the PLR can be affected by how the visual input is selected, processed and interpreted. For example, it has been shown that this response can be triggered by word meaning (Mathôt et al., 2017): when reading or hearing a word that communicates brightness (e.g. sun), the diameter of the pupils was smaller compared to words that communicate darkness (e.g. night). A similar response has also been recorded when maintaining information in spatial working memory (Fabius et al., 2017): when locations on a bright background are being memorised and then retrieved, pupils are smaller compared to locations on a dark background.

Finally, it is important to notice that there is not much information about the computational processes behind the PLR. While this has not been directly studied, there is some evidence of what seems to be binocular interaction in the PLR. Wyatt and Musselman (1981) explain that the PLR is indeed binocular and that it shows both convergence, meaning that one pupil will respond to illumination in either retina, and divergence, meaning that both pupils will respond to illumination of one retina. They also explain that stimulating only one eye will elicit a consensual response in the unstimulated eye, meaning that there will be an equal constriction of the pupils in both the stimulated and unstimulated eyes. This would seem to

suggest the presence of binocular interaction that might be controlled by computational processes similar in nature to the processes controlling binocular combination in the cortex. There are also studies that have shown some evidence of binocular summation of the PLR: when both pupils are being stimulated, they will be smaller compared to when one of the two eyes is occluded (Doesschate and Alpern, 1967; Reeves, 1918; Thomson, 1947).

## 1.4   Pupillometry, EEG, fMRI and silent substitution

To investigate the mechanisms and the computational processes behind the PLR and how the signals from the two eyes are combined, stimuli of flickering light should be used to elicit a continuous and measurable response from the pupils. It is possible to use various techniques to measure these responses such as: pupillometry, EEG and fMRI.

Pupillometry permits direct measurement of the diameter of the pupils and has been used to study pupil responses for more than sixty years, since the publication of three crucial studies in the sixties (Hess and Polt, 1964, 1960; Kahneman and Beatty, 1966). Pupillometry is not only used to study changes in pupil size in response to changes in ambient light, but also to investigate changes in mental states (e.g. changes in arousal levels or increase in mental efforts are reflected by changes in pupil size, Mathôt, 2018), to investigate language behaviour, and memory and decision making (Sirois and Brisson, 2014). It is a very precise technique that can measure very small (down to a micrometer-large) and fast changes, and can provide an accurate and continuous measure whether the participant is aware of changes or not (Laeng et al., 2012).

Electroencephalography (EEG) allows measurement of the electrical activity generated by populations of neurons that fire together and generate a change in electrical polarisation in the brain. This electrical activity is recorded using a varying number of electrodes (from 32 to 128) that are positioned on the surface of the scalp. Presenting flickering lights to the eyes would also generate responses in the visual areas, which, if combined with pupillometric measures, could help to explain how binocular combination happens in the visual cortex and the non-canonical pathways that regulate the pupil response. EEG has excellent temporal resolution, making it ideal for measuring brain responses to fast changing stimuli such as flickering lights. For flickering light, steady-state visually evoked potentials would be measured: these are neural responses that are produced when viewing a repetitive visual stimulus, such as flickering light. Additionally, as binocular combination is being investigated, and the literature suggests that there is high suppression between the eyes to maintain ocularity invariance, steady-state EEG is an excellent tool that allows to record and measure

suppression (Baker et al., 2021).

However, EEG has poor spatial resolution due to the electrical signals having to pass through brain tissue and the scalp (Srinivasan et al., 1996) and this would not permit localisation of where exactly within the visual cortex binocular combination happens. This can be compensated by using functional magnetic resonance imaging (fMRI), which measures brain activity by detecting the magnetic properties associated with blood flow and blood oxygenation (Buxton, 2013; Ogawa et al., 1990). When the brain becomes more active, the neurones require more energy that is provided by glucose, which is not stored by brain cells. The required glucose is transported to the areas in need by the blood, together with oxygenated haemoglobin, and these differences in oxygenation change the magnetic properties of the blood, which are then measured by fMRI. Because the signal depends on changes of blood flow, which are relatively slow, the temporal resolution of fMRI is poor (Glover, 2011; Kim et al., 1997), but its spatial resolution is excellent, allowing precise measurement on the scale of millimetres.

Finally, as was explained in the previous section, the various photoreceptor classes are all involved in controlling the size of the pupils. Their role has been investigated and explained using a technique known as silent substitution, which makes it possible to target one specific class while nominally silencing the others to investigate how the pupils behave when only one specific class is being stimulated. Many studies have used it while pharmacologically dilating and stimulating one eye, and recording responses from the other eye (Cao et al., 2015; Estévez and Spekreijse, 1982; Shapiro et al., 1996; Spitschan et al., 2014; Spitschan and Woelders, 2018). This approach does not permit investigation of the binocular combination rules for specific photoreceptors, which could add more insight about our knowledge of how the pupils combine signals between each other.

## 1.5   Summary

Many studies have been conducted to understand more about the computational processes behind binocular combination. On the other hand, while studies have investigated when and why pupillary response occurs and what kind of stimuli elicit this type of response, there is not much information about the computational processes that regulate pupil diameter in response to different levels of light and how the signals between the two eyes are combined together. It might be reasonable to think that they might be similar in nature and that they might involve binocular interactions as well, such as summation and interocular suppression. Using and combining different techniques such as pupillometry, EEG, fMRI and silent substitution might help to investigate these processes and understand exactly where they happen within the visual

cortex. Moreover, the use of pupillometric measures might offer new insights about basic neural mechanisms that may be affected in clinical disorders, such as amblyopia.

## 1.6   Thesis overview

The main objective of this thesis is to investigate and understand the rules of binocular combination in the cortical pathways (the visual cortex) and the subcortical pathways that govern the pupil diameter using pupillometry, EEG, psychophysics, and fMRI.

Chapter 1 offers a general introduction that includes: an overview of binocular combination and ocularity invariance of spatial patterns; an overview of the PLR and the role of photoreceptors in controlling the pupil size; an overview of pupillometry, EEG, fMRI and silent substitution.

Chapter 2 reports the results of three experiments to investigate monocular and binocular responses to achromatic flickering (2 Hz) discs of luminance with no spatial contrast. The first experiment uses EEG and pupillometry simultaneously. The second experiment reproduces the first experiment using higher temporal frequencies of flicker and uses only EEG. The third experiment uses psychophysics to measure perception of the same flickering stimuli. The results from the three experiments are then accounted for in a single modelling framework, which was based on the Meese et al. (2006) model, where the weight of interocular suppression determines the binocular combination properties. The aim with the implementation of this model was to help describe the data better and not to find a model that would fit the data best. This is the reason why only the one model was used rather than comparing results from the other available alternatives. A similar reasoning was used for the model implemented in Chapter 4.

Chapter 3 uses fMRI to measure monocular and binocular responses to achromatic flickering discs of luminance and achromatic flickering gratings (both at 2 Hz).

Chapter 4 reports the results of four experiments to investigate monocular and binocular responses to flickering stimuli (0.5 Hz) when stimulating one specific class of photoreceptors using pupillometry and silent substitution. The first experiment uses discs of luminance flicker stimulating the periphery of the retina. In the second experiment, the melanopsin-containing ipRGCs are targeted while silencing the S, M and L cones. In the third experiment, the L-M pathway is targeted while silencing the S cones and the ipRGCs. In the fourth experiment, the S-(L+M) pathway is targeted while silencing the L and M cones and the ipRGCs. The results from the four experiments are then accounted for in a single modelling framework adapted from Chapter 2.

Chapter 5 summarises the findings presented in this thesis, discusses the broader implications and suggests avenues for future research.

Appendix 1 presents the EEG and pupillometry results of an experiment that conceptually replicates the first experiment from Chapter 2, but uses an alternative system of hardware and software and only the periphery of the retina is stimulated.

Appendix 2 presents the EEG and pupillometry results of an experiment that selectively tested the S, M, and L cones and the ipRGCs with discs flickering at 2 Hz.

Appendix 3 shows the results of additional analyses made on the results from Chapter 4 to investigate the response of the unstimulated eye during monocular presentation in each experiment.

Appendix 4 shows tables that summarise the statistical results from Chapter 4.

Appendix 5 shows fit examples for the computational model used in Chapter 4.

# 2 Chapter 2: Different rules for binocular combination of luminance flicker in cortical and subcortical pathways

This chapter has been adapted from: Segala FG, Bruno A, Martin JT, Aung MT, Wade AR, Baker DH. 2023. Different rules for binocular combination of luminance flicker in cortical and subcortical pathways. eLife 12. doi:10.7554/elife.87048[1]

## 2.1 Abstract

How does the human brain combine information across the eyes? It has been known for many years that cortical normalisation mechanisms implement 'ocularity invariance': equalising neural responses to spatial patterns presented either monocularly or binocularly. Here we used a novel combination of electrophysiology, psychophysics, pupillometry and computational modelling to ask whether this invariance also holds for flickering luminance stimuli with no spatial contrast. We find dramatic violations of ocularity invariance for these stimuli, both in cortex and also in the subcortical pathways that govern pupil diameter. Specifically, we find substantial binocular facilitation in both pathways with the effect being strongest in cortex. Near-linear binocular additivity (instead of ocularity invariance) was also found using a perceptual luminance matching task. Ocularity invariance is therefore not a ubiquitous feature of visual processing, and the brain appears to repurpose a generic normalisation algorithm for different visual functions by adjusting the amount of interocular suppression.

## 2.2 Introduction

The brain must combine information across multiple sensory inputs to derive a coherent percept of the external world. This involves a process of signal combination both within (Baker and Wade, 2017) and between (Ernst and Banks, 2002) the senses. Binocular vision is a useful test case for signal combination, as the inputs to the two eyes overlap substantially (in species with forward-facing eyes), and the neural locus is well-established (Hubel and Wiesel, 1962). Much of our knowledge about binocular combination derives from studies on the contrast response of the 'canonical' visual pathway, in which signals pass from the eyes to primary visual cortex (V1), via the lateral geniculate nucleus (LGN) (Purves et al., 2008). However, signals are also combined across the eyes in the network of subcortical nuclei that govern pupil diameter in response

---

[1]The author, Federico Segala, designed experiments 2 and 3, collected the data for all experiments, analysed the results and wrote the manuscript under the supervision of Professor Daniel Baker and Dr Aurelio Bruno. Experiment 1 was designed jointly with Professor Daniel Baker. The computational model was developed by Professor Daniel Baker.

to absolute light levels (McDougal and Gamlin, 2008) and much less is known about the computations that operate in these subcortical pathways. Our primary purpose here is to investigate the computations governing signal combination in these two anatomically distinct pathways in response to luminance changes.

For pattern vision, binocular presentation confers greater sensitivity to low contrast targets than monocular presentation. This is known as binocular summation, with summation ratios (the relative improvement under binocular presentation) at detection threshold lying between $\sqrt{2}$ and 2 (Baker et al., 2018; Campbell and Green, 1965). This advantage is lost at high stimulus contrasts, where both psychophysical performance (contrast discrimination thresholds, Legge, 1984; Meese et al., 2006) and neural activity (Baker and Wade, 2017; Moradi and Heeger, 2009) are approximately equal for monocular and binocular presentation. Contemporary models of binocular vision (Ding and Sperling, 2006; Meese et al., 2006) advocate a process of interocular suppression that normalizes the two eyes' inputs at high contrasts and negates the binocular advantage. This is consistent with our everyday experience of 'ocularity invariance' (Baker et al., 2007): perceived contrast does not change when one eye is opened and closed.

The pupillary light reflex is an automatic constriction of the iris sphincter muscles in response to increases in light levels, which causes the pupil to shrink (McDougal and Gamlin, 2008). There is a clear binocular component to this reflex, as stimulation of one eye still causes constriction of the other eye's pupil (termed the consensual response, Wyatt and Musselman, 1981). Importantly, the neuroanatomical pathway involved completely bypasses the canonical cortical pathway (retina to V1), instead involving a network of subcortical nuclei, including the Pretectal Olivary nucleus, Superior Cervical ganglion, and Edinger-Westphal nucleus (Angée et al., 2021; Mathôt, 2018; McDougal and Gamlin, 2008; Wang and Munoz, 2015). To account for the consensual response, these brain regions must combine information from the left and right eyes (Doesschate and Alpern, 1967), yet the computation that achieves this is unclear. The pupil response can be modulated by periodic changes in luminance, and is temporally low-pass (Barrionuevo et al., 2014; Spitschan et al., 2014), most likely due to the mechanical limitations of the iris sphincter and dilator muscles (Privitera and Stark, 2006).

To investigate the binocular combination of light, we designed an experiment that allowed us to simultaneously record electrophysiological and pupillometric responses to monocular and binocular stimuli. We chose a primary flicker frequency of 2 Hz as a compromise between the low-pass pupil response (see Barrionuevo et al., 2014; Spitschan et al., 2014), and the relatively higher-pass EEG response (Regan, 1966). This novel paradigm allowed us to probe both cortical (using EEG) and subcortical (using a binocular eye-tracker) pathways simultaneously in response to flickering light, and make quantitative comparisons between them. Periodic flicker entrains both neural (Norcia et al., 2015) and pupil (Spitschan et al., 2014) responses

at the flicker frequency, enabling precise estimation of response amplitudes in the Fourier domain. Relative to the response to a monocular signal, adding a signal in the other eye can either increase the response (facilitation) or reduce it (suppression). We followed up our main experiment with additional exploration of the effect of stimulus frequency, and a psychophysical matching experiment measuring perceived flicker intensity (i.e. temporal contrast). The results are interpreted using a hierarchical Bayesian computational model of binocular vision, and reveal that subcortical pathways implement stronger interocular suppression than the canonical cortical pathway.

## 2.3 Results

### 2.3.1 Experiment 1
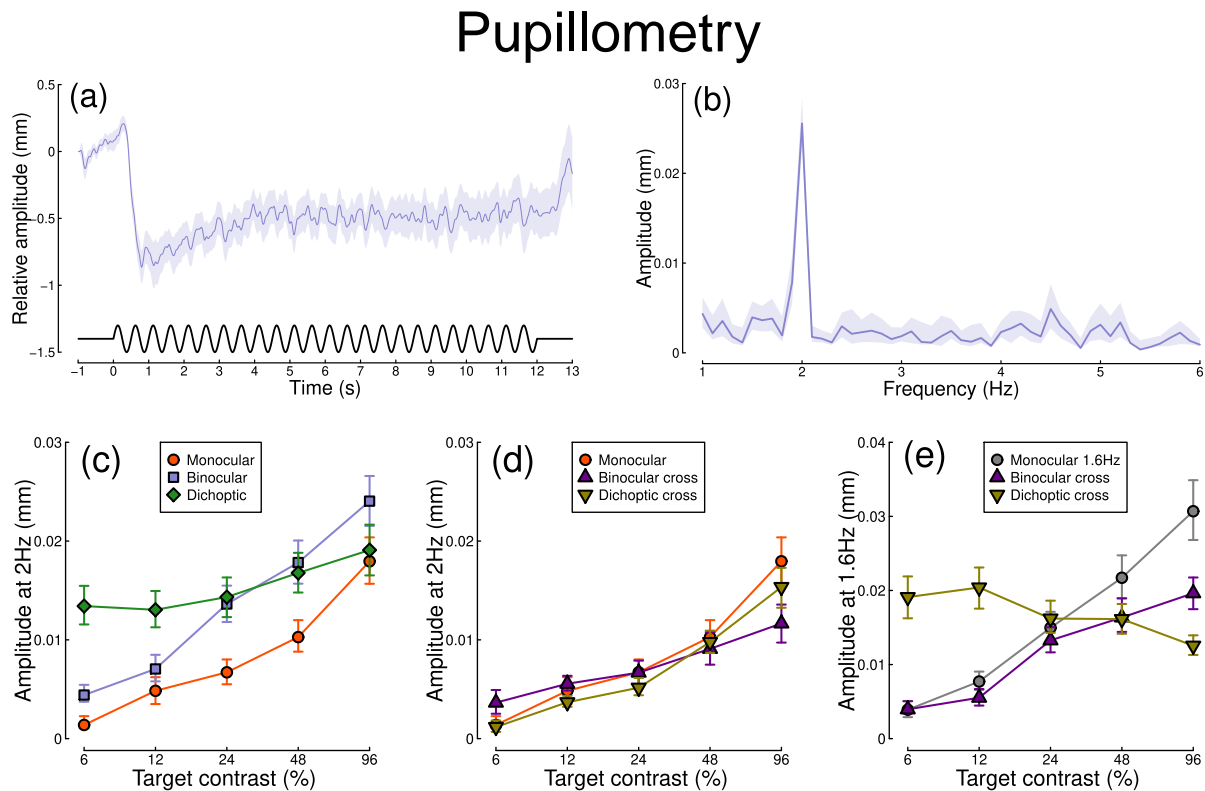


Figure 2.1: Summary of pupillometry results for N=30 participants. Panel (a) shows a group average waveform for binocular presentation (low pass filtered at 5Hz), with the driving signal plotted at the foot. Negative values indicate constriction relative to baseline, and positive values indicate dilation. Panel (b) shows the average Fourier spectrum (absolute amplitude values). Panels (c,d) show contrast response functions for pupil diameter at 2Hz for different conditions (illustrated in Figure 2.8). Panel (e) shows contrast response functions at 1.6Hz for three conditions. Shaded regions and error bars indicate bootstrapped standard errors.

The pupillometry results are summarised in Figure 2.1. The group average waveform for binocular presentation is shown in Figure 2.1a. There is a substantial pupil constriction at stimulus onset, followed by visible oscillations at the flicker frequency (2Hz, see waveform at foot). The average Fourier spectrum is displayed in Figure 2.1b, and shows a clear spike at 2 Hz, but no evidence of a second harmonic response at 4Hz (though see Appendix 1). These results demonstrate that our paradigm can evoke measurable steady-state pupil responses at 2Hz.

Figure 2.1c shows contrast response functions driven by stimuli flickering only at 2Hz. Response amplitudes increased monotonically with target contrast, confirming that our paradigm is suitable for measuring contrast-dependent differences in the pupil response (to our knowledge this is the first time this has been demonstrated). The amplitude of the binocular condition (blue squares) is consistently greater than that of the monocular condition (red circles) across all target contrasts. A $2 \times 5$ repeated measures $ANOVA_{circ}^2$ (Baker, 2021) comparing these conditions revealed a significant main effect of target contrast (F(8,580) = 16.79, $p$ <0.001), a significant effect of condition (F(2,580) = 11.04, $p$ <0.001), and a significant interaction (F(8,580) = 56.25, $p$ <0.001). The dichoptic condition begins at a much higher amplitude, owing to binocular combination of the target and high (48%) contrast mask, and then increases slightly with increasing target contrast (main effect of target contrast: F(8,232) = 3.03, $p < 0.003$).

In Figure 2.1d, we plot responses to monocular target stimuli flickering at 2Hz, when the other eye viewed stimuli flickering at 1.6Hz (the red monocular-only data are replotted from Figure 2.1c for comparison). When the 1.6Hz component had the same contrast as the target (the binocular cross condition, shown in purple) responses were facilitated slightly at low contrasts, and suppressed at the highest target contrasts (interaction between contrast and condition: F(8,580) = 52.94, $p$ <0.001). When the 1.6Hz component had a fixed contrast of 48% (the dichoptic cross condition, shown in yellow), responses were suppressed slightly across the contrast range (interaction between contrast and condition: F(8,580) = 62.05, $p$ <0.001).

Figure 2.1e shows responses at 1.6Hz, for the same conditions, as well as for a condition in which a monocular stimulus flickered at 1.6Hz (grey circles). Here we find strong suppression in both the binocular cross (purple triangles) and dichoptic cross (yellow triangles) conditions. In the binocular cross condition, the amplitudes are reduced relative to the monocular condition (grey circles) (interaction effect: F(8,580) = 41.23, $p$ <0.001). In the dichoptic cross condition, increasing the 2Hz target contrast suppresses the response to the 1.6Hz mask, and the function decreases (see e.g. Busse et al., 2009) (main effect of target contrast F(8,232) = 17, $p$ <0.001).

Figure 2.2 shows equivalent results, measured contemporaneously using EEG. Figure 2.2a shows the group average waveform for binocular presentation, and Figure 2.2b shows the Fourier spectrum for binocular

presentation, both averaged across four posterior electrodes (*Oz, POz, O1* and *O2*, marked on the inset scalp plots). Unlike for the pupillometry data, there are clear responses at both the first harmonic frequency (2Hz), and also the second harmonic frequency (4Hz). We therefore calculated contrast response functions at both first and second harmonic frequencies.

# Electroencephalography
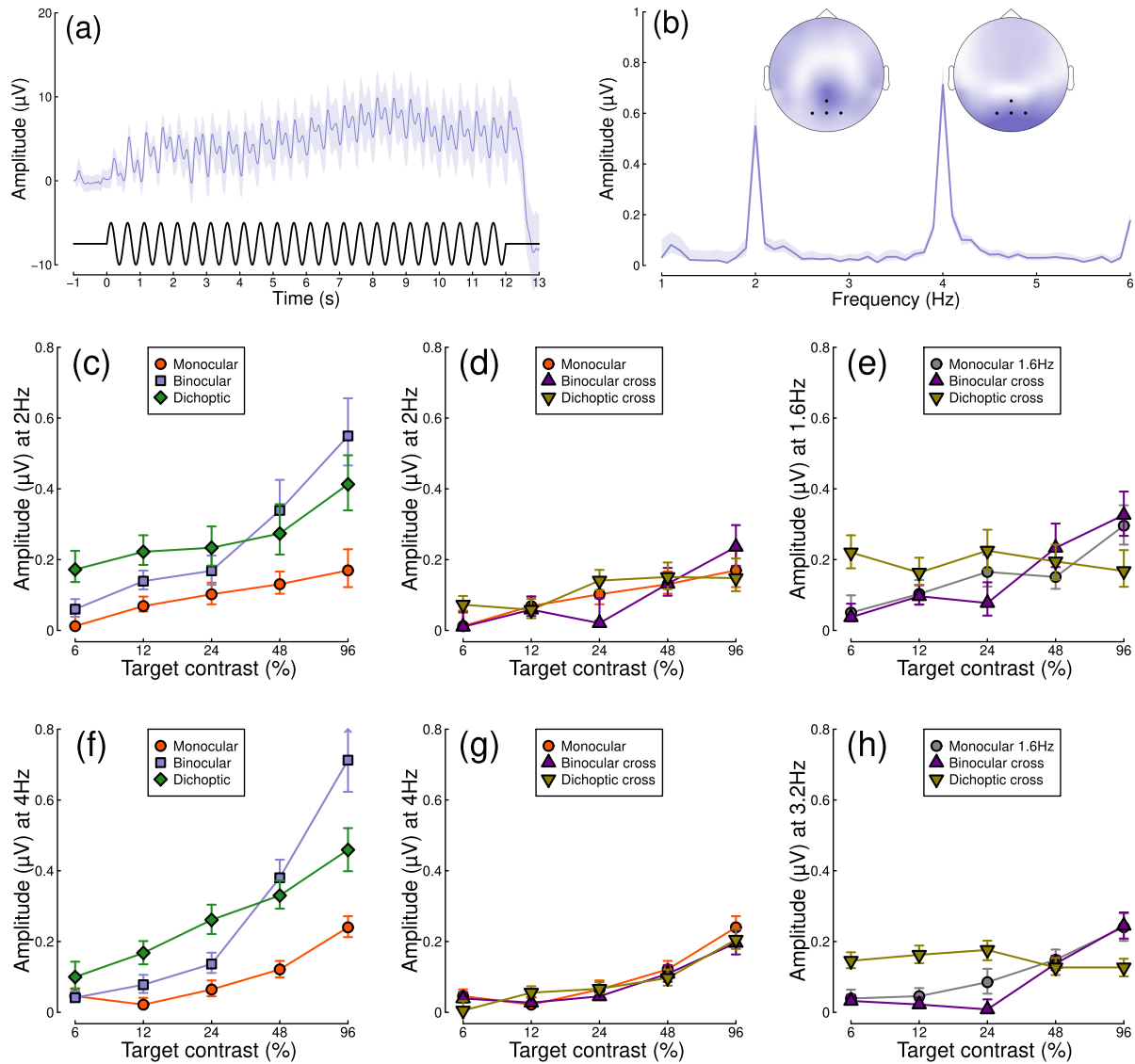


Figure 2.2: Summary of EEG results for N=30 participants. Panel (a) shows a group average waveform for binocular presentation (low pass filtered at 5Hz), with the driving signal plotted at the foot. Panel (b) shows the average Fourier spectrum, and inset scalp distributions. Black dots on the scalp plots indicate electrodes Oz, POz, O1 and O2. Panels (c,d) show contrast response functions at 2Hz for different conditions. Panel (e) shows contrast response functions at 1.6Hz for three conditions. Panels (f-h) are in the same format but for the second harmonic responses. Shaded regions and error bars indicate bootstrapped standard errors.

When stimuli in both eyes flicker at 2Hz, the binocular responses at the first (Figure 2.2c) and second (Figure 2.2f) harmonics are substantially greater than the monocular responses, particularly at high contrasts. Analysis of variance on the complex values ($ANOVA^2_{circ}$) revealed a main effect of contrast (F(8,580) = 4.38, $p$ <0.001) and an interaction effect (F(8,580) = 61.58, $p$ <0.001), but no effect of condition ($p = 0.13$) at the first harmonic, with a similar pattern of results obtained at the second harmonic. For the cross-frequency conditions (Figure 2.2d,g), there was no appreciable effect of adding a 1.6Hz component on the response at 2Hz or 4Hz (no effect of condition, and no interaction). Similarly, there were no clear interocular interactions between frequencies in the responses at 1.6Hz (Figure 2.2e) and 3.2Hz (Figure 2.2h). This pattern of results suggests that processing of temporal luminance modulations happens in a more linear way in visual cortex (indexed by EEG), compared with subcortical pathways (indexed by pupillometry), and shows no evidence of interocular suppression.
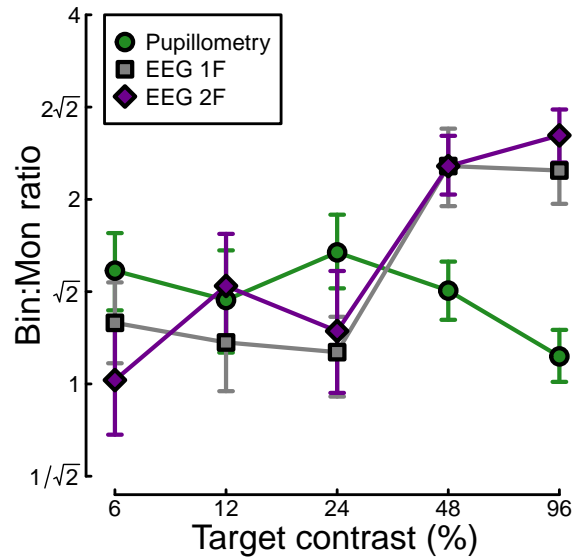


Figure 2.3: Ratio of binocular to monocular response for three data types. These were calculated by dividing the binocular response by the monocular response at each contrast level, using the data underlying Figures 2.1c, 2.2c and 2.2f. Each value is the average ratio across N=30 participants, and error bars indicate bootstrapped standard errors.

Finally, we calculated the ratio of binocular to monocular responses across the three data types from Experiment 1. Figure 2.3 shows that these ratios are approximately $\sqrt{2}$ across the low-to-intermediate contrast range for all three data types. At higher contrasts, we see ratios of 2 or higher for the EEG data,

but much weaker ratios near 1 for the pupillometry data. Note that the ratios here are calculated on a per-participant basis and then averaged, rather than being the ratios of the average values shown in Figures 2.1 and 2.2. A $3 \times 5$ repeated measures ANOVA on the logarithmic (dB) ratios found a main effect of contrast ($F_{(3.08, 89.28)} = 4.53$, $p < 0.002$), no effect of data modality ($F_{(2,58)} = 0.75$, $p = 0.48$), but a highly significant interaction ($F_{(5.54, 160.67)} = 3.84$, $p < 0.001$). All of the key results from Experiment 1 were subsequently replicated for peripheral stimulation (see Appendix 1).

### 2.3.2 Experiment 2
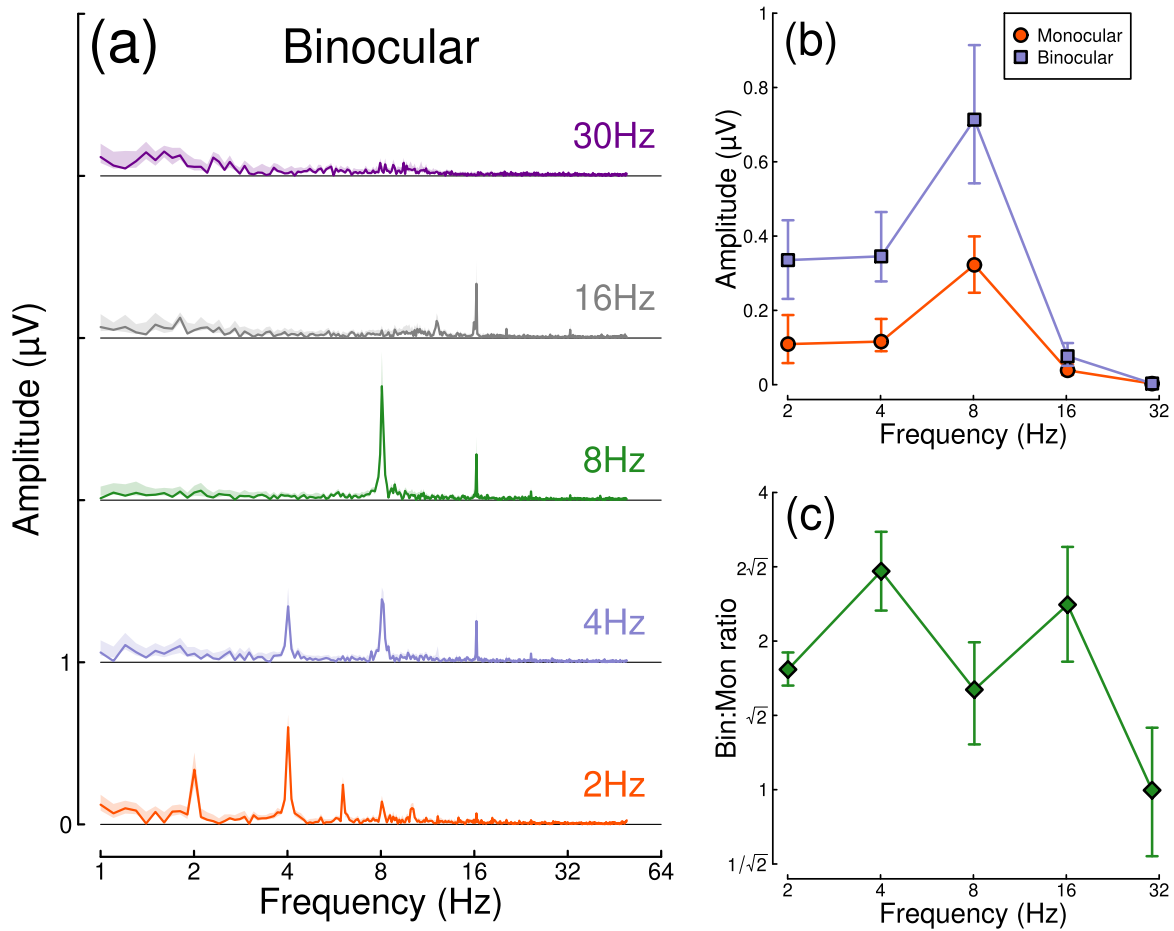


Figure 2.4: Binocular facilitation at different temporal frequencies, measured using EEG. Panel (a) shows Fourier spectra for responses to binocular flicker at 5 different frequencies (offset vertically for clarity). Panel (b) shows the response at each stimulation frequency for monocular (red circles) and binocular (blue squares) presentation. Panel (c) shows the ratio of binocular to monocular responses. Error bars and shaded regions indicate bootstrapped standard errors across N=12 participants.

The strong binocular facilitation and weak interocular suppression in the EEG data from Experiment 1 was very different from previous findings on binocular combination using steady-state EEG with grating stimuli (Baker and Wade, 2017). One possible explanation is that the lower temporal frequency used here (2Hz, vs 5 or 7Hz in previous work) might be responsible for this difference. We therefore ran a second experiment to compare monocular and binocular responses at a range of temporal frequencies. Only EEG data were collected for this experiment, as the pupil response is substantially weaker above around 2Hz (Barrionuevo et al., 2014; Spitschan et al., 2014); note that we originally chose 2Hz because it produces measurable signals for both EEG and pupillometry, yet is unfortunately optimal for neither.

Results from the temporal frequency experiment are shown in Figure 2.4. Figure 2.4a shows the Fourier spectra for responses to binocular flicker at 5 different frequencies (2, 4, 8, 16, and 30 Hz). From 2 to 16 Hz, clear signals are observed at each fundamental frequency, and typically also their higher harmonics (integer multiples of the fundamental). However, at 30 Hz (upper row), the responses recorded were not demonstrably above the noise baseline. Figure 2.4b compares the monocular and binocular responses at each stimulation frequency. Here we replicate the substantial summation effect across frequencies up to and including 16Hz (Fig. 2.4c), demonstrating that strong binocular facilitation in the EEG data of Experiment 1 cannot be attributed to our use of 2Hz flicker.

### 2.3.3   Experiment 3

In Experiment 1 we found evidence of stronger binocular facilitation for cortical responses to luminance flicker (measured using EEG), compared with subcortical responses (measured using pupillometry; see Figure 2.3). Since perception is dependent on cortical responses, these results provide a clear prediction for perceived contrast judgements indexed by psychophysical contrast matching paradigms (e.g. Anstis and Ho, 1998; Legge and Rubin, 1981; Levelt, 1965; Quaia et al., 2018). We therefore conducted such an experiment, in which participants judged which of two stimuli had the greater perceived amplitude of flicker. On each trial, one stimulus was a matching stimulus, that had a fixed binocular flicker amplitude of either 24% or 48% (temporal) contrast. The other stimulus was a target stimulus, the contrast of which was controlled by a staircase algorithm. We tested 9 ratios of target contrast between the left and right eyes.

The results from the matching experiment are shown in Figure 2.5. Each data point indicates the contrast levels required in each eye that were perceptually equivalent to the binocular 24% (red circles) and 48% (blue circles) matching contrasts. At both matching contrasts, we see a very substantial increase in the physical contrast required for a monocular target (data points along the $x$- and $y$-axes), compared to a binocular target (points along the diagonal of $x=y$). For example with a 48% match, the monocular

targets required contrasts close to 100%, whereas binocular targets required a contrast of around 50%. The data points between these extremes also fall close to the predictions of a linear summation model (diagonal dotted lines), and are inconsistent with a winner-takes-all (or MAX) model (dashed lines). Overall, these matching results are consistent with the approximately linear summation effects observed in the EEG data of Experiment 1 (Figure 2.2c,f).
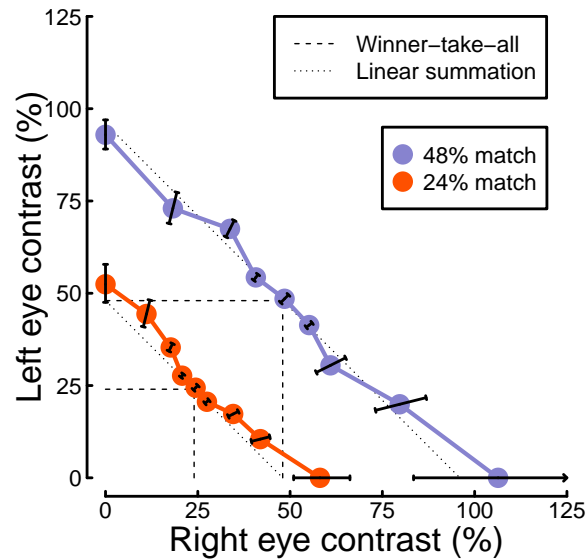


Figure 2.5: Contrast matching functions. Dotted and dashed lines are predictions of canonical summation models involving linear combination (dotted) or a winner-take-all rule (dashed). Error bars indicate the standard error across participants (N=10), and are constrained along radial lines converging at the origin. Note that, for the 48% match, the data point on the x axis falls higher than 100% contrast. This is because the psychometric function fits for some individuals were interpolated such that the PSE fell above 100%, shifting the mean slightly above that value.

### 2.3.4 Computational modelling

We fitted a computational model to the data from Experiments 1 & 3 using a hierarchical Bayesian approach. The model behaviour is displayed in Figure 2.6a-d, with empirical data superimposed for comparison. In general, the model captures the key characteristics of the empirical data, with group-level parameter estimates provided in Table 2.1. We were particularly interested in comparing the weight of interocular suppression across data sets. We therefore plot the posterior distributions for this parameter for all four data sets (see Figure 2.6e). The key finding is that the pupillometry results (green distribution) display a

Table 2.1: Summary of median parameter values.

| Data set | Z | k | w | Rmax |
|---|---|---|---|---|
| Pupillometry | 3.44 | 0.01 | 0.61 | 0.00023 |
| EEG 1F | 2.62 | 0.15 | 0.02 | 0.00336 |
| EEG 2F | 3.71 | 0.07 | 0.02 | 0.0031 |
| Matching | 0.30 | 5.10 | 0.09 | - |

much greater weight of interocular suppression compared with the other data sets (grey, purple and yellow distributions). There is no overlap between the pupillometry distribution and any of the other three. All four distributions are also meaningfully below a weight of 1 – the value that previous work using grating stimuli would predict (Baker and Wade, 2017; Meese et al., 2006), and the peak location of our prior distribution (black curve). These results offer an explanation of the empirical data: the strong interocular suppression for the pupillometry data is consistent with the weak binocular facilitation, and measurable dichoptic masking observed using that method. The weaker suppression for the other experiments is consistent with the near-linear binocular facilitation effects, and absent dichoptic masking.
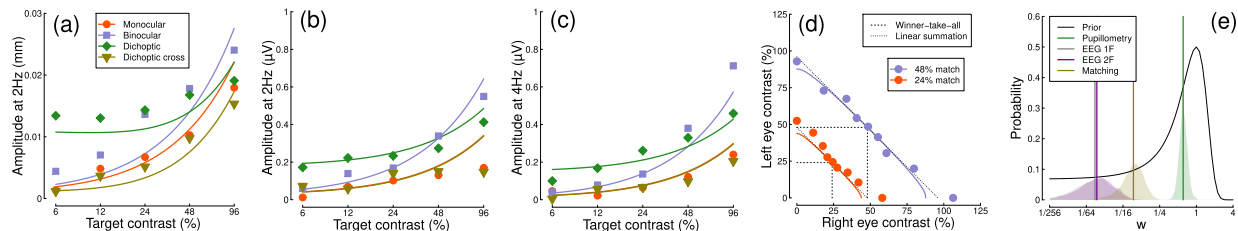


Figure 2.6: Summary of computational modelling. Panels (a-d) show empirical data from key conditions, replotted from earlier figures for the pupillometry (a), first harmonic EEG responses (b), second harmonic EEG responses (c) and contrast matching (d) experiments, with curves showing model behaviour generated using the median group-level parameter values. Panel (e) shows the posterior probability distributions of the interocular suppression parameter for each of the four model fits. The pupillometry distribution (green) is centred about a substantially higher suppressive weight than for the other data types (note the logarithmic x-axis). The black curve shows the (scaled) prior distribution for the weight parameter.

## 2.4 Discussion

Using a novel paradigm that combines EEG and pupillometry, we found surprising results for the binocular integration of flickering light. In the visual cortex response (indexed by EEG), the binocular combination of spatially-uniform temporal luminance modulations seems to happen approximately linearly, with no evidence of interocular suppression. Evidence for this comes from the substantial binocular facilitation effect when comparing monocular and binocular responses, and the lack of a dichoptic suppression effect when the two eyes were stimulated at different frequencies. In the subcortical pathway (indexed by pupillometry),

binocular combination is more non-linear, with evidence of interocular suppression. This was evidenced by a weaker binocular facilitation, and stronger dichoptic suppression, relative to the EEG data. This pattern of results was confirmed by computational modelling, which showed a much greater suppressive weight for the pupillometry data compared to the EEG data. Additionally, we found that perception of flickering light is consistent with a near-linear binocular summation process, consistent with the cortical (EEG) responses.

The results of our main experiment were unexpected for both the pupillometry and the EEG measures. Previous studies investigating binocular combination of spatial patterns (i.e. sine wave grating stimuli) are generally consistent with strong interocular suppression and weak binocular facilitation at high contrasts (Baker and Wade, 2017; Meese et al., 2006; Moradi and Heeger, 2009) (however we note that facilitation as substantial as ours has been reported in previous EEG work by Apkarian et al., 1981). Our second experiment ruled out the possibility that these differences were due to the lower temporal frequency (2Hz) used here. However, there is evidence of more extensive binocular facilitation for a range of other stimuli. Using scleral search coils, Quaia et al. (2018) observed a strong binocular facilitation (or 'supersummation') in the reflexive eye movement response to rapidly moving stimuli (also known as the ocular following response). Spitschan and Cajochen (2019) report a similar result in archival data on melatonin suppression due to light exposure (melatonin is a hormone released by the pineal gland that regulates sleep; its production is suppressed by light exposure and can be measured from saliva assays). Work on the accommodative response indicates that binocular combination there is approximately linear (Flitcroft et al., 1992), and can even cancel when signals are in antiphase (we did not try this configuration here). In the auditory system, interaural suppression of amplitude modulation also appears to be weak when measured using a similar steady-state paradigm (Baker et al., 2020). Finally, psychophysical matching experiments using static stimuli also show near-linear behaviour for luminance increments (Anstis and Ho, 1998; Baker et al., 2012; Levelt, 1965), though not for luminance decrements (Anstis and Ho, 1998). Overall, this suggests that strong interocular normalization may be specific to spatial pattern vision, and not a general feature of binocular signal combination (or combination across multiple inputs in other senses).

Given the above, where does this leave our understanding of the overarching purpose of signal combination? Baker and Wade (2017) point out that strong suppression between channels that are subsequently summed is equivalent to a Kalman filter, which is the optimal method for combining two noisy inputs (see also Ernst and Banks, 2002). Functionally, interocular suppression may therefore act to dynamically suppress noise, rendering binocular vision more stable. This account has intuitive appeal, and is consistent with other models that propose binocular combination as a means of redundancy reduction (Li and Atick, 1994; May and Zhaoping, 2022). One possibility is that optimal combination is useful for visual perception — a

critical system for interacting with the local environment — and is therefore worth devoting the additional resource of inhibitory wiring between ocular channels. However the other examples of binocular combination discussed above are primarily physiological responses (pupil size, eye movements, hormone release) that may benefit more from an increased signal-to-noise ratio, or otherwise be phylogenetically older than binocular pattern vision. Conceptualised another way, the brain can repurpose a generic architecture for different situational demands by adjusting parameter values (here the weight of interocular suppression) to achieve different outcomes. Our future work in this area intends to compare binocular combination for specific photoreceptor pathways, including different cone classes, and intrinsically photoreceptive retinal ganglion cells.

Pupil size affects the total amount of light falling on the retina. It is therefore the case that fluctuations in pupil diameter will have a downstream effect on the signals reaching cortex. We did not incorporate such interactions into our computational model, though in principle this might be worthwhile. However we anticipate than any such effects would be small, since pupil modulations at 2Hz are in the order of 2% of overall diameter (e.g. Spitschan et al., 2014). It is also the case that cortical activity can modulate pupil diameter, usually through arousal and attention mechanisms (e.g. Bradley et al., 2008). We think it unlikely that these temporally coarse processes would have a differential effect on e.g. monocular and binocular stimulation conditions in our experiment, and any fluctuations during an experimental session (perhaps owing to fatigue) will be equivalent for our comparisons of interest. Therefore we make the simplifying assumption that the pupil and perceptual pathways are effectively distinct, but hope to investigate this more directly in future neuroimaging work. Using fMRI to simultaneously image cortical and subcortical brain regions will also allow us to check that the differences we report here are not a consequence of the different measurement techniques we used (pupillometry and EEG).

Classic studies investigating the neurophysiological architecture of V1 reported that cells in cytochrome-oxidase 'blobs' (Horton and Hubel, 1981; Livingstone and Hubel, 1984) are biased towards low spatial frequencies (Edwards et al., 1995; Tootell et al., 1988), and relatively insensitive to stimulus orientation (Horton and Hubel, 1981; Livingstone and Hubel, 1984; though see Economides et al., 2011). As the blob regions are embedded within ocular dominance columns (Horton and Hubel, 1981), they are also largely monocular (Livingstone and Hubel, 1984; Tychsen et al., 2004). More recent work has reported psychophysical evidence for unoriented chromatic (Gheiratmand et al., 2013) and achromatic (Meese and Baker, 2011) mechanisms, that also appear to be monocular. Our use of luminance flicker might preferentially stimulate these mechanisms, perhaps explaining why our EEG data show little evidence of binocular interactions. Indeed, our EEG results could potentially be explained by a model involving entirely non-interacting monocular channels, with the

binocular facilitation effects we find (e.g. Figures 2.3 & 2.4) owing to additivity of the electrophysiological response across independent monocular cells, rather than within binocular neurons. We therefore performed an additional analysis to investigate this possibility.
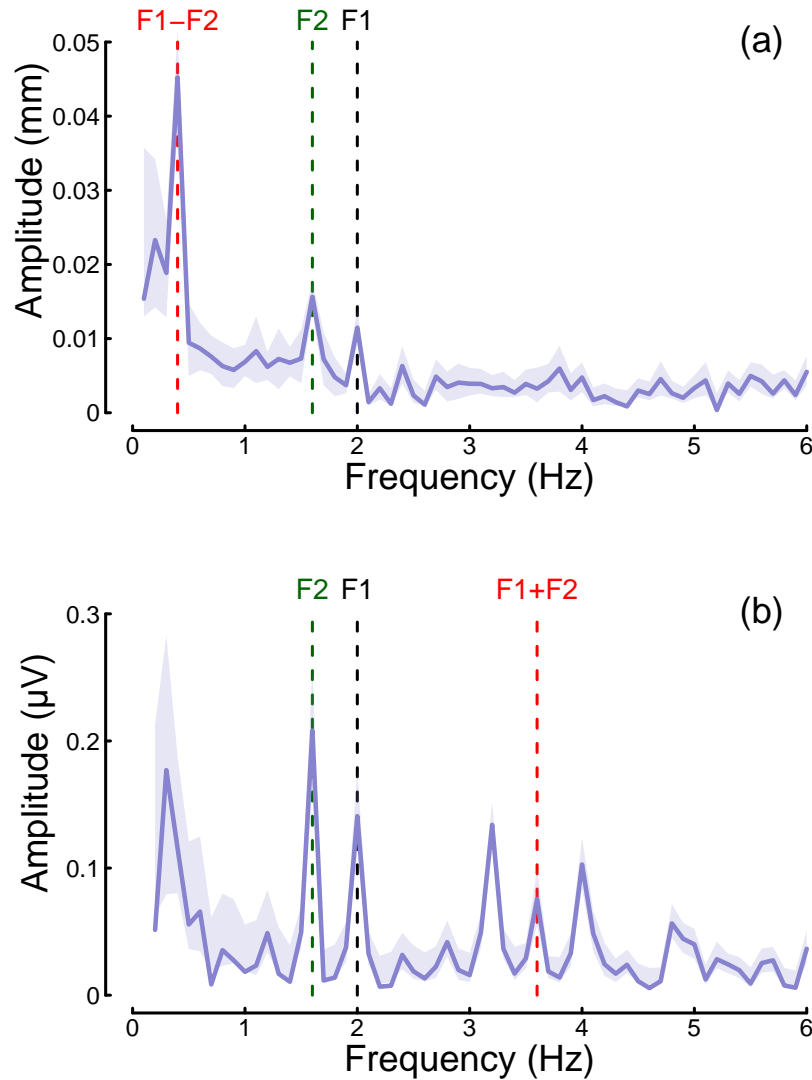


Figure 2.7: Summary of intermodulation responses in pupillometry (a) and EEG (b) data. The data are pooled across the binocular cross and dichoptic cross conditions of Experiment 1, with a target contrast of 48%. Vertical dashed lines indicate the fundamental flicker frequencies of 2Hz (F1; black) and 1.6Hz (F2; green), and the intermodulation difference (F1-F2 = 0.4Hz) and sum (F1+F2 = 3.6Hz) frequencies (red). Data are averaged across N = 30 participants, and shaded regions indicate ±1 standard error.

In the steady-state literature, one hallmark of a non-linear system that pools inputs is the presence of intermodulation responses at the sums and differences of the fundamental flicker frequencies (Baitch and Levi, 1988; Tsai et al., 2012). In Figure 2.7 we plot the amplitude spectra of conditions from Experiment

1 in which the two eyes were stimulated at different frequencies (2Hz and 1.6Hz) but at the same contrast (48%; these correspond to the binocular cross and dichoptic cross conditions in Figures 2.1d,e and 2.2d,e). Figure 2.7a reveals a strong intermodulation difference response at 0.4Hz (red dashed line), and Figure 2.7b reveals an intermodulation sum response at 3.6Hz (red dashed line). It seems likely that the absence of a sum response for pupillometry data, and of a difference responses for the EEG data, is a consequence of the temporal constraints of these methods. The presence of intermodulation terms is predicted by non-linear gain control models of the type considered here (Baker and Wade, 2017; Tsai et al., 2012), and indicates that the processing of monocular flicker signals is not fully linear prior to the point at which they are combined across the eyes. Indeed, our model architecture (Meese et al., 2006) makes specific predictions about the location of interocular suppression - it impacts before binocular combination, consistent with results from primate physiology (Dougherty et al., 2019).

## 2.5 Conclusions

We have demonstrated that binocular combination of flickering light differs between cortical and subcortical pathways. Flicker was also associated with substantially weaker interocular suppression, and stronger binocular facilitation, compared to combination of spatial luminance modulations in visual cortex. Our computational framework for understanding signal combination permits direct comparisons between disparate experimental paradigms and data types. We anticipate that this will help elucidate the constraints the brain faces when combining different types of signals to govern perception, action and biological function.

## 2.6 Methods

### 2.6.1 Participants

Thirty (20 females), twelve (7 females) and ten (3 females) adult participants, whose ages ranged from 18 to 45, were recruited for Experiments 1, 2 and 3 respectively. All participants had normal or corrected to normal binocular vision, and gave written informed consent. Our procedures were approved by the Ethics Committee of the Department of Psychology at the University of York (identification number 792).

### 2.6.2 Apparatus & stimuli

The stimuli were two discs of achromatic flickering light with a diameter of 3.74 degrees, presented on a black background. The same stimuli were used for all three experiments. Four dark red lines were added

around both discs to help with their perceptual fusion, giving the appearance of a single binocular disc (see upper left insert in Figure 2.8 for an example of the fused stimulus). The discs were viewed through a four-mirror stereoscope, which used front silvered mirrors to avoid internal reflections, and meant that participants saw a single fused disc. The use of a stereoscope allowed us to modulate the stimuli in three different ocular configurations: monocular, binocular, and dichoptic. Note that during monocular presentation of flicker, the unstimulated eye still saw the static (non-flickering) disc of mean luminance.

All stimuli had a mean luminance of 42 cd/m$^2$ and were displayed on an Iiyama VisionMaster™ Pro 510 display (800 x 600 pixels, 60 Hz refresh rate), which was gamma corrected using a Minolta LS-110 photometer (Minolta Camera Co. Ltd., Japan). For experiments 1 and 2, the stimuli were presented using Psychopy (v3.0.7). For experiment 3, the stimuli were presented using Psychopy (v2022.1.1).

EEG data were collected for Experiments 1 and 2 using a 64-electrode ANT WaveGuard cap and the signals were recorded at 1 kHz using the ASA software (ANT Neuro, Netherlands). Pupillometry data were collected for Experiment 1 using a binocular Pupil Core eye-tracker (Pupil Labs GmbH, Berlin, Germany; Kassner et al., 2014) running at 120 Hz, and the signals were recorded with the Pupil Capture software.

### 2.6.3 Procedure

Before each experiment, participants adjusted the angle of the stereoscope mirrors to achieve binocular fusion. This was done so that they would perceive the two discs as one fused disc when looking at the screen through the stereoscope.

#### 2.6.3.1 Experiment 1: simultaneous EEG and pupillometry

The experiment was conducted in a windowless room, in which the only light source was the monitor. The participants sat at 99 cm from the monitor and the total optical viewing distance (through the stereoscope) was 107 cm. The experiment was carried out in a single session lasting 45 minutes in total, divided into three blocks of 15 minutes each. In each block, there were 60 trials lasting 15 seconds each (12s of stimulus presentation, with an interstimulus interval of 3s). The participants were given no task other than to look at the fixation cross in the middle of the disc while trying to minimise their blinking during the presentation period.
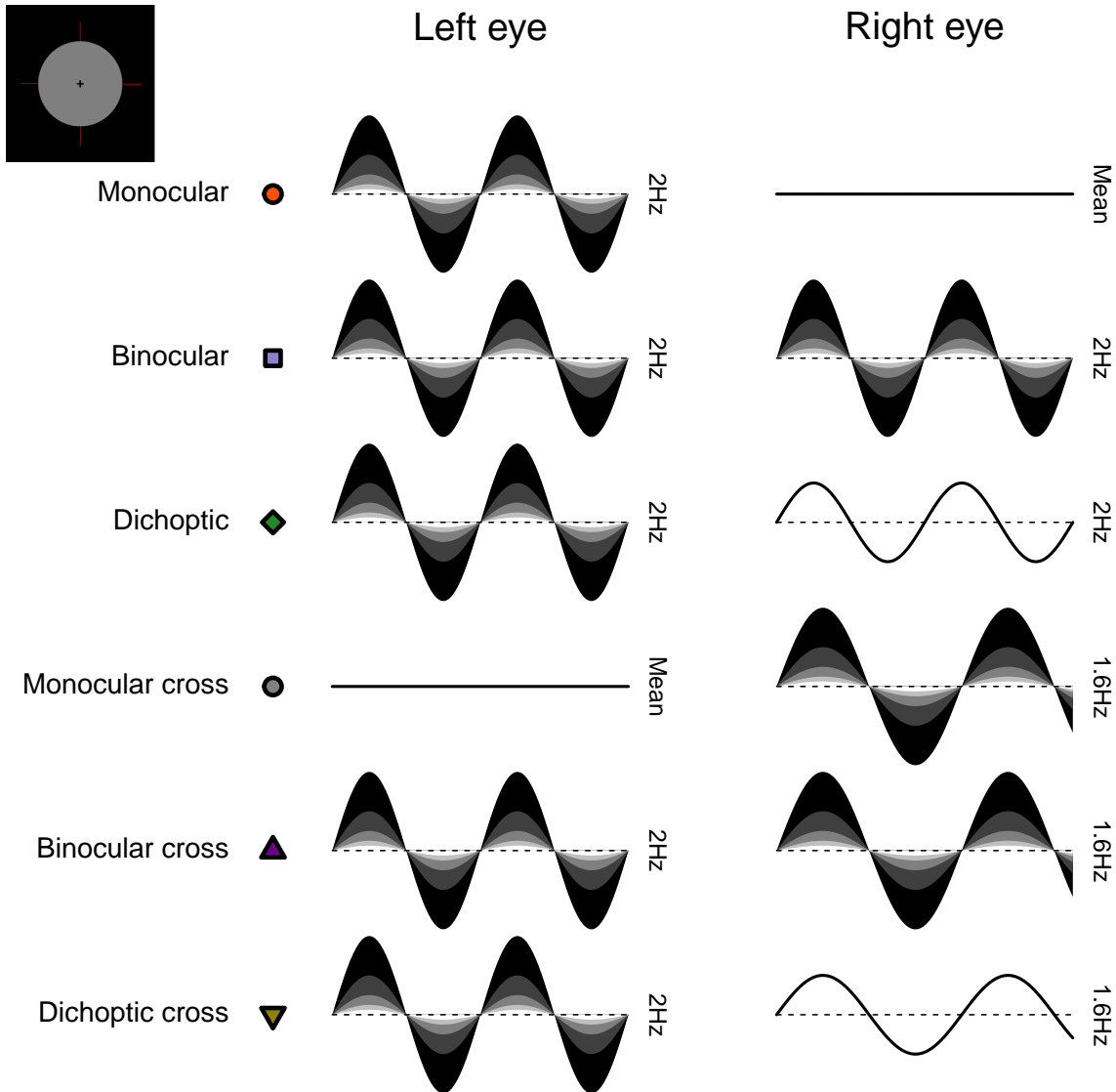
Figure 2.8: Schematic diagram illustrating the ocular arrangements, and temporal waveforms of the luminance modulations used in Experiment 1. Shaded waveforms indicate a target stimulus, that was presented at one of five contrasts on each trial (denoted by the shading levels). Unshaded waveforms indicate mask stimuli, that were presented at a fixed contrast level of 48% regardless of the target contrast. Each waveform corresponds to a 1 second period of a 12 second trial, and coloured symbols are for consistency with Figures 2.1 and 2.2. The icon in the upper left corner illustrates the stimulus appearance (a luminous disc against a black background). The left and right eye assignments were counterbalanced across trials in the experiment (i.e. the monocular stimulus could be shown to either eye with equal probability).

We included six distinct ocular conditions, each at five temporal contrast levels (combined factorially) relative to the mean luminance: 6, 12, 24, 48 and 96%. Contrast was defined as temporal Michelson contrast; the difference between maximum and minimum luminances, scaled by the mean and expressed as a percentage. In the first three conditions, the discs flickered at 2 Hz, in either a monocular, binocular, or

dichoptic arrangement (see upper rows of Figure 2.8). In the dichoptic condition the non-target eye saw a fixed temporal contrast of 48%. The rationale for including the monocular and binocular conditions is that they permit us to measure empirically any binocular facilitation, by comparing the response amplitudes across these two conditions. The rationale for including the dichoptic condition is that it provides additional contraints to computational models, and further explores the binocular contrast-response space (see Baker et al., 2007).

In the remaining three conditions (termed the cross-frequency conditions) an additional flicker frequency of 1.6Hz was introduced. We chose this frequency because it is sufficiently well-isolated from the target frequency (2Hz) in the Fourier spectrum for 10-second trials. We repeated the monocular condition with this stimulus (one eye sees 1.6Hz flicker, the other sees mean luminance), as well as testing in a binocular cross configuration (one eye sees each frequency at the target contrast). The rationale for the binocular cross condition is that it allows us to see the effects of suppression between the eyes without the additional complication of signal summation (which occurs when both eyes receive the same frequency), because the response of each eye can be resolved independently by frequency. Finally, in the dichoptic cross condition, one eye saw the target stimulus flickering at 2Hz, the other eye saw flicker at 1.6Hz with a contrast of 48% - again this reveals the presence of suppression (by comparison with the 2Hz monocular condition). A schematic overview of the cross-frequency conditions is shown in the lower rows of Figure 2.8. In all conditions, we counterbalanced presentation of the target stimulus across the left and right eyes.

### 2.6.3.2 Experiment 2: EEG responses across temporal frequency

This experiment used the same equipment set up as Experiment 1, except that the eye tracker was not used. Unlike the first experiment, only one contrast level was used (96%) and the discs were set to flicker at five different frequencies (2, 4, 8, 16 and 30 Hz). Only two ocular configurations, monocular and binocular, were included, with the latter having both discs flickering at the same frequency. The experiment was carried out in one session lasting 25 minutes in total, divided into five blocks of 5 minutes each. In each block, there were 20 trials in total with the same timing as for Experiment 1.

### 2.6.3.3 Experiment 3: temporal contrast matching

The experiment was conducted in a darkened room with a blacked-out window. The display equipment (monitor and stereoscope) were the same as for the two previous experiments, but no EEG or pupillometry data were collected. A two-interval contrast matching procedure was used to collect data. In one interval, participants were presented with a standard fused disc that flickered at a set contrast level (either 24 or

48%), which was selected by the experimenter at the beginning of each block. In the other interval, a target disc was displayed, flickering at different contrast levels on each trial, but with a fixed interocular contrast ratio across the block. The contrast level of the target was controlled by a 1-up, 1-down staircase moving in logarithmic (dB) steps of contrast. The ratio of flicker amplitudes in the left and right eyes was varied across blocks and was set to be 0, 0.25, 0.5, 0.75 or 1 (9 distinct conditions). The standard and target discs were displayed for 1 second each, with an interstimulus interval of 0.5 seconds. After both discs had appeared on screen, the participants had to indicate which interval they perceived as having the more intense flicker. The intervals were randomly ordered, and all discs flickered at a frequency of 2 Hz (two cycles in sine phase).

Due to its long duration (approximately 3 hours in total), the participants completed the experiment across multiple sessions initiated at their own convenience. The experiment was divided into 54 blocks (3 repetitions × 2 standard contrasts × 9 target ratios), which lasted on average 3 minutes each, depending on the response speed of the participant. In each block, there was a total of 50 trials. No auditory feedback was given for this subjective task.

### 2.6.4   Data analysis

EEG data were converted from the ANT-EEProbe format to a compressed csv text file using a custom Matlab script (available at: https://github.com/bakerdh/PupillometryEEG/, Segala et al., 2023a) and components of the EEGlab toolbox (Delorme and Makeig, 2004). The data for each participant were then loaded into R for analysis, where a ten-second waveform for each trial at each electrode was extracted (omitting the first two seconds). The Fourier transform of each waveform was calculated, and the complex spectrum stored in a matrix. All repetitions of each condition were then averaged for each electrode. They were then averaged across four occipital electrodes (*POz*, *Oz*, *O1*, *O2*), to obtain individual results. Finally, these were averaged across participants to obtain the group results. All averaging was performed in the complex domain and therefore retained the phase information (i.e. coherent averaging), and at each stage we excluded data points with a Mahalanobis distance exceeding $D = 3$ from the complex-valued mean (see Baker, 2021). For statistical comparisons of complex-valued data, we use the $ANOVA^2_{circ}$ statistic described by Baker (2021). This is a multivariate extension of ANOVA that assumes equal variance of the real and imaginary Fourier components, or equivalently, an extension of the $T^2_{circ}$ statistic of Victor and Mast (1991) that can compare more than two conditions.

A similar analysis pipeline was adopted for the pupillometry data. The data were converted from mp4 videos to a csv text file using the Pupil Player software (Kassner et al., 2014), which estimated pupil diameter for each eye on each frame using a 3D model of the eyeball. The individual data were then loaded into R for

analysis, where again a ten-second waveform for each trial in each eye was extracted (excluding the first two seconds after stimulus onset). We interpolated across any dropped or missing frames to ensure regular and continuous sampling over time. The Fourier transform was calculated for each waveform, and all repetitions of each condition were pooled across eye and then averaged. We confirmed in additional analyses that the monocular consensual pupil response was complete, justifying our pooling of data across the eyes. Finally, data were averaged across all participants to obtain the group results. Again, we used coherent averaging, and excluded outlying data points in the same way as for the EEG data. Note that previous pupillometry studies using luminance flicker have tended to fit a single sine-wave at the fundamental frequency, rather than using Fourier analysis (e.g. Spitschan et al., 2014). The Fourier approach is more robust to noise at other frequencies (which can make the phase and amplitude of a fitted sine wave unstable) and has been used in some previous studies (see Barrionuevo et al., 2014; Barrionuevo and Cao, 2016). Additionally, it makes the pupillometry analysis consistent with standard practice in steady-state EEG analysis (e.g. Figueira et al., 2022).

To analyse the matching data, we pooled the trial responses across all repetitions of a given condition for each participant. We then fitted a cumulative normal psychometric function to estimate the point of subjective equality at the 50% level. Thresholds were averaged across participants in logarithmic (dB) units.

For all experiments, we used a bootstrapping procedure with 1000 iterations to estimate standard errors across participants. All analysis and figure construction was conducted using a single R-script, available online, making this study fully computationally reproducible.

### 2.6.5   Computational model and parameter estimation

To describe our data, we chose a model of binocular contrast gain control with the same general form as the first stage of the model proposed by Meese et al. (2006). The second gain control stage was omitted (consistent with Baker and Wade, 2017) to simplify the model and reduce the number of free parameters. The response of the left eye's channel is given by:

$$Resp_L = \frac{L^2}{Z + L + wR}, \tag{2}$$

with an equivalent expression for the right eye:

$$Resp_R = \frac{R^2}{Z + R + wL}. \tag{3}$$

In both equations, $L$ and $R$ are the contrast signals from the left and right eyes, $Z$ is a saturation constant that shifts the contrast-response function laterally, and $w$ is the weight of suppression from the other eye.

The responses from the two eyes are then summed binocularly:

$$Resp_B = R_{max}(Resp_L + Resp_R) + n, \tag{4}$$

where $n$ is a noise parameter, and $R_{max}$ scales the overall response amplitude. The $R_{max}$ parameter was omitted when modelling the contrast matching data, as it has no effect in this paradigm.

Despite being derived from the model proposed by Meese et al. (2006), the simplifications applied to this architecture make it very similar to other models (e.g. Ding and Sperling, 2006; Doesschate and Alpern, 1967; Legge, 1984; Schrödinger, 1926). In particular we fixed the numerator exponent at 2 in our model, because otherwise this value tends to trade off with the weight of interocular suppression (see Baker et al., 2012; Kingdom and Libenson, 2015). Our key parameter of interest is the weight of interocular suppression. Large values around $w = 1$ result in a very small or nonexistent binocular advantage at suprathreshold contrasts, consistent with previous work using grating stimuli (Baker and Wade, 2017). Low values around $w = 0$ produce substantial, near-linear binocular facilitation (Baker et al., 2020). Models from this family can handle both scalar contrast values and continuous waveforms (Tsai et al., 2012) or images (Meese and Summers, 2007) as inputs. For time-varying inputs, the calculations are performed at each time point, and the output waveform can then be analysed using Fourier analysis in the same way as for empirical data. This means that the model can make predictions for the entire Fourier spectrum, including harmonic and intermodulation responses that arise as a consequence of non-linearities in the model (Baker and Wade, 2017). However for computational tractability, we performed fitting here using scalar contrast values.

We implemented the model within a Bayesian framework using the Stan software (Carpenter et al., 2017). This allowed us to estimate group-level posterior parameter distributions for the weight of interocular suppression, $w$, and the other free model parameters $R_{max}$, $Z$ and $n$. The prior distributions for all parameters were Gaussian, with means and standard deviations of 1 and 0.5 for $w$ and $R_{max}$, and 5 and 2 for $Z$ and $n$, with these values chosen based on previous literature (Baker et al., 2012; Meese et al., 2006). We sampled from a Student's t-distribution for the amplitudes in the pupillometry and EEG experiments, and from a Bernoulli distribution for the single trial matching data. The models were fit using the individual data across all participants, independently for each data set. We used coherent averaging to combine the data across participants, but this was not implemented in the model, so to compensate we corrected the

group-level model by scaling the estimated noise parameter ($n$) by the square root of the number of participants ($n_{group} = \frac{n}{\sqrt{30}}$). We took posterior samples at over a million steps for each data set, using a computer cluster, and retained 10% of samples for plotting.

### 2.6.6   Preregistration, data and code availability

We initially preregistered our main hypotheses and analysis intentions for the first experiment. We then conducted a pilot study with N = 12 participants, before making some minor changes to the stimulus (we added dim red lines to aid binocular fusion). We then ran the main experiment, followed by two additional experiments that were not preregistered. The preregistration document, raw data files, and experimental and analysis code, are available on the project repository: https://doi.org/10.17605/OSF.IO/TBEMA.

# 3 Chapter 3: Binocular combination of achromatic flickering light in the visual cortex

## 3.1 Abstract

Many studies have investigated how the brain combines information across the two eyes: for spatial patterns, the visual areas perform ocularity invariance, where the response to monocular and binocular stimuli is equalised. On the other hand, flickering luminance stimuli with no spatial contrast show substantial binocular facilitation in the visual areas measured using EEG. Here, we tested flickering luminance discs using fMRI to test where this facilitation happens within the visual cortex: whether it happens only in V1 or also in V2, V3 and V4. We also tested flickering gratings. For the latter stimuli, our results confirm the ocularity invariance mechanisms that have been described in the literature. However, for the former stimuli, while we found that there is facilitation for binocular stimuli, this facilitation is not as strong as the facilitation described in the previous literature and is constant throughout all four visual areas.

## 3.2 Introduction

Information is combined by the brain to provide a meaningful understanding of the surrounding world. Evidence of this is provided by binocular vision, which combines the individual images from both eyes to form a cyclopean image of the world. Many studies have investigated how this combination happens for spatial contrast within the visual cortex. At low contrast, binocular summation is observed: binocular presentation elicits a bigger response than monocular presentation, with the summation ratios varying between $\sqrt{2}$ and 2 (Baker et al., 2018; Campbell and Green, 1965). At high contrast, binocular summation for spatial pattern vision is lost: the response to monocularly-presented and binocularly-presented stimuli is equalised (Ding and Sperling, 2006; Meese et al., 2006). This process is known as ocularity invariance (Baker et al., 2007) and has been observed in psychophysical performance, tested with contrast discrimination thresholds (Legge, 1984), and in neural activity, tested with electroencephalograms (EEG, Baker and Wade, 2017) and with functional magnetic resonance imaging (fMRI, Lygo et al., 2021; Moradi and Heeger, 2009).

We recently investigated binocular combination of spatially-uniform temporal luminance flickering light in the visual cortex and in the subcortical pathways that determine pupil size (Segala et al., 2023b). At high contrast, we found that ocularity invariance is violated, with a substantial binocular facilitation effect found in the visual cortex when comparing monocular and binocular responses. Within the primary visual cortex (V1), there are cells found within the blob regions that are biased towards low spatial frequencies

(Edwards et al., 1995; Tootell et al., 1988) and that are also largely monocular (Livingstone and Hubel, 1984; Tychsen et al., 2004). In our discussion, we suggested that these cells and these mechanisms might be the ones that are primarily being stimulated by a luminance flicker and why the EEG was showing little interocular interaction.

To investigate whether this binocular facilitation is present only in V1, we designed an fMRI experiment to record BOLD responses to monocular and binocular stimuli. We presented participants with luminance discs containing no spatial modulation flickering at 2 Hz to reproduce our previous experiment (Segala et al., 2023b). We also used luminance gratings flickering at 2 Hz to test for ocularity invariance. We analysed the results within the four primary visual cortices (V1, V2, V3, V4) predicting that we would observe no binocular summation for the flickering gratings throughout all four visual areas and that we would observe strong binocular facilitation in V1 only for the flickering luminance discs.

## 3.3 Methods

The current experiment was performed within the scope of a bigger project funded by a BBSRC grant which aimed to investigate binocular combination in the non-canonical pathways and to understand how reflexive eye movements are driven by motion in one or both eyes, and explore how this differs across chromatic pathways. This was done by using five different stimulus conditions that will all be described in this methods section to make sure that the experiment is fully understandable to the reader. However, for the sake of remaining within the context of this thesis, only a portion of the analyses and of the results will be reported and presented in the results section of this chapter: the flickering luminance disc and flickering grating conditions.

### 3.3.1 Participants

Thirty-six (23 females) adult participants were recruited for the experiment, whose age ranged from 18 to 50. All participants had normal or corrected to normal binocular vision and normal colour vision, and gave written informed consent. Our procedures were approved by the Research Governance Committee of the York Neuroimaging Centre at the University of York.

### 3.3.2 Stimuli and task

The stimuli used in the main experiment included an annular luminance disc and radial sinewave grating patterns (0.25 cycles per degree) that were designed specifically to isolate the achromatic post-

receptoral, L/M-cone opponent, and S-cone opponent mechanisms (Figure 3.1). The stimuli spanned from 3 to 10 degrees of visual angle in eccentricity, from the central fixation (total 20 degrees visual angle in diameter). The central 6 degrees diameter was set to the background mean luminance (Figure 3.1) and contained a fixation point composed of overlapping multicoloured dots (about 0.5 degrees of visual angle diameter). The fixation point was updated into different configurations (by randomly re-generating the dot positions) at random time points throughout the experiment: this served as an attentional task for the participants, who were asked to count how many times the fixation point changed throughout the scan. The experiment had a 12 second on-off block design: participants were presented with 2 Hz sinusoidal flicker for 12 seconds, followed by a 12 second blank period. There were five different conditions presented throughout the scan under binocular and monocular configurations: a flickering luminance disc containing no spatial modulation and counterphase flickering (Figure 3.1a); a flickering luminance grating (Figure 3.1b); three drifting gratings conditions (16 deg/sec, direction reversing every 1 second) for each of luminance, L-M and S-cone isolating stimuli (Figure 3.1c-e). All gratings conditions were presented flickering on/off at 2 Hz (i.e. not a counterphase flicker). Each run of the main experiment included four trials of the five principal stimulus types, two of which were binocular and two were monocular (one left eye, one right eye).
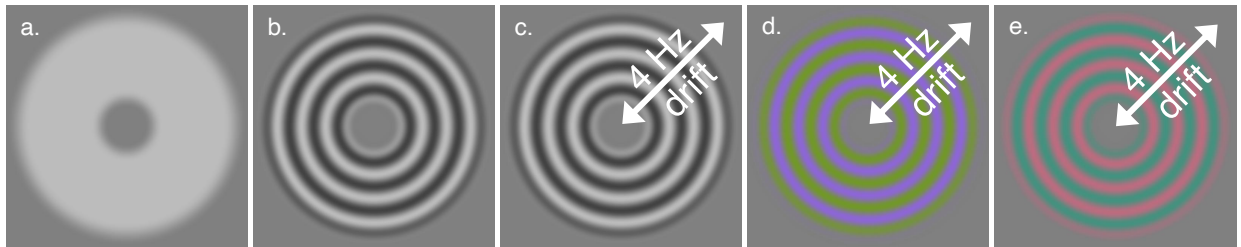


Figure 3.1: Stimuli used in the main functional experiment. Panel (a) is the disc of luminance flicker. Panel (b) is the grating flicker. Panel (c) is the grating flicker with drift. Panel (d) is the blue-yellow isoluminant flicker with drift. Panel (e) is the red-green isoluminant flicker with drift. All stimuli flickered sinusoidally at 2 Hz. All grating patterns had a spatial frequency of 0.25 cycles/deg. Michelson contrast was 48% for all achromatic stimuli, 34% for L-M cones and 95% for S cones.

In addition to the main experiment stimulus, two further functional scans were performed to obtain retinotopic information from the visual cortex; one expanding ring stimulus, and one rotating wedge stimulus, both containing a checkerboard flickering at 6 Hz, which completed 8 cycles (36 seconds per cycle) per scan, and spanned a radius of 14.34 degrees.

Because stimulus requirements for isoluminance vary between subjects due to differences in lens yellowing, L/M cone ratio, macular pigment density, and other factors, a perceptual calibration was performed based on minimum flicker luminance measurements (Anstis and Cavanagh, 1983; Cavanagh et al., 1987) and it was obtained as participants underwent structural scans. On each trial of the perceptual calibration,

participants aimed to minimize the flicker of radial stimuli used in the main experiment. An example of a typical calibration result for one participant can be seen in Figure 3.2.
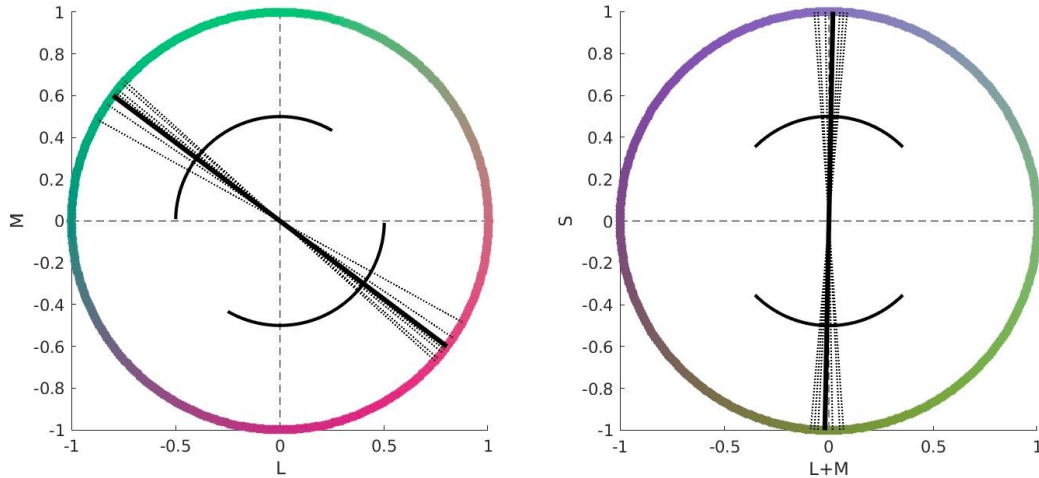


Figure 3.2: Example of typical results for the perceptual calibration task. The left panel shows the results of the calibration within the L and M space and the right panel shows the results of the calibration within the S and L+M space. The dotted lines show the settings selected by the participant in each trial. The bold lines show the average of the individual responses and the settings that were selected during the experiment for the participant.

### 3.3.3 Apparatus

Stimuli were presented using a PROPixx DLP Projector (Vpixx Ltd., Quebec, Canada) with 1920 x 1080 pixel resolution and 120 Hz refresh rate. Image frames intended for the left and right eyes were interleaved with a circular 3D Polarizer (Vpixx Ltd., Quebec, Canada), giving an effective refresh rate of 60 Hz per eye. The images were back-projected onto a custom acrylic display panel that preserved polarization. Participants viewed the display from a distance of about 62 cm through passive stereo polarizer glasses and a first-surface right-angle mirror attached to the head coil.

The spectral emissions of the red, green and blue channels of the projector were measured at the corneal plane using a wavelength- and irradiance-calibrated OceanOptics JAZ spectrometer optic (Ocean Insight Inc., Oxford, UK) and the Smith and Pokorny 10-degree fundamentals (Smith and Pokorny, 1975) were used to define the spectral sensitivities of S-, M- and L-cones.

### 3.3.4 MRI acquisition

Magnetic resonance images were obtained with a 3-Tesla Siemens Magnetom Prisma MRI scanner and a Siemens 64-channel head and neck coil. We acquired high resolution T1-weighted (TR 2.4s; TE 2.28ms; voxel size 0.8 x 0.8 x 0.8 mm; 8° flip angle; FOV 256 x 256 x 256 mm) and T2-weighted (TR 3.2s; TE 563ms; voxel size 0.8 x 0.8 x 0.8 mm; 120° flip angle; FOV 256 x 256 x 256 mm, aligned from the centre of the slice group from the T1-weighted scan prescription) structural scans using a generalized auto-calibrating partially parallel acquisition (GRAPPA) with a multi-band acceleration factor of 2.

Functional images portraying blood-oxygen level dependent (BOLD) contrasts (Ogawa et al., 1990) were acquired with a T2*-sensitive gradient-recalled echo pulse sequence (TR 3s; TE 36.6ms; voxel size 2.3 x 2.3 x 2.0 mm; 75° flip-angle; FOV 280 x 280 mm; 72 slices). Slices were acquired in the standard interleaved fashion using a multiband acceleration factor of 2 and with a slice prescription that incorporated the occipital pole and calcarine sulcus (for the majority of subjects the whole brain was covered by the slices, for some subjects a small number of voxels were lost from the top of the brain in order to ensure the occipital pole was included within the slices). Each functional scan lasted 8 minutes and yielded 164 volumes. We additionally acquired in-plane gradient field map images (TR 850ms; TE1 4.92ms; TE2 7.38ms; echo time differences 2.46ms; voxel size 3.0 x 3.0 x 3.0 mm; 60° flip-angle, FOV 240 x 240 mm; 44 slices; aligned from the centre of the slice group from the functional scan prescription), to apply B0 unwarping to functional images (Jenkinson, 2003, 2001; Jezzard and Balaban, 1995), and an in-plane proton density scan to aid structural scan alignment (TR 7.2s; TE 9.2ms; voxel size 2.1875 x 2.1875 x 2 mm; 160° flip-angle; FOV 280 x 280 mm; 72 slices).

### 3.3.5 Data analysis

As stated before, all the conditions were analysed but only the conditions (flickering luminance discs and flickering gratings) pertaining to the theme of this thesis have been reported here.

#### 3.3.5.1 Processing of structural data

A detailed reconstruction of each subject's brain was created from the T1-weighted and T2-weighted structural scans, using a combination of FSL v5.0 (http://fsl.fmrib.ox.ac.uk/fsl/fslwiki/) and Freesurfer v6.0 (http://surfer.nmr.mgh.harvard.edu/), using the recon-all function. Grey and white matter were segmented during the reconstruction process so that analyses could be restricted to the segmented cortical grey matter.

### 3.3.5.2 FSL analysis

To produce brain images, data were analysed using the FMRIB's Software Library (FSL, https://fsl.fmrib.ox.ac.uk/fsl/: Jenkinson et al., 2012).

#### 3.3.5.2.1 Preprocessing of the functional data

FMRI data for each of the four functional runs were subject to a standard image preprocessing pipeline using custom Python scripts and FEAT (FMRI Expert Analysis Tool) Version 6.00, part of FSL. Functional images were coregistered to the subject's own in-session high resolution T1 structural image using the boundary-based registration algorithm (Greve and Fischl, 2009) and then warped into 2-mm MNI152 space (Montreal Neurological Institute: Mazziotta et al., 2001) using FLIRT (Jenkinson et al., 2002; Jenkinson and Smith, 2001). The registration from high-resolution structural to standard space was further refined using FNIRT (Andersson et al., 2007a, 2007b).

The following pre-statistics processing was applied to each 4D image dataset: correction for B0 distortions (Jenkinson, 2003, 2001; Jezzard and Balaban, 1995); removal of non-brain tissue with BET (Smith, 2002); motion correction with MCFLIRT (Jenkinson et al., 2002); slice time correction using Fourier-space time-series phase-shifting; spatial smoothing with a 10 mm full width at half-maximum (FWHM) Gaussian kernel (Smith and Brady, 1997); grand-mean intensity normalisation of the entire 4D dataset by a single multiplicative factor; high-pass temporal filtering to compensate for baseline drifts in the signal (Gaussian-weighted least-squares straight line fitting, with sigma = 45 s).

#### 3.3.5.2.2 Statistical analysis

Voxel-wise time-series statistical analysis was carried out using FILM (FMRIB's Improved Linear Model, https://www.fmrib.ox.ac.uk/datasets/techrep/tr04ss2/tr04ss2/node3.html) with local autocorrelation correction (Woolrich et al., 2001). The time series model included four regressors of interest, one each for the monocular (collapsed across left and right eyes) and binocular presentations of the stimuli shown in Figure 3.1a-b (i.e. mononcular disc, binocular disc, monocular grating, binocular grating). These regressors were constructed by convolving the stimulus on-off timing vector (two 12 s trials per functional run for each regressor) with a canonical double gamma haemodynamic response function (HRF) waveform. Temporal derivatives for each of the stimulus regressors were also included in the model to compensate for timing discrepancies between the actual and modelled HRF, and six nuisance regressors were included to capture variance explained by motion artefacts (extended motion parameter basis set). The resulting general linear model was implemented at each voxel in the fMRI time series to identify regions showing significant

stimulus-related BOLD activation for each condition. A set of contrast vectors (T-tests) were also constructed to compare the parameter estimates for binocular and monocular stimulus conditions (i.e. binocular > monocular) and for stimulation and resting periods (i.e. stimulus on > stimulus off).

The contrasts of parameter estimates from functional runs within each subject were combined in a second level fixed-effects analysis by forcing the random effects variance to zero in FLAME (FMRIB's Local Analysis of Mixed Effects). A final group level analysis was then carried out on the contrast images for each subject using FLAME stage 1 (Beckmann et al., 2003; Woolrich, 2008; Woolrich et al., 2004). Z (Gaussianised T/F) statistic images were thresholded non-parametrically using clusters determined by Z > 2 and a (corrected) cluster significance threshold of $p = 0.05$ (Worsley, 2001).

### 3.3.5.3 mrVista analysis

The outputted T1.mgz file for each subject from the recon-all process was converted into a RAS orientation nifti file using the mri_convert function from freesurfer, and the ribbon file (containing the segmented grey matter information) was updated to correctly label the left and right hemispheres for use in mrVista, using function fs_ribbon2itk from the VISTA software (https://web.stanford.edu/group/vista/cgi-bin/wiki/index.php/Software, downloaded 2022; Vista Lab, Stanford University).

#### 3.3.5.3.1 Preprocessing of the functional data

The functional scans were processed using mrVista, running on MATLAB R2019a (The MathWorks Inc., Natick, MA, USA). Alignment of the functional data to the detailed structural image was performed by first using FSL's FLIRT, to align the PD scan, which was aligned to the functional scan prescription, to the converted T1 nifti file, and then loading the resulting transform file into mrVista when editing the alignment (via the FSL Transform option, rxLoadFSLTransform), where the PD scan was used as the inplane image. Motion correction between and within functional scans from each session was performed using a maximum likelihood alignment routine within mrVista .

A travelling wave analysis (8 cycles) was performed on the retinotopic scans to view eccentricity and polar angle information from the ring and wedge scans, respectively, in line with standard retinotopy analysis techniques. The output of this analysis was used to draw our V1-V4 regions of interest, as described below.

#### 3.3.5.3.2 Defining the regions of interest (ROIs) V1-V4

Primary visual areas were localised for each subject using the output of the travelling wave analysis from retinotopic scans (ring and wedge scans). Flat maps were created in mrVista from the centre of

the approximate foveal location in V1 (in the posterior occipital region, along the calcarine sulcus). The boundaries of the visual areas were identified based on the phase reversals from the polar angle phase maps, to define V1, V2, V3, and V4. These ROIs were then restricted using the eccentricity information from the travelling wave analysis to create ROIs that spanned the radius of the actual stimuli (i.e. 3-10 degrees of visual angle).

## 3.4   Results
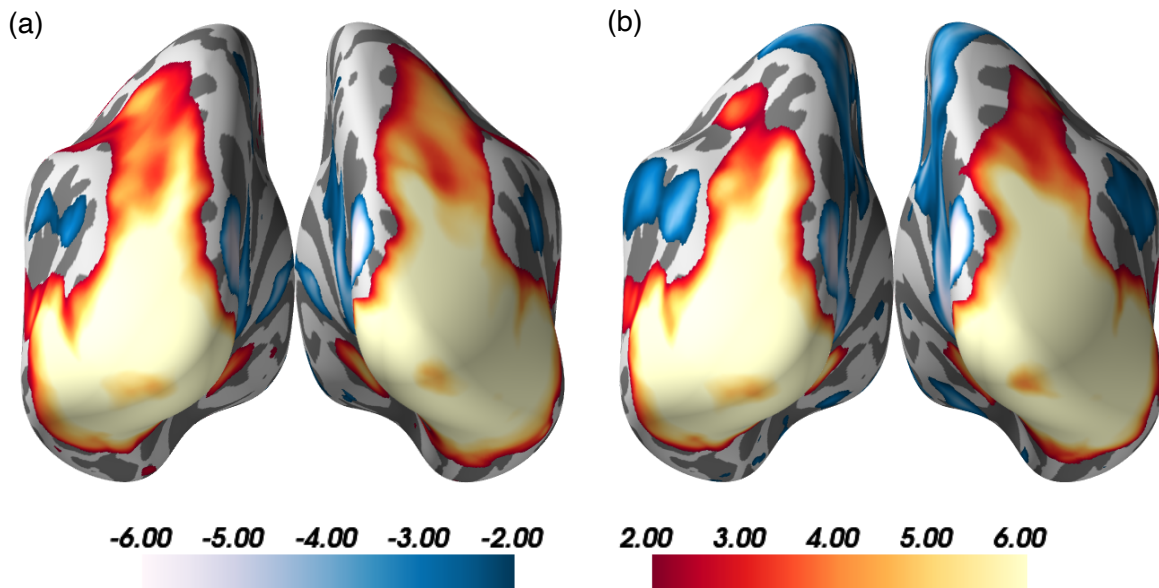


Figure 3.3: Surface average activation across 36 participants when responding to monocular and binocular stimuli. Panel (a) shows the results for the on > off contrast for flickering luminance discs. Panel (b) shows the results for the on > off contrast for flickering gratings.

The results from the FSL analysis were plotted on inflated brain surfaces. Figure 3.3a shows the results for the on > off contrast for luminance flickering discs. Figure 3.3b shows the results for the on > off contrast for flickering gratings. During stimulus presentation periods, for both discs and gratings, there is higher activation in the visual areas compared to the periods where no stimulus was present.

Figure 3.4 shows the results for the binocular > monocular contrast for flickering discs and Figure 3.5 shows the results for the binocular > monocular contrast for flickering gratings.

Figure 3.4 shows a significant higher activation in the visual cortex to binocularly presented luminance discs than to monocularly presented luminance discs.
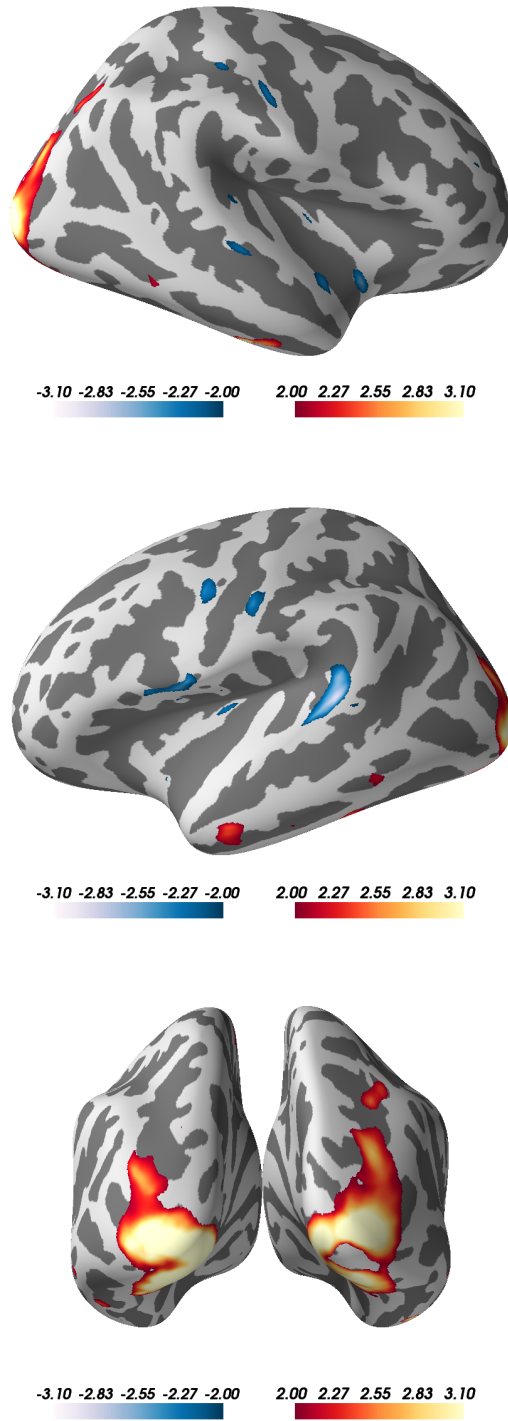
Figure 3.4: Surface average activation across 36 participants when responding to flickering luminance discs presented monocularly and binocularly. In the visual cortex, binocular stimulation elicits a bigger response than monocular stimulation.
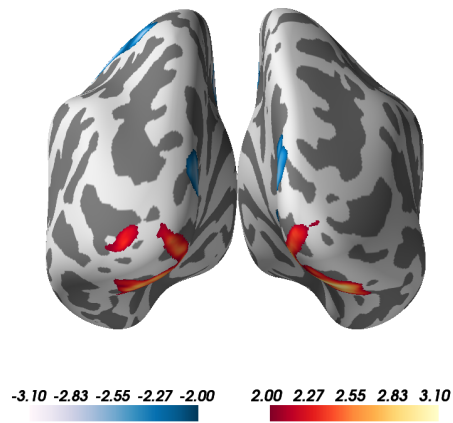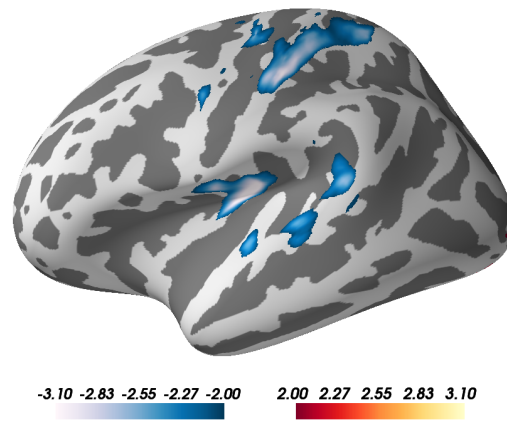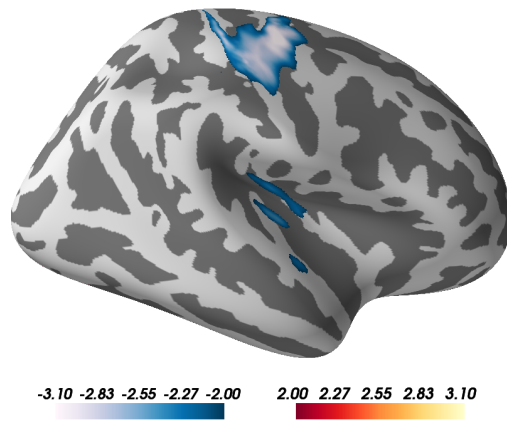
Figure 3.5: Surface average activation across 36 participants when responding to flickering gratings presented monocularly and binocularly. In the visual cortex, monocular and binocular stimulations elicit a similar response.

On the other hand, figure 3.5 shows a similar activation in the visual cortex to binocularly presented

gratings and to monocularly presented gratings. Additionally, we observe some negative activation in the parietal cortex. This is probably due to a physiological response, where the increased blood flow towards the visual areas resulted in decreased blood flow in the adjacent regions.
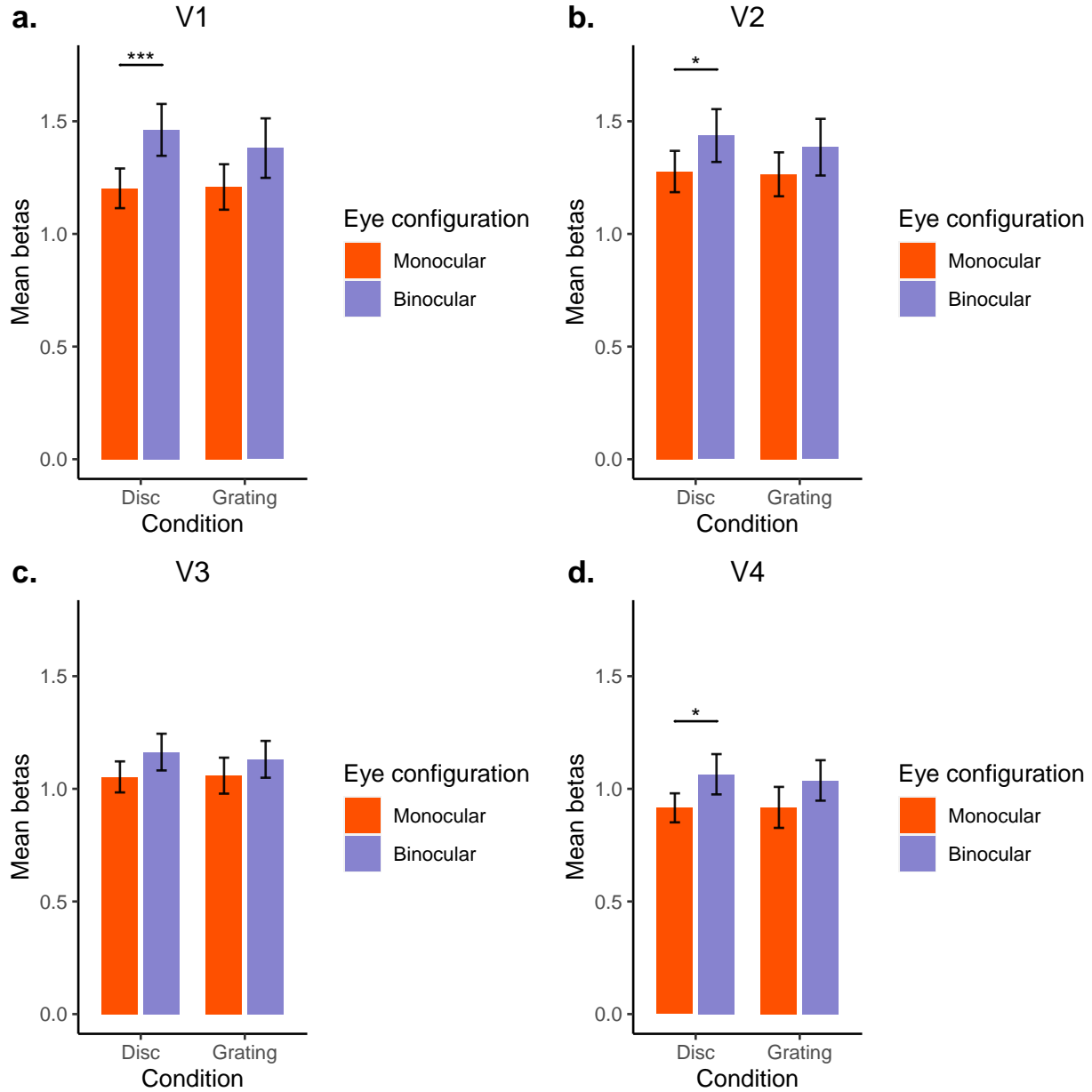


Figure 3.6: Mean betas (N = 36) for flickering luminance discs and flickering gratings presented monocularly and binocularly measured in V1 to V4. In V1, V2 and V4, response to binocular flickering luminance discs is significantly bigger than response to monocular flickering luminance discs. The difference is not significant for the flickering gratings in V1, V2, V3 and V4 and for the flickering luminance discs in V3. Error bars indicate the standard error of the mean.

Using a general linear model in mrVista, the beta weights were extracted for both conditions and both

ocular configurations. The beta weights averaged across the 36 participants for both conditions are shown in Figure 3.6. Four two-way repeated measures ANOVAs were run in R to check whether there was a significant effect of stimulus presentation (one- or two-eye presentation), of stimulus type (disc or grating) and whether there was a significant interaction between the two within each visual areas. There was a significant effect of stimulus presentation (for V1 $F(1,35) = 13.04$, $p < 0.001$; for V2 ($F(1,35) = 7.73$, $p < 0.001$; for V3 ($F(1,35) = 7.12$, $p < 0.001$; for V4 ($F(1,35) = 7.4$, $p < 0.001$). However, there was no significant effect of stimulus type (for V1 $F(1,35) = 0.64$, $p = 0.43$; for V2 $F(1,35) = 0.71$, $p = 0.41$; for V3 $F(1,35) = 0.23$, $p = 0.64$; for V4 $F(1,35) = 0.14$, $p = 0.71$), nor there was a significant interaction (for V1 $F(1,35) = 1.29$, $p = 0.26$; for V2 $F(1,35) = 0.22$, $p = 0.64$; for V3 $F(1,35) = 0.25$, $p = 0.62$; for V4 $F(1,35) = 0.17$, $p = 0.69$). Bonferroni-corrected pairwise t tests were run in R between each monocular and binocular condition pair within each ROI (e.g. flickering monocular luminance disc and flickering binocular luminance disc in V1).
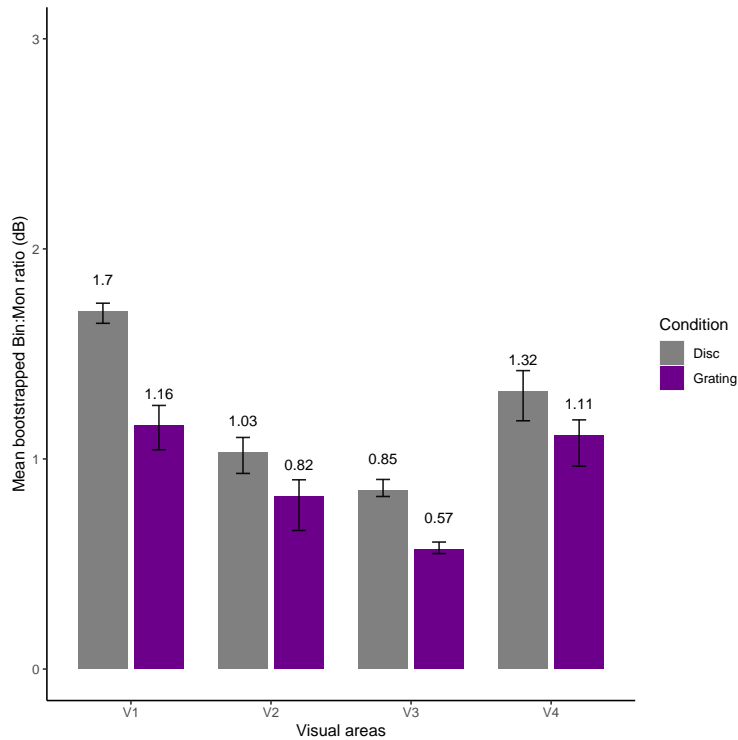


Figure 3.7: Logarithmic binocular to monocular ratios for the disc and grating conditions in the four visual areas. 0 represents the value for equal monocular and binocular responses. Error bars indicate the standard error of the mean.

Figure 3.6a shows the mean betas in V1. The flickering disc condition elicits a significantly larger response during binocular presentation compared to monocular presentation ($t(35) = 4.09$, $p = 0.001$). On the other hand, while the flickering grating condition also elicits a bigger response during binocular presentation compared to monocular presentation, the difference is not significant ($t(35) = 2.21$, $p = 0.2$).

71

Figure 3.6b shows the mean betas in V2. Here too, the flickering disc condition elicits a significantly larger response during binocular presentation compared to monocular presentation ($t(35) = 3.11$, $p = 0.022$), while the response elicited by binocular flickering gratings compared to monocular flickering gratings is not significantly different ($t(35) = 1.56$, $p = 0.762$).
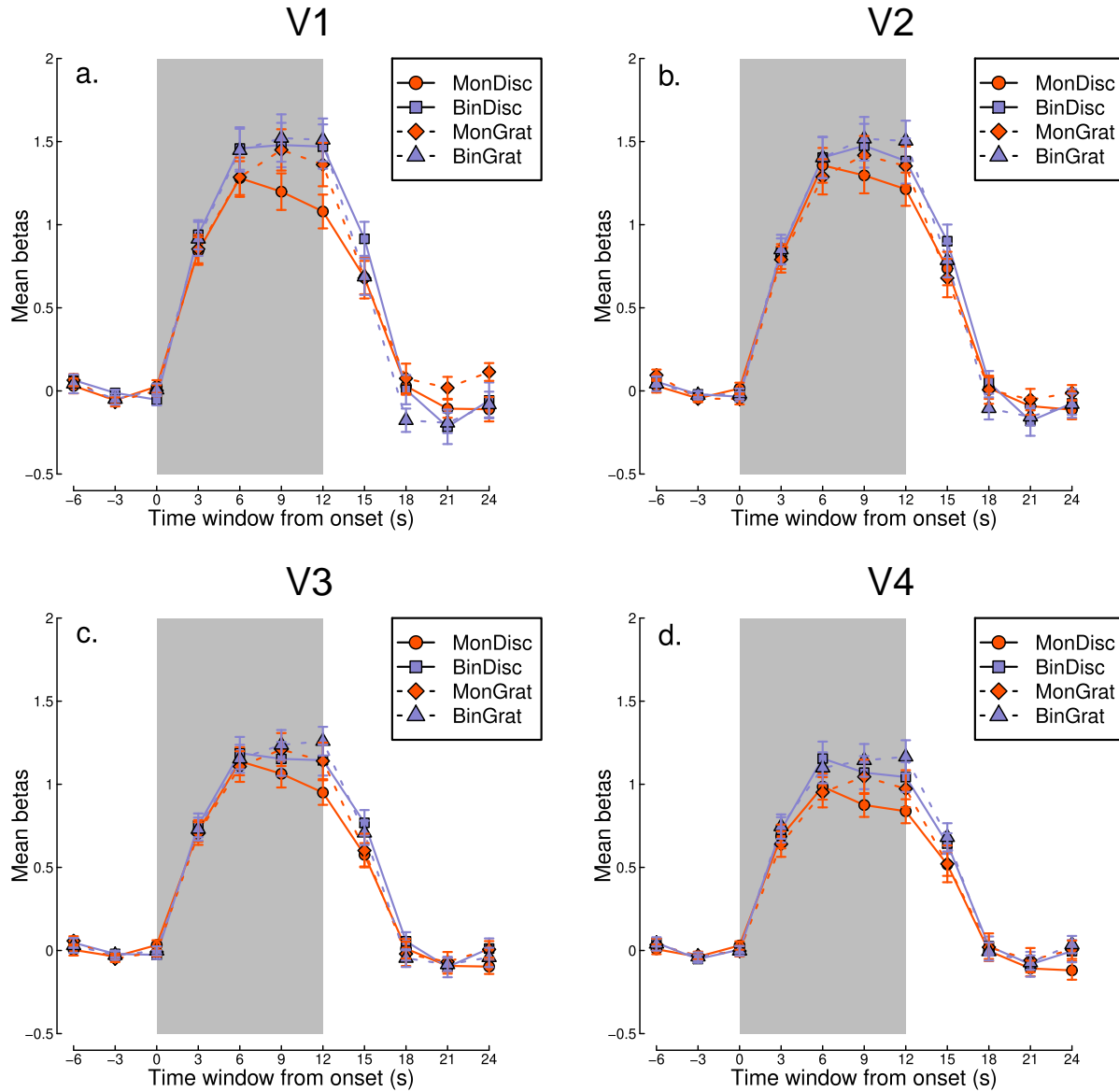


Figure 3.8: Timecourses of the mean betas in the four visual areas. Panel (a) shows the timecourse in V1. Panel (b) shows the timecourse in V2. Panel (c) shows the timecourse in V3. Panel (d) shows the timecourse in V4. The grey shaded area shows the period when the participants saw the stimuli on the screen. Error bars indicate the standard error of the mean.

Figure 3.6c shows the mean betas in V3. Both conditions elicit bigger binocular responses than monoc-

ular responses. However, both the flickering luminance disc condition ($t(35) = 2.54$, $p = 0.094$) and the flickering grating condition ($t(35) = 1.26$, $p = 1$) are not significant.

Finally, figure 3.6d shows the mean betas in V4. Similar to what was observed in V1 and V2, the flickering luminance disc condition elicits a significantly larger response during binocular presentation compared to monocular presentation ($t(35) = 2.97$, $p = 0.032$). The flickering grating condition also elicits a bigger response during binocular presentation compared to monocular presentation. However, the difference is not significant ($t(35) = 1.7$, $p = 0.586$).

We computed the binocular to monocular ratios of the mean betas presented in figure 3.6 for both conditions in each visual area. We used a bootstrapping procedure with 1000 iterations to obtain the means of the binocular and monocular conditions and calculated the ratios from these values. The ratios are shown in figure 3.7 in logarithmic form. In V1 to V4, we observe that the binocular to monocular ratio of the flickering discs is bigger than the ratio of the flickering gratings. In V2-V4, the difference in ratios between the two conditions is smaller compared to V1. Additionally, the ratios of both conditions decrease from V1 to V3 and then increase again in V4, although, for the flickering disc condition, it remains smaller than the ratio obtained in V1.

Finally, we plotted the timecourses of the mean betas in figure 3.8, with figures 3.8a-d showing the timecourses for V1 to V4 respectively over a period of 30 seconds. In all four visual areas, there is no activation in the period preceding the presentation of the stimuli (-6-0s). Once the stimuli appear on screen, the activation increases, with a steep increase in the first 6 seconds (0-6s) of stimulus presentation for both ocular configurations in both conditions. During the last 6 seconds of stimulus presentation (6-12s), the activation plateaus for the monocular and binocular gratings and the binocular luminance discs. For the monocular luminance discs, we observe a small decrease of the activation. After the stimuli disappear from the screen, we observe a steep decrease of the activation in the first 6 seconds (12-18s) for both ocular configurations in both conditions. Finally, in the last 6 seconds (18-24s), the activation levels stabilise to the same levels as the pre-stimulus period for all conditions.

## 3.5   Discussion

Using fMRI, we compared monocular and binocular responses to luminance flickering discs and flickering gratings in V1, V2, V3 and V4. As expected, for flickering gratings, we found bigger responses during binocular presentation compared to monocular presentation but this difference was shown to be not significant in all four visual cortices, indicating non-linear combination and interocular suppression for spatial pattern

vision. This could suggest that normalisation may happen later for these stimuli, in extrastriate visual areas. For the flickering luminance discs, we found that responses to binocular stimuli were bigger than to monocular stimuli in all four visual cortices, with the difference being significant in V1, V2 and V4 but not in V3. However, contrary to what we had predicted, the results for the flickering luminance discs seem to suggest that the binocular combination of spatially-uniform temporal luminance modulations seems to happen in a non-linear manner, with evidence of interocular suppression, as indicated by the low binocular to monocular ratios.

The results for the flickering gratings were expected and consistent with previous research studying binocular combination of spatial patterns (Baker and Wade, 2017; Lygo et al., 2021; Moradi and Heeger, 2009). The weak binocular facilitation and strong interocular suppression observed are in line with the idea of ocularity invariance, where monocular and binocular responses are equalised. On the other hand, the results for the flickering discs of luminance were surprising. In our previous experiment (Segala et al., 2023b), we observed strong binocular facilitation to spatially-uniform temporal luminance modulations, especially at high contrasts. Here, on the contrary, our results seem to suggest that summation for this stimulus is weak. Where might this difference come from?

Our current experiment was different in two aspects: the way the stimuli were designed and the method of data collection. In our previous study (Segala et al., 2023b), we presented our stimuli on a black background, while, here, we presented our stimuli on a grey background. The difference in luminance between the background and the stimuli was therefore bigger in our previous experiment compared to our current one, which could possibly result in a bigger response observed. Additionally, in the current experiment, the luminance stimuli were designed as annular discs where the central 6 degrees diameter was set to the background mean luminance, meaning that there was no foveal stimulation during the presentation, while, in the EEG experiment, the stimuli were a full disc stimulating the fovea. This difference in presentation might also explain the difference in binocular summation observed. Indeed, if we look at the EEG results when the fovea is not stimulated (see Figure A1.2), we can observe that the summation is similar to what was observed in the current fMRI experiment (see Figure A1.3). The other aspect that differed was that, here, we used fMRI, while previously we used EEG. These two techniques record two different types of signals that work in different ways: the latter measures electrical activity using electrodes on the surface of the scalp and has high temporal resolution, making it able to record fast changing stimuli; the former measures brain activity by detecting the magnetic properties associated with blood flow and blood oxygenation (Buxton, 2013; Ogawa et al., 1990), giving it an excellent spatial resolution but a limited temporal resolution due to the slow haemodynamic response (Glover, 2011; Kim et al., 1997). These differences could explain why the

summation that we observe here is less than the strong facilitation that we observed previously (Segala et al., 2023b): from our timecourses, we observe that halfway through the stimulus presentation period, the activation plateaus, suggesting that maybe the haemodynamic response is saturating. Therefore, this would not allow us to record higher responses and would explain why we did not observe facilitation. Another possibility for why we observed this difference in summation could be the neurons that drive the responses for EEG and fMRI. EEG responses are mainly derived from the pyramidal cells (Bruyns-Haylett et al., 2017), which are excitatory neurons. On the other hand, MRI responses are driven by the entire neuronal population, including excitatory and inhibitory neurons. This could suggest that the reduced summation observed in our fMRI experiment could also be due to a partial inhibition caused by neurons that were not recorded when using EEG.

Finally, we looked at the differences in summation between V1, V2, V3 and V4. From our results, V1 seem to show stronger summation for flickering luminance discs than the other three visual areas. While, again, this summation is not as strong as the facilitation we described in our previous study (Segala et al., 2023b), it seems to agree with our idea that the cells found within the blob regions in V1 (Livingstone and Hubel, 1984; Tychsen et al., 2004) might be the ones that are primarily being stimulated by a luminance flicker and why summation might be stronger in V1.

## 3.6   Conclusions

Using fMRI, we have demonstrated that there is stronger summation of spatially-uniform temporal luminance modulations in V1 compared to V2, V3 and V4, although this summation is less strong than the facilitation observed using EEG. We have also demonstrated that, for spatial pattern vision, monocular and binocular stimuli are equalised and this equalisation is maintained from V1 to V4.

# 4 Chapter 4: Binocular combination in the Autonomic Nervous System

## 4.1 Abstract

The size of the pupils changes in response to levels of ambient light and is regulated by the autonomic nervous system. The role of the retinal photoreceptors in determining pupil size has been investigated using silent substitution. They have been shown to be directly involved in controlling and maintaining the size of the pupils, with the cones and rods driving the initial constriction and the intrinsically photosensitive retinal ganglion cells maintaining the size over prolonged time periods. Here, we used silent substitution and pupillometry to investigate binocular combination while targeting the intrinsically-photoreceptive retinal ganglion cells, the L-M pathway and the S-(L+M) pathway. We found that the signals between the two pupils are combined in a non-linear manner when targeting all the different photoreceptor classes and that the non-linear combination was different between each class, as reflected by the different magnitudes of interocular suppression measured for each pathway.

## 4.2 Introduction

The autonomic nervous system regulates many involuntary bodily processes, including the constriction and dilation of the pupils in response to light (McDougal and Gamlin, 2015). The anatomical pathway from the retina to the subcortical nuclei controlling the pupillary light response (PLR) is well established: it includes the Pretectal Olivary nucleus (PON), the Superior Cervical ganglion and the Edinger-Westphal nucleus, which project to the iris sphincter muscles that directly control the pupil size (McDougal and Gamlin, 2015, 2008; Wang and Munoz, 2015). Additionally, the retinal photoreceptors (cones, rods and the recently discovered melanopsin-containing intrinsically photosensitive retinal ganglion cells, ipRGCs) have been shown to be directly involved in controlling and maintaining the size of the pupils (Barrionuevo et al., 2018, 2014; Dacey et al., 2005; Murray et al., 2018; Spitschan, 2019; Spitschan et al., 2014; Woelders et al., 2018). The cones have been shown to drive the initial rapid constriction of the pupils (Mathôt, 2018), while the slower and longer activation of the ipRGCs shows their role in maintaining the constriction over a prolonged period of time and in regulating the post-illumination pupillary response (Markwell et al., 2010; McDougal and Gamlin, 2010).

The ipRGCs are a unique photoreceptor class that has been discovered recently (Provencio et al., 2000). They express the photopigment melanopsin, which is involved in the regulation of the circadian

rhythm (Panda et al., 2002; Provencio et al., 2000; Ruby et al., 2002), and form a major input to the PON (Dacey et al., 2003). The first direct evidence of the involvement of the ipRGCs in the PLR was shown in rats by Lucas et al. (2003) who genetically deleted the melanopsin gene from rats, resulting in the loss of the intrinsic photosensitivity of the cells and a reduced pupil constriction. This same behaviour was later also observed in primates and humans (Gamlin et al., 2007), where it was demonstrated that the PLR continues during light presentation even when cone and rod signalling is blocked. This also demonstrates the primary role of the ipRGCs in maintaining pupil constriction over a prolonged time. It has also been shown that the ipRGCs receive inputs from the other photoreceptors (cones and rods) and are activated by them (Dacey et al., 2005).

To investigate how specific photoreceptor classes control the size of the pupils, a technique known as silent substitution is used. Silent substitution exploits the fact that each photoreceptor class has a distinct spectral tuning that overlaps with the others. Using a multiprimary system, in which the primaries have different spectra, it is possible to target one class of photoreceptors while maintaining the others at a constant activity level, effectively silencing them (Shapiro et al., 1996; Spitschan and Woelders, 2018, this paper also offers a clear explanation of how to implement silent substitution). Studies using silent substitution have shown that the pupils behave differently depending on which photoreceptor or pathway is being stimulated. For example, pupil responses have been shown to be out of phase when the S cones are stimulated, relative to when the ipRGCs or the L+M cones are stimulated (Cao et al., 2015; Spitschan et al., 2014). Additionally, when L and M cones are stimulated individually, there appears to be a paradoxical pupil response: increments in L cone stimulation cause a constriction of the pupil, while increments in M cone stimulation lead to a dilation of the pupil (Murray et al., 2018; Woelders et al., 2018).

Interaction between the two eyes and the rules of binocular combination have been extensively studied. For pattern vision in the visual cortex, at low contrast, binocular summation occurs (binocular presentation confers higher sensitivity than monocular presentation, Baker et al., 2018; Campbell and Green, 1965; Legge, 1984), while, at high contrast, ocularity invariance is implemented (the response to monocularly- and binocularly-presented patterns is equalised, Baker et al., 2007; Ding and Sperling, 2006; Meese et al., 2006). Additionally, evidence of a binocular component to the PLR is shown by the existence of a consensual response of the pupil (the stimulation of one eye will cause constriction of the other eye, Wyatt and Musselman, 1981) and we have also recently investigated the rules of binocular combination between the pupils (Segala et al., 2023b), finding that combination happens non-linearly with evidence of interocular suppression. In our previous study, we have also observed the presence of a pupil response at the second harmonic when stimulating the periphery of the retina (as demonstrated by the average Fourier spectrum shown in Figure

A1.1b), which was not present during foveal presentation (see the average Fourier spectrum shown in Figure 2.1b). In steady-state literature, this second harmonic response has been linked to the presence of non-linearities (Norcia et al., 2015; Regan and Regan, 1988) and investigating the second harmonics might give additional information about the nature of these non-linearities (e.g. squaring, exponentiation, rectification).

Most of the studies that use silent substitution and that investigate the PLR stimulate only one eye. If the stimulated eye is pharmacologically dilated to control pupil size, the response from the unstimulated eye (known as the consensual response) can be recorded (e.g. McDougal and Gamlin, 2010; Spitschan et al., 2014). While this approach controls the total amount of light incident at the retina, it does not permit investigation of binocular combination for specific photoreceptor pathways. Seeing that it is possible to directly investigate binocular combination of signals between the pupils, we decided to investigate this by designing an experiment that allowed us to binocularly target the ipRGCs, the L-M pathway and the S-(L+M) pathway individually while recording binocular pupillometric measures. We decided to investigate the L-M pathway rather than the L and M cones separately as this allows us to investigate directly the post retinal pathway. Additionally, investigating L and M cones would be equivalent to look at the luminance pathway, which would be redundant as we are already running a separate experiment to investigate the pupil response to peripheral stimulation by luminance flicker. We chose a primary flicker frequency of 0.5 Hz, which has been shown to elicit pupil responses from all three pathways (Spitschan et al., 2014). Based on previous results, we expect to observe non-linear binocular combination with evidence of interocular suppression, where different magnitudes of interocular suppression should be observed depending on the pathway that is being stimulated. The final results are interpreted using a hierarchical Bayesian computational model of binocular vision.

## 4.3 Methods

### 4.3.1 Participants

Twelve participants were recruited for each of the four experiments for a total of forty-eight (27 females) adult participants, whose age ranged from 18 to 41. All participants had normal or corrected to normal binocular vision and normal colour vision, and gave written informed consent. Our procedures were approved by the Ethics Committee of the Department of Psychology at the University of York (identification number 184).

### 4.3.2 Apparatus & stimuli
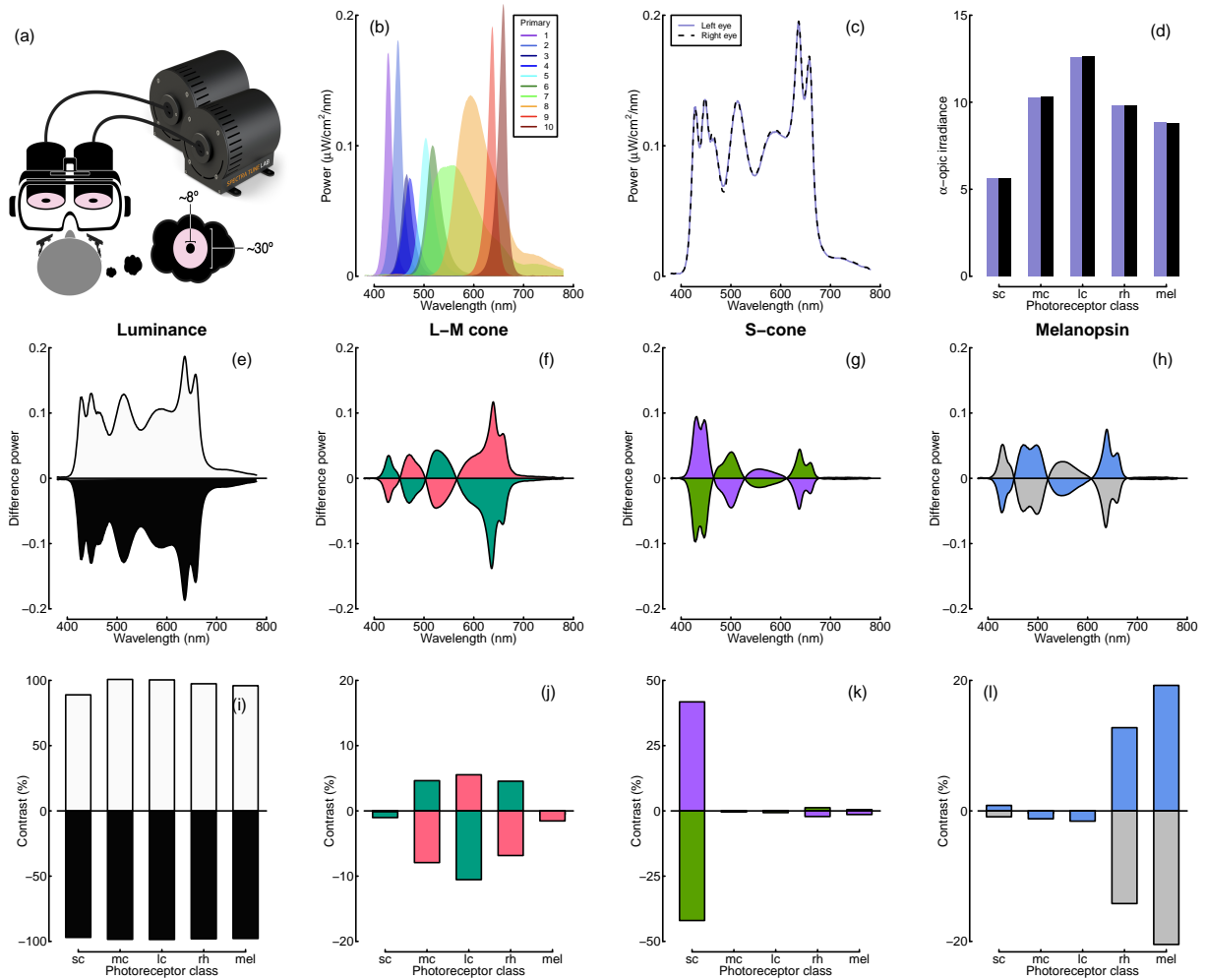


Figure 4.1: Summary of the spectral power distributions and alpha-opic irradiances for the background and each experiment. Panel (a) shows a schematic of the binocular stimulation system for presenting spectrally tuned modulations independently to each eye. The VR headset was attached to a clamp stand that the experimenters could use to adjust the height and align the headset with the eyes of the participant. The participant's head was supported by a chin rest to keep it in position throughout the experiment. Panel (b) shows the outputs of each LED primary at maximum intensity, and panels (c) and (d) show the overall spectral power distributions and the alpha-opic irradiances of the background spectra used for both eyes. The subsequent rows show the power differences (e-h), and photoreceptor contrasts (i-l) relative to the background. Column headings indicate the pathway stimulated.

To present synchronised silent substitution contrast modulations independently to each eye, two light engines, each with 10 independently addressable LED colour channels (SpectraTuneLAB: LEDMOTIVE Technologies, LLC, Barcelona, Spain), were integrated into a customised viewing system. The light engines were operated via a Python interface to their REST API (Martin et al., 2022), which supports synchronous launch and playback of spectral sequences prepared in advance and stored in JSON format. When preparing

the spectral sequences, the age of participants was recorded to account for the yellowing of the lenses. We calculated silent substitution solutions using the *PySilSub* toolbox (Martin et al., 2023), using linear algebra. The outputs of the two light engines (see Figures 4.1b,c) were calibrated using an Ocean Optics Jaz spectroradiometer, which was wavelength-calibrated to an Argon lamp and intensity calibrated using a NIST-traceable light source. We used the Stockman and Sharpe (2000) 10-degree cone fundamentals, and estimates of melanopsin absorbance spectra from CIE S 026 (discussed in Martin et al., 2023) to calculate $\alpha$-opic irradiance.

The output from the light engines was directed through liquid light guides (LLG3-8H: Thorlabs Ltd, Cambridgeshire, UK) and diffused onto semi-opaque and highly diffusive white glass discs with a diameter of 50 mm for even illumination (34-473: Edmund Optics, York, UK). The light guide gaskets were butt-coupled to the light engine diffusers with threaded adapters (SM1A9, AD3LLG: Thorlabs Ltd, Cambridgeshire, UK) and the exiting ends of the light guides were mated with 51 mm depth optical cylinders (SM2L20: Thorlabs Ltd, Cambridgeshire, UK) via appropriately threaded adapters (AD3LLG, SM2A6: Thorlabs Ltd, Cambridgeshire, UK). The stimulus diffuser discs were retained at the front end of the optical cylinders approximately 51 mm from the light source, at which distance the output beam was sufficiently dispersed to afford even illumination of the diffuser when viewed from the front. To guarantee safe illumination levels, a circular neutral-density filter with the same diameter of the white glass discs (50 mm) and an optical density of 0.6 log units was placed in the optical path between the light source and the diffusers. A small circular piece of blackout material with a diameter of approximately 8 degrees (10 mm) was positioned centrally on the front of each diffuser disc to aid as a fusion lock, as a fixation point and to occlude the fovea.

The diffuser discs were positioned in the objective planes of the lenses of a modified VR headset (SHINECON SC-G01, Dongguan Shinecon Industrial Co. Ltd), which was used by the participants to view the stimuli. The stimuli were two discs of flickering light with a diameter of approximately 30 degrees, which were fused together into a cyclopean percept resembling a donut-shaped ring of light, similar to that used in other studies (e.g., Barrionuevo and Cao, 2016; Murray et al., 2018; Spitschan et al., 2014; Zele et al., 2018). The VR headset modifications allowed for small adjustments to account for individual differences in interpupillary distance and focal length. The use of this set up allowed us to modulate the stimuli in three different ocular configurations, similar to the ones we used in our previous experiment (Segala et al., 2023b): monocular, binocular and dichoptic. In the monocular configuration, the unstimulated eye still saw a non-flickering disc of mean luminance. A schematic of the stimulation system is shown in Figure 4.1a. Pupillometry data were collected using a binocular Pupil Core eye-tracker headset (Pupil Labs GmbH, Berlin, Germany, Kassner et al., 2014) running at 120 Hz, and the signals were recorded with the Pupil

Capture software.

### 4.3.3  Procedure

Before the start of each experiment, participants adjusted the objective planes of the lenses with the help of the experimenter until the stimulus was in focus and they perceived the two pieces of blackout material as one fused piece.

We initially planned to examine pupil responses and EEG responses simultaneously to temporal modulations flickering at 2 Hz and 1.6 Hz while stimulating the periphery of the retina. While the experiment produced clear responses when presenting an achromatic light (see Figures A1.1 and A1.2 in Appendix 1), the responses were very noisy for the targeted photoreceptor class experiments (see Figures A2.1-A2.8 in Appendix 2) for both the pupillometry and the EEG data. Therefore, we decided to lower the main frequency to achieve clear responses from all photoreceptor classes.

In their article, Spitschan et al. (2014) investigated the amplitude of the pupil response (expressed in percent change units) at different frequencies (0.01, 0.05, 0.1 and 0.5 Hz). For S cones, the amplitude of the response remained approximately constant (~2% change) across all these frequencies. However, for the ipRGCs pathway, they showed that the amplitude of the response decreased from approximately 7% change at 0.01 Hz, to approximately 5% change at 0.05 Hz, and to approximately 2% change at 0.1 and 0.5 Hz. In other words, choosing a frequency of 0.5 Hz would limit the amplitude of the pupil response, making it almost 3 times smaller than a response caused by a modulation at 0.01 Hz. While choosing the new frequency, we also took into the account the length of a trial. In our original experiment, run at 2 Hz, each 12-second trial included a total of 24 full cycles. At 0.5 Hz, the same trial length would include 6 full cycles, while, at the lowest frequency of 0.01 Hz, one trial would need to be 100s long to include a full flickering cycle. Because we wanted to use different eye configurations (monocular, binocular and dichoptic) and present the stimuli at different contrast levels (6, 12, 24, 48 and 96%), choosing a frequency of 0.01 or 0.05 Hz would have made the experiment unbearably long for the participants. Additionally, at 0.1 and 0.5 Hz, the amplitude of the response is the same for S cones and the ipRGCs pathway, so choosing a frequency of 0.5 Hz would allow us to have more flickering cycles within each trial (and so more data to analyse). Therefore, while understanding that the response amplitude would be limited to 3 times smaller than the amplitude available at the lowest frequency, we decided to lower the main frequency to 0.5 Hz as it was slow enough to elicit a pupil response from all photoreceptor classes and we focussed on only recording pupillometry data as this frequency would be well below the minimum threshold to elicit EEG responses (Norcia et al., 2015).

Pupil responses to binocular temporal contrast modulations were examined in a factorial design that combined six ocular conditions, two temporal frequencies (0.4 and 0.5 Hz) and five temporal contrast levels relative to the mean illuminance (6, 12, 24, 48 and 96%). This design, similar to what we used in our previous study (Segala et al., 2023b), was applied in four separate experiments, each with a different mode of photoreceptor stimulation. In the first three conditions, the discs flickered at 0.5 Hz, in either a monocular, binocular or dichoptic arrangement. In the dichoptic condition the non-target eye saw a flickering fixed contrast of 48%. In the remaining three conditions (the cross-frequency conditions) one eye's disc flickered at 0.4 Hz, and the other eye's disc flickered at 0.5 Hz. We also tested monocular responses at 0.4 Hz, as well as binocular (one eye sees each frequency at the target contrast) and dichoptic (target stimulus flickering at 0.5 Hz, mask contrast of 48% at 0.4 Hz in the other eye) arrangements. We counterbalanced presentation of the target stimulus across the left and right eyes.

For all experiments, sinusoidal contrast modulations were presented against the same background spectrum (matched between the eyes), which was used to achieve silent substitution in the three photoreceptor modulation experiments using the method described by Spitschan and Woelders (2018). Participants adapted to the background spectrum, which had a known spectral power distribution (see Figure 4.1c), and were then presented the stimuli that modulated around this spectrum. Based on which pathway we were stimulating, the light was increased near the peak of the photoreceptor pathway that was being targeted and decreased near the peak spectral sensitivity of the other photoreceptor pathways. The increases and decreases were done relative to the background spectrum. The background spectrum was defined by setting all channels to half maximum output for the brighter of the two devices (STLab 1, left eye) and then using the STLab 1/STLab 2 calibration ratio to find the equivalent settings for the companion device (STLab 2, right eye). The background spectrum illuminance was approximately 74 lux or 68.5 cd/m$^2$. The spectral power distributions and alpha-opic irradiances of the background spectra for both eyes are shown in Figures 4.1c,d.

### 4.3.3.1 Experiment 5: luminance

The experiment was conducted in a windowless room, in which the only source of light was the modified VR headset. The participants sat as close as possible to the VR headset, leaving enough space for the eye-tracker to record the eyes. The experiment was carried out in a single session of 45 minutes, divided into three blocks of 15 minutes each. In each block, there were a total of 60 trials lasting 15 seconds each (12s of stimulus presentation, followed by 3s of interstimulus interval). The participants were given no task other than look at the black fixation dot while trying to minimise their blinking during the presentation period.
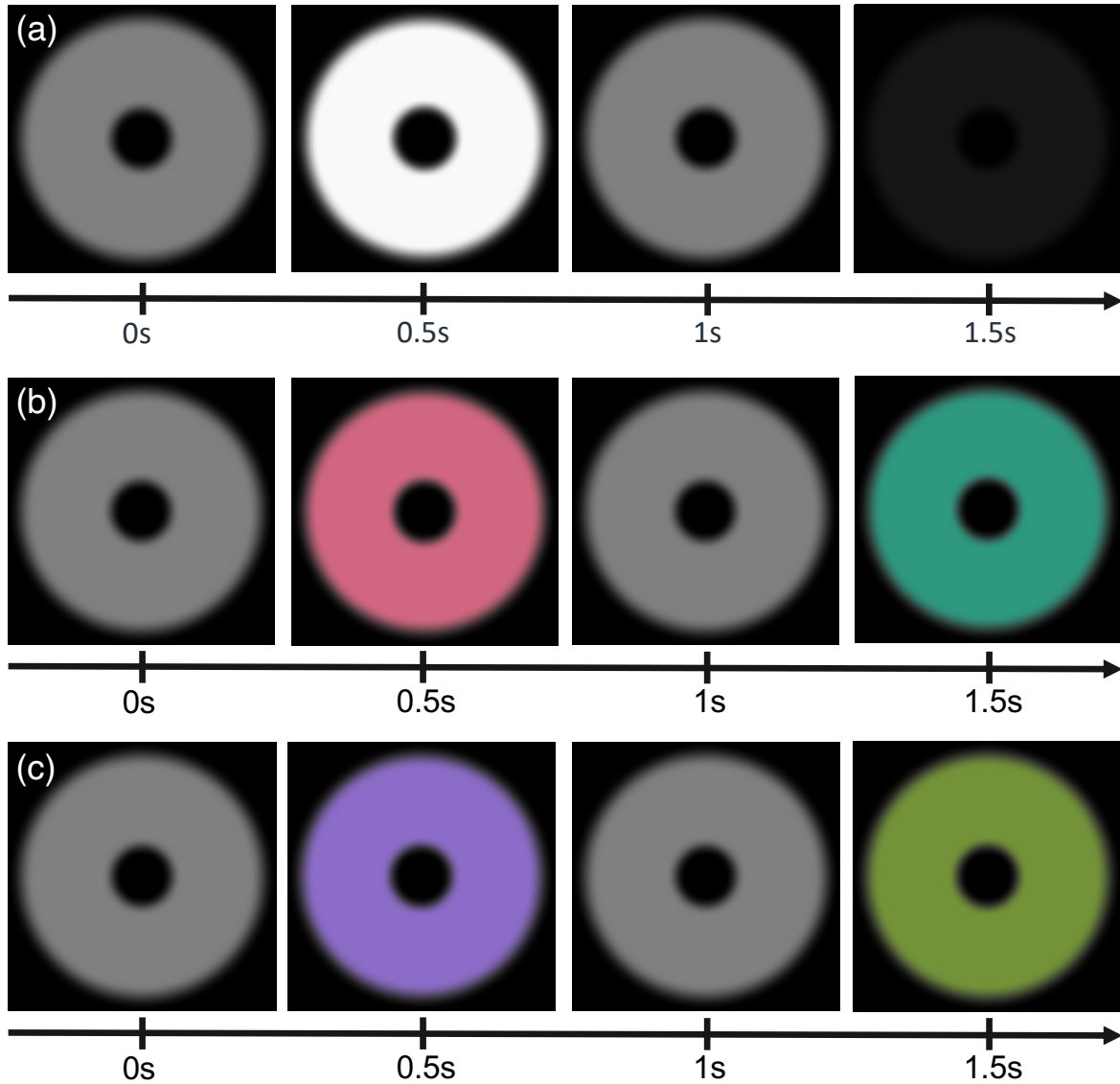
Figure 4.2: Example of the different experimental conditions. Panel (a) shows one cycle of flicker in the achromatic luminance experiment. In this experiment, the stimulus flickers between black and white. At the beginning of the cycle (0s), the stimulus appears at half the intesity and appears grey to the viewer. At 0.5s, the stimulus reaches the maximum intensity of the flicker and appears white to the viewer. At 1s, the stimulus appears again at half maximum and once again appears to be grey to the viewer. At 1.5s, the stimulus reaches the minimum intensity of the flicker and appears black to the viewer. Panel (b) shows one cycle of the flickering in the L-M pathway experiment. In this experiment, the stimulus flickers between magenta (+L-M) and cyan (-L+M). At the beginning of the cycle (0s), the stimulus appears at zero cone contrast and appears to be grey to the viewer. At 0.5s, the stimulus reaches the maximum L-cone contrast and appears magenta to the viewer. At 1s, the stimulus appears again at zero cone contrast and switches colour, once again appearing to be grey to the viewer. At 1.5s, the stimulus reaches the minimum L-cone contrast and appears cyan to the viewer. Panel (c) shows one cycle of the flickering in the S-(L+M) pathway experiment. In this experiment, the stimulus flickers between purple (+S-(L+M)) and lime (-S+(L+M)). At the beginning of the cycle (0s), the stimulus appears at zero cone contrast and appears to be grey to the viewer. At 0.5s, the stimulus reaches the maximum S-cone contrast and appears purple to the viewer. At 1s, the stimulus appears again at zero cone contrast and switches colour, once again appearing to be grey to the viewer. At 1.5s, the stimulus reaches the minimum S-cone contrast and appears lime to the viewer.

In this experiment, the participants saw a disc of achromatic flickering light (average illuminance of approximately 74 lux or 68.5 cd/m$^2$), flickering between black and white, at the different contrast levels defined earlier. An example of one cycle of flickering for the luminance experiment is shown in Figure 4.2a. The spectral power distributions and alpha-opic irradiances relative to the background for the luminance experiment are shown in Figures 4.1e,i.

### 4.3.3.2 Experiment 6: melanopsin

The experiment used the same equipment set-up and the same experimental conditions as Experiment 5. The procedure was also the same. However, at the beginning of each block, participants habituated for 2 minutes to the background that would be present throughout the entire experiment. During this adaptation period, participants were asked to fixate on the same black fixation dot positioned in the middle of the stimulus and were told that they could blink normally. At the end of the adaptation period, the experiment started immediately and the participants followed the same instructions given in Experiment 5.

In this experiment, the participants experienced contrast modulations that targeted the melanopsin-containing intrinsically photosensitive Retinal Ganglion cells, while ignoring rods and nominally silencing the cones. Michelson contrast levels represented a percentage of the maximum melanopic contrast available, which was predetermined to be approximately 22 %. Under perfect silent substitution conditions, these modulations do not entail any changes in brightness or chromaticity: it is therefore very difficult to include an example to visualise the stimulus. However, silent substitution is never perfect, so participants reported small fluctuations in reddishness, greenishness and brightness due to open-field cone contrast artefacts. These fluctuations were especially present at higher contrasts. This can be observed in the alpha-opic irradiances relative to the background for the melanopsin experiment shown in Figure 4.1h, where a small activation of the S, L and M cones is observable. The spectral power distributions relative to the background for the melanopsin experiment is also shown in Figure 4.1l.

### 4.3.3.3 Experiment 7: L-M postreceptoral 'parvocellular' pathway

The experiment used the same equipment set-up and the same experimental conditions as Experiment 5. The procedure was the same as Experiment 6, including the presence of a 2-minute adaptation period at the beginning of each block. Additionally, before the start of the experiment, participants completed a luminance nulling perceptual calibration procedure in L-M cone space on an Iiyama VisionMaster$^{\text{TM}}$ Pro 510 display (800 x 600 pixels, 60 Hz refresh rate). During the task, participants were presented with a disc flickering within the L-M cone space (between magenta and cyan). Using a trackball, participants adjusted

the angle in cone space to find their subjective isoluminant point, which resulted in changing the flickering intensity of the stimulus until the amplitude of the flicker appeared to be minimised. The result was used to modify the requested contrasts during stimulus preparation so as to account for individual differences affecting perceived illuminance, principally the L:M cone ratio (Carroll et al., 2002; Hofer et al., 2005).

In this experiment, the participants experienced contrast modulations that targeted the L-M postreceptoral 'parvocellular' pathway while ignoring rods and nominally silencing S-cones and melanopsin. Michelson contrast levels represented a percentage of the maximum L-M contrast available for the background spectrum, which was determined in advance to be approximately 10 %. As shown in Figure 4.2b, participants experienced an isoluminant chromatic modulation between magenta (+L-M) and cyan (-L+M). The spectral power distributions and alpha-opic irradiances relative to the background for the L-M pathway experiment are shown in Figures 4.1f,j.

### 4.3.3.4  Experiment 8: S-(L+M) 'koniocelluar' pathway

The experiment used the same equipment set-up and the same experimental conditions as Experiment 5. The procedure was the same as Experiment 6, including the presence of a 2-minute adaptation period at the beginning of each block.

In this experiment, the participants experienced contrast modulations that targeted the S-(L+M) 'koniocellular' pathway while ignoring rods and nominally silencing L/M cones and melanopsin. Michelson contrast levels represented a percentage of the maximum S-cone contrast available for the background spectrum, which was predetermined to be approximately 45 %. As shown in Figure 4.2c, participants experienced an isoluminant chromatic modulation between purple (+S-(L+M)) and lime (-S+(L+M)). The spectral power distributions and alpha-opic irradiances relative to the background for the S-(L+M) pathway experiment are shown in Figures 4.1g,k.

### 4.3.4  Data analysis

The pupillometry data were analysed using the same method we used in our previous study (Segala et al., 2023b). The data were converted from mp4 videos to a csv text file using the Pupil Player software (Kassner et al., 2014), which estimated pupil diameter for each eye on each frame using a 3D model of the eyeball. The individual data were then loaded into R for analysis, where a ten-second waveform for each trial in each eye was extracted (excluding the first two seconds after stimulus onset). We interpolated across any dropped or missing frames to ensure regular and continuous sampling over time. The Fourier transform

was calculated for each waveform, and all repetitions of each condition were pooled across eye and then averaged. Finally, data were averaged across all participants to obtain the group results. We used coherent averaging and at each stage we excluded data points with a Mahalanobis distance exceeding $D = 3$ from the complex-valued mean. The consensual response was also analysed (see Appendix 3 for more details and the results).

For all experiments, we used a bootstrapping procedure with 1000 iterations to estimate standard errors across participants. All analysis and figure construction was conducted using a single R-script, available online, making this study fully computationally reproducible: https://osf.io/gdvt4/.

### 4.3.5    Computational model and parameter estimation

To describe our data, we chose the same model described in our previous study (Segala et al., 2023b). The model has the same general form as the first stage of the contrast gain control model proposed by Meese et al. (2006) and omits the second stage. For the previous model that we used (Segala et al., 2023b), the exponent of the numerator had a fixed value of 2. Here, we allow this parameter (called $p$) to be free, in order to permit different shapes of contrast response function, e.g. saturating or super-saturating. The responses of the left eye and right eye channels are as follows:

$$Resp_L = \frac{L^p}{Z + L^q + wR^q},$$

(5)

$$Resp_R = \frac{R^p}{Z + R^q + wL^q},$$

(6)

where $L$ and $R$ are the contrast signals from the left and right eyes, $p$ and $q$ are exponents, $Z$ is a saturation constant that shifts the contrast-response function laterally, and $w$ is the weight of suppression from the other eye.

The responses from the two eyes are then summed binocularly:

$$Resp_B = R_{max}(Resp_L + Resp_R) + k,$$

(7)

where $k$ is a noise parameter, and $R_{max}$ scales the overall response amplitude.

We performed model fitting on the normalised amplitudes to account for amplitude differences between the experiments. Fit examples have been computed and are shown in Figures A5.1 and A5.2 in Appendix 5.

# Luminance
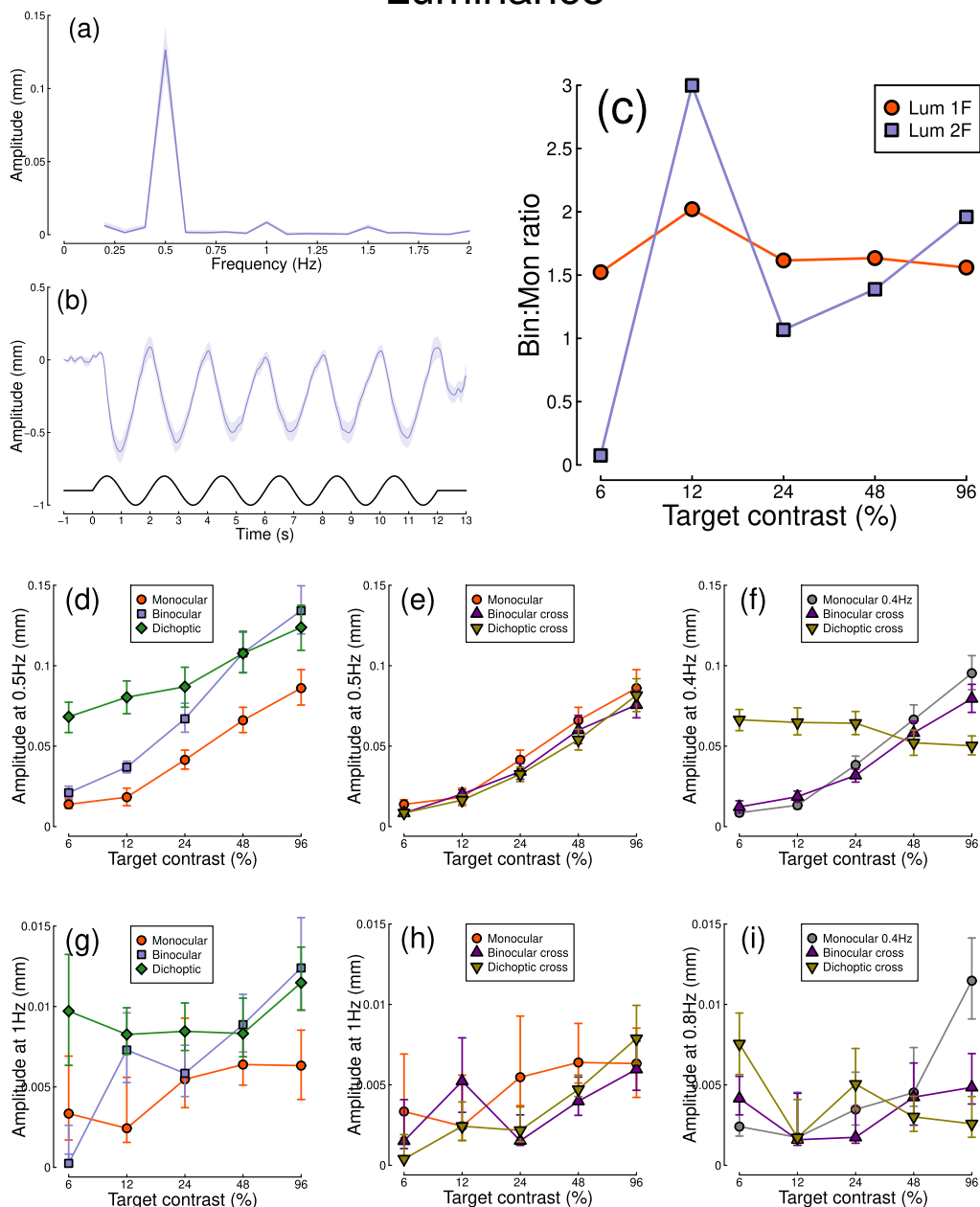


Figure 4.3: Summary of pupillometry results for the luminance experiment for N=12 participants. Panel (a) shows the average Fourier spectrum. Panel (b) shows a group average waveform for binocular presentation (low pass filtered at 5 Hz), with the driving signal plotted at the foot. Panel (c) shows the ratio of binocular to monocular response. The red circles show the ratios at the first harmonic (0.5 Hz) and the blue squares show the ratios at the second harmonic (1 Hz). Panels (d,e) show contrast response functions at 0.5 Hz for different conditions. Panel (f) shows contrast response functions at 0.4 Hz for three conditions. Panels (g-i) are in the same format but for the second harmonic responses. Shaded regions and error bars indicate bootstrapped standard errors.

## 4.4 Results

### 4.4.1 Experiment 5

The results of the luminance experiment are summarised in Figure 4.3. The average Fourier spectrum is displayed in Figure 4.3a, and shows a strong response at the first harmonic frequency (0.5 Hz) and a weaker but still clear response at the second harmonic frequency (1 Hz). These results demonstrate that we can evoke measurable steady-state pupil responses at 0.5 Hz by stimulating the periphery of the retina. The group average waveform for binocular presentation is shown in Figure 4.3b. There is a substantial pupil constriction at stimulus onset, followed by very visible oscillations at the flicker frequency (0.5 Hz, see waveform at foot).

Figure 4.3d shows contrast response functions in response to stimuli flickering only at 0.5 Hz. The amplitude of the binocular condition (blue squares) is consistently greater than that of the monocular condition (red circles) across all target contrasts. A $2 \times 5$ repeated measures $ANOVA^2_{circ}$ (Baker, 2021) comparing these conditions revealed a significant main effect of target contrast (F(8,220) = 80.82, $p < 0.001$), a significant effect of condition (F(2,220) = 52.88, $p < 0.001$), and a significant interaction (F(8,220) = 32.69, $p < 0.001$). The dichoptic condition (green diamonds) begins at a much higher amplitude, owing to binocular combination of the target and high (48%) contrast mask, and then increases with increasing target contrast (main effect of target contrast: F(8,88) = 23.07, $p < 0.001$). Similar results can be observed at the second harmonic in Figure 4.3g (see Tables A4.7 and A4.8 for summary of statistical results).

In Figure 4.3e, we plot responses to monocular target stimuli flickering at 0.5 Hz, when the other eye viewed stimuli flickering at 0.4 Hz (the red monocular-only data are replotted from Figure 4.3d for comparison). When the 0.4 Hz component had the same contrast as the target (the binocular cross condition, shown in purple) responses were suppressed slightly across all target contrasts (interaction between contrast and condition: F(8,220) = 29.51, $p < 0.001$). When the 0.4 Hz component had a fixed contrast of 48 % (the dichoptic cross condition, shown in yellow), responses were also suppressed slightly across the contrast range (interaction between contrast and condition: F(8,220) = 27.52, $p < 0.001$). The same pattern of results was generally observed at the second harmonic (Figure 4.3h, see Tables A4.9 and A4.10 for summary of statistical results).

Figure 4.3f shows responses at 0.4 Hz, for the same conditions, as well as for a condition in which a monocular stimulus flickered at 0.4 Hz (grey circles). Again there was evidence of weak suppression between the eyes, as the purple triangles fall below the grey circles (see Table A4.5 for summary of statistical results). The dichoptic cross condition also shows evidence of suppressive modulation with target contrast (see Table

A4.6 for summary of statistical results). The same pattern is also observed at the second harmonic (Figure 4.3i, see Tables A4.11 and A4.12 for summary of statistical results).

Finally, we calculated the binocular to monocular ratio at the first and second harmonic frequencies. Figure 4.3c shows that these ratios are generally below 2 at both frequencies, suggesting that there is summation happening between the eyes but also interocular suppression, therefore suggesting that the signals between the eyes are combined non-linearly. At the highest contrast at the second harmonic, the ratio is close to 2, perhaps indicating that a more linear combination is happening for higher contrasts.

### 4.4.2 Experiment 6

The results of the melanopsin experiment are summarised in Figure 4.4. The average Fourier spectrum is displayed in Figure 4.4a, and also shows clear responses at both the first harmonic frequency (0.5 Hz) and the second harmonic frequency (1 Hz) of approximately equal amplitude. These results demonstrate that we can evoke measurable steady-state pupil responses at 0.5 Hz by selectively stimulating the melanopsin-containing retinal ganglion cells whilst ignoring rods and nominally silencing all three cone classes. The group average waveform for binocular presentation is shown in Figure 4.4b and shows a substantial pupil constriction at stimulus onset, followed by visible oscillations at approximately the flicker frequency (0.5 Hz, see waveform at foot).

Figure 4.4d shows contrast response functions for melanopsin-directed stimuli flickering at 0.5 Hz. The amplitude of the binocular condition (blue squares) is similar to that of the monocular condition (red circles) across all target contrasts (all error bars overlap, see Table A4.13 for summary of statistical results). At the second harmonic the binocular response is substantially greater than the monocular response at higher contrasts where the response is above baseline (Figure 4.4g, see Table A4.19 for summary of statistical results).

In Figure 4.4e, we again plot responses to monocular target stimuli flickering at 0.5 Hz, when the other eye viewed stimuli flickering at 0.4 Hz (here too, the red monocular-only data are replotted from Figure 4.4d for comparison). For the binocular cross condition (shown in purple), responses were slightly suppressed across all target contrasts (see Table A4.15 for summary of statistical results). For the dichoptic cross condition (shown in yellow), responses were also slightly suppressed across the contrast range (see Table A4.16 for summary of statistical results). This pattern is also observed at the second harmonic (Figure 4.4h, see Tables A4.21 and A4.22 for summary of statistical results).
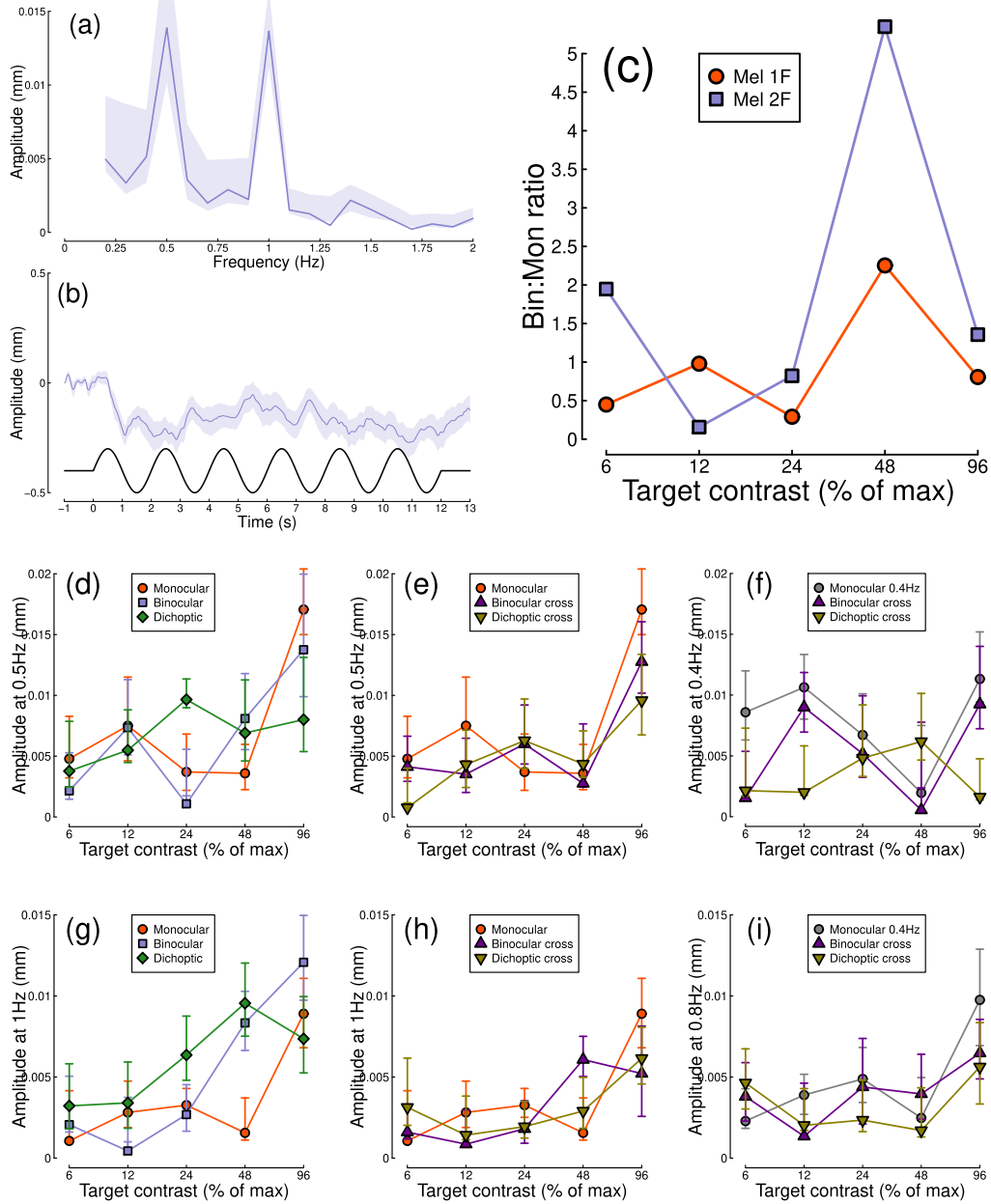
Figure 4.4: Summary of pupillometry results for the melanopsin experiment for N=12 participants. Panel (a) shows the average Fourier spectrum. Panel (b) shows a group average waveform for binocular presentation (low pass filtered at 5 Hz), with the driving signal plotted at the foot. Panel (c) shows the ratio of binocular to monocular response. The red circles show the ratios at the first harmonic (0.5 Hz) and the blue squares show the ratios at the second harmonic (1 Hz). Panels (d,e) show contrast response functions at 0.5 Hz for different conditions. Panel (f) shows contrast response functions at 0.4 Hz for three conditions. Panels (g-i) are in the same format but for the second harmonic responses. Shaded regions and error bars indicate bootstrapped standard errors.

Figure 4.5: Summary of pupillometry results for the L-M pathway experiment for N=12 participants. Panel (a) shows the average Fourier spectrum. Panel (b) shows a group average waveform for binocular presentation (low pass filtered at 5 Hz), with the driving signal plotted at the foot. Panel (c) shows the ratio of binocular to monocular response. The red circles show the ratios at the first harmonic (0.5 Hz) and the blue squares show the ratios at the second harmonic (1 Hz). Panels (d,e) show contrast response functions at 0.5 Hz for different conditions. Panel (f) shows contrast response functions at 0.4 Hz for three conditions. Panels (g-i) are in the same format but for the second harmonic responses. Shaded regions and error bars indicate bootstrapped standard errors.

Figure 4.6: Summary of pupillometry results for the S-(L+M) pathway experiment for N=12 participants. Panel (a) shows the average Fourier spectrum. Panel (b) shows a group average waveform for binocular presentation (low pass filtered at 5 Hz), with the driving signal plotted at the foot. Panel (c) shows the ratio of binocular to monocular response. The red circles show the ratios at the first harmonic (0.5 Hz) and the blue squares show the ratios at the second harmonic (1 Hz). Panels (d,e) show contrast response functions at 0.5 Hz for different conditions. Panel (f) shows contrast response functions at 0.4 Hz for three conditions. Panels (g-i) are in the same format but for the second harmonic responses. Shaded regions and error bars indicate bootstrapped standard errors.

Figure 4.4f shows responses at 0.4 Hz, for the same conditions, as well as for a condition in which a monocular stimulus flickered at 0.4 Hz (grey circles). These data are perhaps too noisy to interpret, though we note that the binocular cross data (purple triangles) are generally below the monocular data (grey circles), perhaps indicating suppression (see Table A4.17 for summary of statistical results). The same pattern is generally also observed at the second harmonic (Figure 4.4i, see Table A4.23 for summary of statistical results).

Finally, we calculated the binocular to monocular ratio at the first and second harmonic frequencies. Figure 4.4c shows that these ratios are around 1 at the first harmonic, suggesting that there is strong interocular suppression between the eyes, and binocular signal combination is therefore strongly non-linear.

### 4.4.3   Experiment 7

The results of the L-M pathway experiment are summarised in Figure 4.5. The average Fourier spectrum is displayed in Figure 4.5a, and shows clear responses at both the first harmonic frequency (0.5 Hz) and the second harmonic frequency (1 Hz) of approximately equal amplitude. These results demonstrate that we can evoke measurable steady-state pupil responses at 0.5 Hz by selectively stimulating the L-M postreceptoral 'parvocellular' pathway whilst ignoring rods and nominally silencing S-cones and melanopsin. The group average waveform for binocular presentation is shown in Figure 4.5b and, as observed in the previous experiments, there is a substantial pupil constriction at stimulus onset, followed by visible oscillations at the flicker frequency (0.5 Hz, see waveform at foot) and its second harmonic (i.e. there are two peaks in the data for every one peak in the driving waveform).

Figure 4.5d shows contrast response functions in response to stimuli flickering only at 0.5 Hz. The amplitude of the binocular condition (blue squares) is substantially smaller than that of the monocular condition (red circles) across the range of target contrasts, indicating a process of binocular suppression (see Table A4.25 for summary of statistical results). At the second harmonic, the pattern is reversed, with the binocular responses being larger than the monocular responses (Figure 4.5g, see Table A4.31 for summary of statistical results).

In Figure 4.5e, we plot responses to monocular target stimuli flickering at 0.5 Hz, when the other eye viewed stimuli flickering at 0.4 Hz (the red monocular-only data are replotted from Figure 4.5d for comparison). For the binocular cross (purple triangles) and dichoptic cross (yellow triangles) conditions, we again observed a very strong suppression of the responses across all target contrasts (see Tables A4.27 and A4.28 for summary of statistical results). This was not observed at the second harmonic (Figure 4.5h), where

monocular and binocular responses appeared to be quite similar (see Tables A4.33 and A4.34 for summary of statistical results).

Figure 4.5f shows responses at 0.4 Hz, for the same conditions, as well as for a condition in which a monocular stimulus flickered at 0.4 Hz (grey circles). Again, strong suppression can be observed across the contrast range (see Table A4.29 for summary of statistical results). The dichoptic cross condition shows a clear modulation with target contrast, as we can see by the decrease of the response as the contrast increases (see Table A4.30 for summary of statistical results). The same pattern is also observed at the second harmonic (Figure 4.5i), though the suppression in the binocular cross condition is less extreme at the second harmonic (see Tables A4.35 and A4.36 for summary of statistical results).

Finally, we calculated the binocular to monocular ratio at the first and second harmonics. Figure 4.5c shows that these ratios are generally below 1 at the first harmonic, again indicating very strong interocular suppression, and suggesting that the combination of the signals between the eyes is strongly non-linear. At the second harmonic, the ratios are generally between 1 and 2, suggesting that suppression between the eyes is weaker, but overall the combination remains non-linear.

### 4.4.4    Experiment 8

The results of the S-(L+M) pathway experiment are summarised in Figure 4.6. The average Fourier spectrum is displayed in Figure 4.6a, and shows a clear response at both the first harmonic frequency (0.5 Hz) and a stronger response (by around 50%) at the second harmonic frequency (1 Hz). These results demonstrate that we can evoke measurable steady-state pupil responses at 0.5 Hz by selectively stimulating the S-(L+M) 'koniocelluar' pathway whilst ignoring rods and nominally silencing L/M cones and melanopsin. The group average waveform for binocular presentation is shown in Figure 4.6b. There is a substantial pupil constriction at stimulus onset, followed by very visible oscillations at the flicker frequency (0.5 Hz, see waveform at foot) and its second harmonic.

Figure 4.6d shows contrast response functions in response to stimuli flickering only at 0.5 Hz. For the first 3 target contrasts, response amplitudes increased monotonically with target contrast. At the higher contrasts, we observe a roll-over of the pupil response shown by the drop in the signals. This suggests that the S cones saturate at higher contrasts, and so are not able to drive larger pupil modulations. The amplitude of the binocular condition (blue squares) is consistently greater than that of the monocular condition (red circles) across the range of target contrasts (see Table A4.37 for summary of statistical results). At the second harmonic, we observe quite different results, with the binocular and monocular conditions having the

same amplitudes across the contrast range (Figure 4.6g), and no evidence of saturation (see Table A4.43 for summary of statistical results).

In Figure 4.6e, we plot responses to monocular target stimuli flickering at 0.5 Hz, when the other eye viewed stimuli flickering at 0.4 Hz (the red monocular data are replotted from Figure 4.6d for comparison). There was very little evidence of suppression in the binocular cross (purple triangles) or dichoptic cross (yellow triangles) conditions at the first harmonic (see Tables A4.39 and A4.40 for summary of statistical results). However at the second harmonic (Figure 4.6h), strong suppression was apparent at the higher target contrasts (see Tables A4.45 and A4.46 for summary of statistical results).

Figure 4.6f shows responses at 0.4 Hz, for the same conditions, as well as for a condition in which a monocular stimulus flickered at 0.4 Hz (grey circles). At this frequency there was some evidence of suppression at the higher target contrasts (purple triangles below grey circles, see Table A4.41 for summary of statistical results). At the second harmonic (Figure 4.6i), the binocular cross condition (purple triangles) shows a very strong suppression and the dichoptic cross condition shows a clear modulation with target contrast (yellow triangles), visible as a decrease of the response as the target contrast increases (see Tables A4.47 and A4.48 for summary of statistical results).

Finally, we calculated the binocular to monocular ratio at the first and second harmonics. Figure 4.6c shows that these ratios are generally between 1 and 2 at the first harmonic, indicating summation between the eyes with intermediate levels of interocular suppression. At the second harmonic, the ratios were around 1 for the three highest target contrasts, again consistent with strong interocular suppression.

### 4.4.5   Computational modelling

We fitted a computational model to the data from Experiments 1, 2, 3 and 4 using a hierarchical Bayesian approach. The model behaviour is displayed in Figure 4.7a-d for the first harmonic frequency and in Figure 4.7f-i for the second harmonic frequency. The empirical data is superimposed for comparison. In general, the model captures the key characteristics of the empirical data, with group-level parameter estimates provided in Tables 4.1 and 4.2 for the first and second harmonic frequencies respectively. We were particularly interested in comparing the weight of interocular suppression across data sets. We therefore plot the posterior distributions for this parameter for all four data sets (see Figure 4.7e for the distributions at the first harmonic and Figure 4.7j for the distributions at the second harmonic).

At the first harmonic, the key finding is that the luminance results (grey distribution) display a much smaller weight of interocular suppression than the other data sets. The melanopsin and S-(L+M) results

(gold and blue distributions) display a similar weight of interocular suppression. The L-M results (red distribution) display the greatest weight of interocular suppression of all data sets. There is minimal overlap between the luminance distribution and the other three distributions. For the luminance, the distribution is meaningfully below a weight of 1, while it is well above a weight of 1 for the L-M results. The distributions of melanopsin and S-(L+M) are around a weight of 1. These results offer an explanation of the empirical data: the weaker suppression for the luminance experiment is consistent with the weaker suppression effects and the weaker dichoptic masking, while the stronger suppression for the L-M experiment is consistent with the stronger suppression observed at the first harmonic and the stronger dichoptic masking.
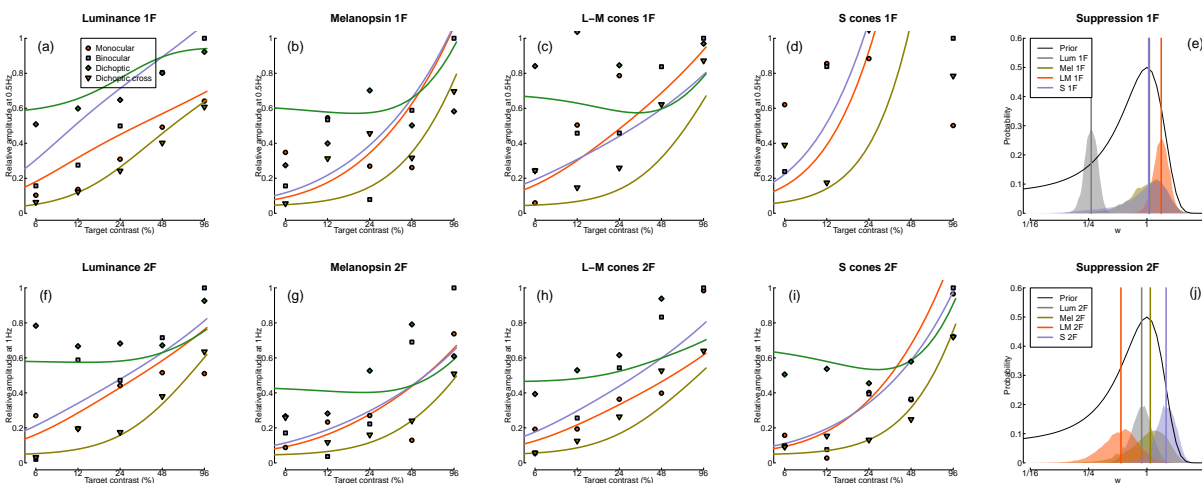


Figure 4.7: Summary of computational modelling. Panels (a-d) and (f-i) show empirical data from key conditions at the first and the second harmonic frequencies respectively. The data are replotted from earlier figures for the luminance experiment at the first (a) and the second (f) harmonic frequencies, the melanopsin experiment at the first (b) and the second (g) harmonic frequencies, the L-M pathway experiment at the first (c) and the second (h) harmonic frequencies, and the S-(L+M) pathway experiment at the first (d) and the second (i) harmonic frequencies. The curves show model behaviour generated using the median group-level parameter values. Panels (e) and (j) show the posterior probability distributions of the interocular suppression parameter for each of the four model fits at the first and the second harmonic frequencies respectively. In panel (e), the luminance distribution (grey) is centred about a substantially lower suppressive weight than for the other data types (note the logarithmic x-axis), while the L-M distribution (red) is centred about a higher suppressive weight than for the other data types. On the other hand, in panel (j), the L-M distribution is centred about a substantially lower suppressive weight than for the other data types, while it is the S-(L+M) distribution (blue) that is centred about a higher suppressive weight than for the other data types. The black curves show the (scaled) prior distribution for the weight parameter.

At the second harmonic, the key finding is that the S-(L+M) results display a greater weight of interocular suppression compared to the other data sets. On the other hand, the L-M results display the smallest weight of interocular suppression. The luminance and melanopsin results display weights of interocular suppression that are quite close to each other. For the L-M results, the distribution is meaningfully below a weight of 1, while it is well above a weight of 1 for the S-(L+M) results. The distributions of

Table 4.1: Summary of median parameter values at the first harmonic frequency.

| Experiment | Z | k | w | p | q | Rmax |
|---|---|---|---|---|---|---|
| Luminance 1F | 21.15 | 0.02 | 0.27 | 1.91 | 1.66 | 0.21373 |
| Melanopsin 1F | 20.62 | 0.04 | 1.06 | 1.90 | 1.22 | 0.05084 |
| L-M 1F | 22.14 | 0.04 | 1.40 | 1.96 | 1.55 | 0.13861 |
| S 1F | 21.53 | 0.04 | 1.04 | 1.98 | 1.16 | 0.10229 |

Table 4.2: Summary of median parameter values at the second harmonic frequency.

| Experiment | Z | k | w | p | q | Rmax |
|---|---|---|---|---|---|---|
| Luminance 2F | 21.75 | 0.04 | 0.88 | 1.98 | 1.61 | 0.13592 |
| Melanopsin 2F | 20.67 | 0.04 | 1.08 | 1.91 | 1.36 | 0.05348 |
| L-M 2F | 21.70 | 0.04 | 0.54 | 1.95 | 1.55 | 0.09385 |
| S 2F | 21.42 | 0.04 | 1.57 | 1.97 | 1.24 | 0.04321 |

luminance and melanospin are around a weight of 1, with the former being slightly below and the latter being slightly above. These results offer an explanation of the empirical data: the weaker suppression for the L-M experiment is consistent with the weaker suppression effects and the weaker dichoptic masking observed at the second harmonic, while the stronger suppression for the S-(L+M) experiment is consistent with the stronger suppression observed at the second harmonic and the stronger dichoptic masking.

### 4.4.6 Phase analysis

In a previous study, Spitschan et al. (2014) analysed the phase of the pupil response and compared it between L+M-cone stimulation, S-cone stimulation, melanopsin stimulation and brightness stimulation. In their study, they found that, at a flicker frequency of 0.5 Hz, L+M and melanopsin responses were in phase, while brightness and S-cone responses were in anti-phase. Additionally, they found that, at the second harmonic frequency, S-cone and melanospin responses seem to be in phase with each other and in anti-phase to L+M-cone responses. We reproduced this analysis with our data and the results are summarised in Figure 4.8. At the first harmonic frequency, the amplitudes from the luminance experiment have been scaled down by a factor of 10 to make it possible to compare them directly with the results from the other experiments.

Figure 4.8a shows the results to monocular responses at the first harmonic frequency. The L-M pathway stimulation produces an anti-phase pupil response relative to luminance stimulation. The S-(L+M) pathway and luminance results are desynchronised in quadrature phase. This same pattern of results is also observable in Figure 4.8b, which summarises the results to binocular responses at the first harmonic frequency.

Figure 4.8c shows the results to monocular responses at the second harmonic frequency. Here, results are noisier compared to the first harmonic results, but a pattern is still observable. In general, it seems that

melanopsin and S-(L+M) stimulations produce in-phase responses to each other, but produce anti-phase responses to luminance stimulation. On the other hand, L-M pathway responses seem to be desynchronised in quadrature phase from the the results of the other experiments. The same pattern of results is also observable in Figure 4.8d, which summarises the results to binocular responses at the second harmonic frequency.
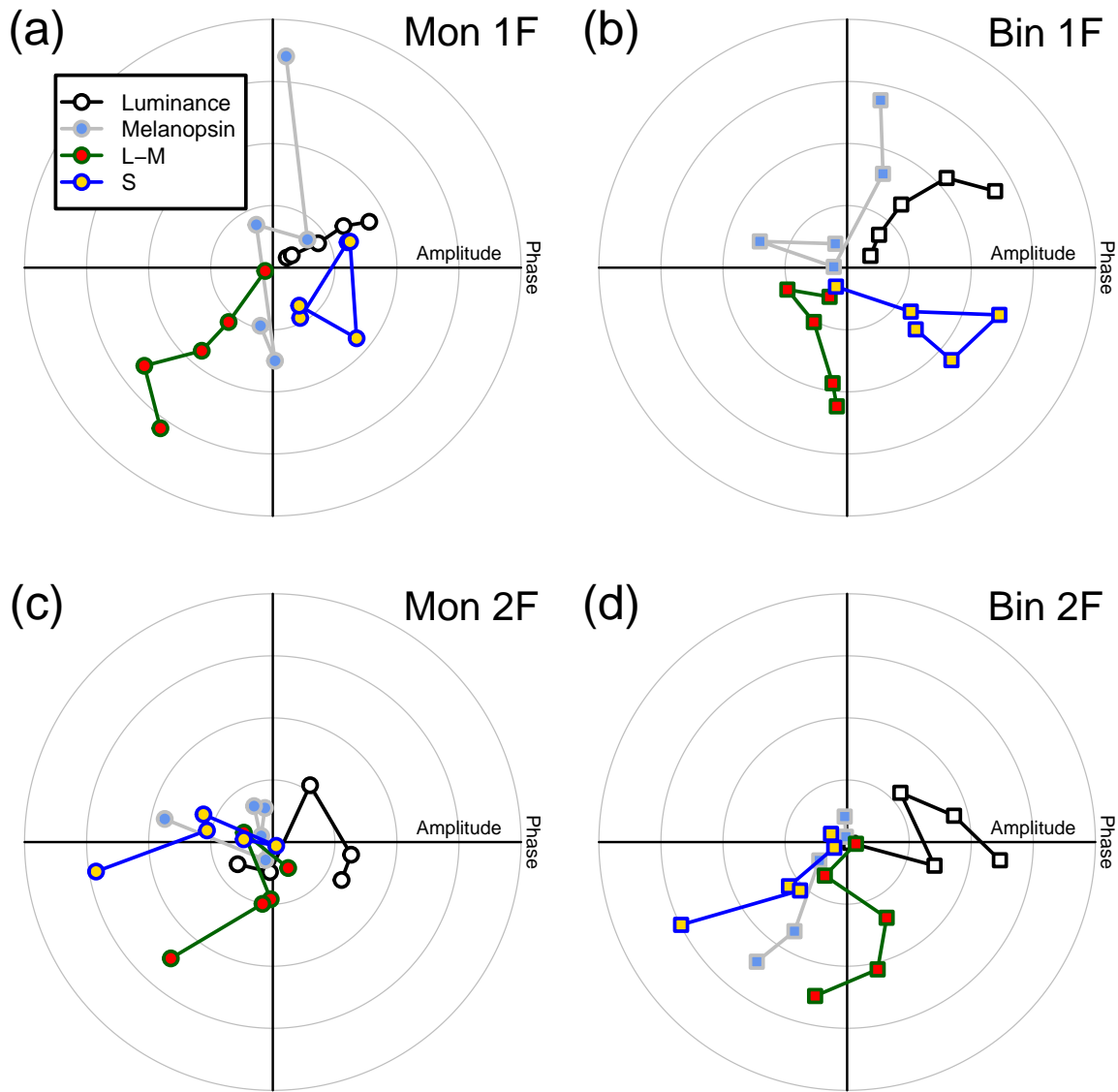


Figure 4.8: Pupil phase plots at the first and second harmonic frequencies for the luminance, melanopsin, L-M pathway and the S-(L+M) pathway experiments. Panel (a) shows the pupil response during monocular stimulation at the first harmonic frequency. Panel (b) shows the pupil response during binocular stimulation at the first harmonic frequency. Panel (c) shows the pupil response during monocular stimulation at the second harmonic frequency. Panel (d) shows the pupil response during binocular stimulation at the second harmonic frequency. In panels (a) and (b), the luminance amplitudes have been scaled down by a factor of 10 to be compared with the other experiments' results.

## 4.5   Discussion

We used pupillometry and silent substitution to measure monocular and binocular responses of the pupils to flickering stimuli when stimulating specific photoreceptor pathways. In our luminance experiment, we found that peripheral stimulation of the retina can elicit a pupillary response and we were also able to record a response at the second harmonic, which was not seen when we stimulated the fovea (Segala et al., 2023b). In all four experiments, we were able to record contrast response functions at both the first and the second harmonics. All experiments showed that binocular combination in the autonomic nervous system happens in a non-linear manner, with evidence of different magnitudes of interocular suppression depending on the photoreceptor pathway. This pattern of results was confirmed by a computational model, which allowed us to compare the weight of interocular suppression for each pathway. We found that, at the first harmonic frequency, the L-M pathway had a bigger suppression weight than the other pathways, while, at the second harmonic frequency, the S-(L+M) pathway had a bigger suppression weight. Finally, we looked at the pupil phases and observed different behaviours for the different pathways at the first and second harmonic frequencies. While the patterns differed between the first and second harmonics, within the same harmonic, whether the stimuli were presented monocularly or binocularly, the patterns were similar.

Our four experiments produced results that we were expecting based on our previous pupillometry findings (Segala et al., 2023b): the signals between the 2 pupils are combined non-linearly regardless of which photoreceptor pathway is being stimulated and whether the fovea or the periphery of the retina is being stimulated. We also observed responses at both the first and the second harmonic frequencies, which were expected based on previous literature (Spitschan et al., 2014; Stark and Sherman, 1957; Verdon and Howarth, 1988). There was, however, one aspect of our results that we were surprised to observe: the amplitude of this second harmonic response in the different photoreceptor pathways. It is true that we had already observed second harmonic responses when stimulating the periphery of the retina with achromatic luminance modulations flickering at 2 Hz (see Figure A1.1b), but the peak was very small when compared to the first harmonic peak, which is similar to what we observed in the luminance experiment here. On the other hand, in the melanopsin and L-M pathway experiments, the first and second harmonics are similar in amplitudes, and in the S-(L+M) pathway experiment, the peak of the second harmonic is even bigger than the peak of the first harmonic. One reason for why this might be happening may be because the driving signal is stronger when using a lower flicker frequency (indeed, pupillometry is more responsive to slow flicker frequencies of less than 1 Hz, Spitschan et al., 2014) and when stimulating the periphery of the retina (we have a very clear waveform for the luminance experiment in Figure 4.3b). However, this explanation is not entirely satisfactory: we observed a second harmonic when stimulating the periphery using a higher flicker

frequency and the pupil waveforms from the other three experiments are not as clear as the one from the luminance experiment. The presence of a second harmonic might indicate the existence of non-linearities that are not observable in the fovea: indeed, steady-state visual responses can contain activity beyond the first harmonic and these harmonics reflect non-linearities (e.g. squaring, exponentiation, rectification) in the visual response (Norcia et al., 2015). Additionally, it can be the case that, when these non-linearities are strong, then the higher harmonics can have equal or even higher peaks than the first harmonic. Here, we did observe strong non-linearities in our photoreceptor pathways, as reflected by the interocular suppression weights that were output by our computational model. For the S-(L+M) pathway specifically, it seems that the higher peak of the second harmonic is a behaviour intrinsic to S cones, as this was observed previously (Spitschan et al., 2014).

The pupil phases shown in Figure 4.8 give us more information about the pathways controlling the pupil response. The first thing that we notice is that the luminance and L-M pathway responses are in anti-phase. It is important to note that, for our L-M pathway stimulation, the stimulus flickered between magenta (first half of the cycle) and cyan (second half of the cycle), which means that the pupil was dilating during the magenta stimulation and then constricting during the cyan presentation. This seems to suggest that increments in magenta would correspond to decrements in brightness and increments in cyan would correspond to increments in brightness. It is possible that, if we had reversed the presentation cycle for the L-M pathway, the pupil response would have been in phase with the luminance responses. It has been recently shown that L-cone and melanopsin stimulation induce an opponent pupillary response to M- and S-cone stimulation (Murray et al., 2018; Woelders et al., 2018). Our melanopsin and S-(L+M) results show a similar behaviour both for monocular and binocular responses. The L-M pathways results are desynchronised approximately in quadrature phase from the melanopsin and S-(L+M) results. These results also seem to align with what was previously found: combining L and M responses should display results that are between the opponency shown by the isolated cone stimulation. Additionally, this could explain the very strong suppression that binocular (L-M) stimulation displays compared to the monocular stimulation: if L and M produce pupil responses that are in anti-phase with each other, then combining the two together should elicit smaller responses. Finally, since the results from our experiments are not in phase, it would suggest that the photoreceptors control the pupil diameter through different pathways.

## 4.6   Conclusions

We have demonstrated that binocular combination of temporal flickering light in the autonomic nervous system depends on the photoreceptor pathway. We were able to elicit pupil responses by stimulating only

the periphery of the retina and we were able to record contrast response functions for all photoreceptor pathways. While all pathways showed non-linear combination, they showed a variation in how the signals are combined, particularly in the weight of interocular suppression.

# 5 Chapter 5: General discussion and conclusions

## 5.1 Summary of findings

The aim of this thesis was to investigate and understand the rules of binocular combination and binocular interactions in the canonical cortical pathways (the visual cortex) and the non-canonical subcortical pathways that govern pupil diameter using EEG, pupillometry, psychophysics, and fMRI.

Chapter 2 investigated the binocular combination of spatially-uniform temporal luminance modulations in the cortical and subcortical pathways. Combining pupillometry and EEG allowed to simultaneously record responses from the visual cortex and the subcortical pathways controlling the pupil response to light. The results were very surprising showing differences in binocular integration of flickering light. In the visual cortex, binocular combination was shown to happen approximately linearly, with no evidence of interocular suppression, highlighted by the substantial binocular facilitation effect when comparing monocular and binocular responses. On the other hand, in the subcortical pathways, it was found that combination happens in a more non-linear way, with evidence of interocular suppression, with weaker binocular facilitation observed compared to the EEG results. Because the EEG results were very different from previous findings on binocular combination using steady-state EEG with grating stimuli (Baker and Wade, 2017), EEG responses were recorded to monocular and binocular stimuli flickering at a range of higher temporal frequencies. The results show substantial facilitation at all frequencies, except at the highest one, where responses were not demonstrably above the noise baseline, making it clear that the facilitation was not caused by the original low frequency. Finally, a temporal contrast matching experiment showed that perception of flickering light is consistent with near-linear binocular summation processes. This pattern of results was confirmed by computational modelling, which showed a much greater suppressive weight for the pupillometry data compared to the EEG and matching data. One explanation given for the strong binocular facilitation observed in the cortical pathways is that, within the primary visual cortex (V1) there are cells found within the blob regions that are biased towards low spatial frequencies (Edwards et al., 1995; Tootell et al., 1988) and are also largely monocular (Livingstone and Hubel, 1984; Tychsen et al., 2004), and it might be these cells and mechanisms that are mainly stimulated by luminance flicker.

Chapter 3 investigated this: fMRI was used to compare monocular and binocular responses to luminance flickering discs and flickering gratings in V1, V2, V3 and V4. The results showed that the difference between monocular and binocular responses to flickering gratings was not significant in all four visual cortices, indicating non-linear combination and interocular suppression for spatial pattern vision. For the flickering luminance discs, the responses to binocular stimuli were significantly bigger than to monocular stimuli in

V1, V2 and V4, with a stronger summation being observed in V1. These results aligned with the previous literature, with ocularity invariance being observed for flickering gratings (Lygo et al., 2021; Moradi and Heeger, 2009). However, the summation observed for the luminance flickering discs was weaker than the strong facilitation observed in Chapter 2. Three explanations were offered to explain this difference. The first explanation is based on the design of the stimuli: the discs used in experiment 4 were not stimulating the fovea as the centre of the stimuli was set to the background mean luminance, which might result in weaker cortical responses. The second explanation is based on the timecourses that show that activation plateaus half way through stimulus presentation, indicating that the haemodynamic response is saturating and therefore it is not possible to record higher responses. The third explanation is based on the nature of the neurons that drive fMRI responses and EEG responses: EEG responses are mainly stimulated by the excitatory pyramidal cells (Bruyns-Haylett et al., 2017), while MRI responses are driven by the entire neuronal population, including the inhibitory neurons. Therefore, the reduced summation observed in this experiment could be due to a partial inhibition caused by those neurons.

Finally, Chapter 4 investigated binocular combination of flickering light in the autonomic nervous system and how this combination depends on the photoreceptor pathway. Four experiments were completed to record monocular and binocular responses to peripheral stimulation of the retina with discs of achromatic flickering light, modulations targeting the melanopsin-containing intrinsically photosensitive Retinal Ganglion cells, the L-M pathway and the S-(L+M) pathway. For all experiments, responses were elicited at the first and second harmonic frequencies and contrast response functions were recorded. The explanation that was given for these observations is that they are most likely caused by the presence of non-linearities (Norcia et al., 2015) that are not present when stimulating the fovea, and that these non-linearities are strong, causing the high amplitudes of the second harmonic frequencies observed in the photoreceptor pathway experiments. The results reflect this: non-linear combination was observed in all four experiments, but different amounts of interocular suppression were observed. Using a computational model, these differences in behaviours were investigated, with a particular interest in comparing the weight of interocular suppression for each pathway. At the first harmonic frequency, the L-M pathway had a bigger suppressive weight than the other pathways, while, at the second harmonic frequency, the S-(L+M) pathway had a bigger suppression weight. One explanation that was given for this behaviour is based on the opponency of the pupil response shown when individually stimulating M- and L- cones (Murray et al., 2018; Woelders et al., 2018): because M- and L-cone stimulations produce anti-phase responses, then combining the two together will cause higher suppression between the two eyes. The phase of the pupils was also analysed and the results showed different pupil behaviour for each photoreceptor pathway and for luminance stimulation, with the pattern of

the results remaining the same whether stimulation was monocular or binocular. These results suggest that each photoreceptor class control the size of the pupils through separate pathways.

## 5.2 Limitations

As discussed in the *Procedure* of Chapter 4 (section 4.3.3), choosing a high frequency might limit the amplitude of the pupil responses and might also affect the phase of the pupil response. Choosing a frequency of 2 Hz for the experiments of Chapter 2 and a frequency of 0.5 Hz for the experiments of Chapter 4 was a limitation of the experiments. However, this was a compromise to be made in exchange of being able to record simultaneous EEG and pupillometry signals in Chapter 2 and to be able to run multiple trials with different ocular configurations for the experiments in Chapter 4.

For experiment 1, while the response was very small for both the pupillometry and the EEG, it was still significantly above the noise baseline. Additionally, the luminance results from experiment 5 show that, at a lower frequency, while the amplitude of the response is bigger, the pattern of the results remain the same. From this, it's possible to conclude that using a 2 Hz frequency was the correct choice.

In Chapter 4, choosing an even lower frequency (0.01 or 0.05 Hz) would have yielded a bigger amplitude of the response within the ipRGCs pathway, but it would have elicited the same amplitude for the S cones (Spitschan et al., 2014). An additional analysis by Spitschan et al. (2014) shows that the phase of the pupil response of shifts depending on the frequency, but the shift between the pathways remains the same. Therefore, using a frequency might have limited the response elicited by the ipRGCs pathway, but not for the other pathways. Additionally, the phase would not have been impacted by the frequency chosen.

## 5.3 Future directions

This thesis presented important findings about the pupillary light response and the computational processes behind this response. Particularly, it extended the knowledge about the combination of the signals between the two eyes in the subcortical pathways that control the size of the pupils. Many studies had used silent substitution while pharmacologically dilating and stimulating one eye and recording the other eye's responses (Cao et al., 2015; Estévez and Spekreijse, 1982; Shapiro et al., 1996; Spitschan et al., 2014; Spitschan and Woelders, 2018) to investigate and compare the involvement of the different photoreceptor classes in determining the pupil size. By showing that it is also possible to do so while stimulating and recording responses from both eyes simultaneously, new research directions have opened. It would be of particular interest to investigate binocular interactions between different photoreceptor pathways: how would

the signals be combined if one photoreceptor pathway is targeted in one eye and a different pathway is targeted in the other eye? To give an example, previous research has shown that L-cone and melanopsin stimulation induce an opponent pupillary response to M- and S-cone stimulation (Murray et al., 2018; Woelders et al., 2018), so it would be interesting to understand how the pupils would respond if one eye was undergoing L-cone stimulation and the other M-cone stimulation: would the combined pupil response be reduced? Would the responses cancel each others out and therefore no constriction observed?

The results of this thesis can also benefit researchers studying binocular combination disorders, such as amblyopia. Amblyopia, commonly referred to as 'lazy eye', is a visual disorder in which the input to one eye is impoverished during childhood and binocular vision fails to develop. It is a relative common disorder of binocular vision, affecting between 1% and 3% of the population (Fu et al., 2020; Hess et al., 2010). The eyes themselves are unaffected: the input from the amblyopic eye is suppressed by the brain to avoid conflicting visual inputs. Therefore, amblyopia is generally considered a cortical disorder. It would therefore be of interest to investigate the non-canonical pathways and see whether they remain unaffected or not in the amblyopic population. If preserved binocular pathways were to be found, this could lead to the development of novel treatments that could be provide additional options and efficiency to the current available treatments for this disorder, as they have been shown to not be always effective (Repka et al., 2003, 2004, 2005).

## 5.4 Overall conclusions

The experiments in this thesis contribute to widening our understanding of the signals between the two eyes in the cortical pathways, connecting the retina to the visual cortex, and the subcortical pathway that govern the diameter of the pupils. The results have shown that the mechanisms within the two pathways are different, reflecting how the two pathways are anatomically separate. While these two might not be completely segregated from each other and interactions might happen between the two, the experiments and the analyses that have been completed do not allow for that level of detail to be picked up.

Different experimental approaches have been used, with novel paradigms being developed: as far as we are aware, for the first time, EEG and binocular pupillometry were combined to record simultaneously responses from the visual areas and the pupils, and these results were directly compared to each other. These findings have shown that ocularity invariance is not a ubiquitous feature of visual processing, and the brain repurposes a generic normalisation algorithm for different visual functions by adjusting the amount of interocular suppression.

The experiments have also shown that there is a difference in visual response between discs and gratings, probably due to the nature of the stimuli: while discs are just uniform shapes, gratings may vary in their spatial frequency and their orientation. These characteristics may affect other mechanisms that will not be involved during presentation of discs.

As mentioned earlier in the thesis, much of this work has already been published in article (Segala et al., 2023b) and abstract (Segala et al., 2022, 2021) format, as well as being presented at international conferences, with plans to submit Chapter 3 and 4 for publication. These experiments form part of a corpus of research on binocular combination in the cortical and subcortical pathways that govern the diameter of the pupils, supported by a BBSRC grant. Ultimately, it is hoped that this collection of work will stimulate further research into binocular combination of signals.

# Appendix 1: Replication of Experiment 1 with peripheral stimulation

We conducted a conceptual replication of Experiment 1 using an alternative system of hardware and software (Martin et al., 2023, 2022). A pair of Spectra Tune Lab multiprimary devices (LEDmotive Technologies LLC, Barcelona, Spain) were coupled to a binocular headset using liquid light guides. The light was imaged onto a circular diffuser for each eye (field size 30 deg) with the central 8 degrees masked off using a black occluder. Therefore the replication experiment (experiment 9) involved peripheral stimulation, unlike experiment 1 which stimulated the central ~4 degrees of the visual field. All conditions were otherwise as described for the main experiment, and we tested 12 participants in total.

## Pupillometry
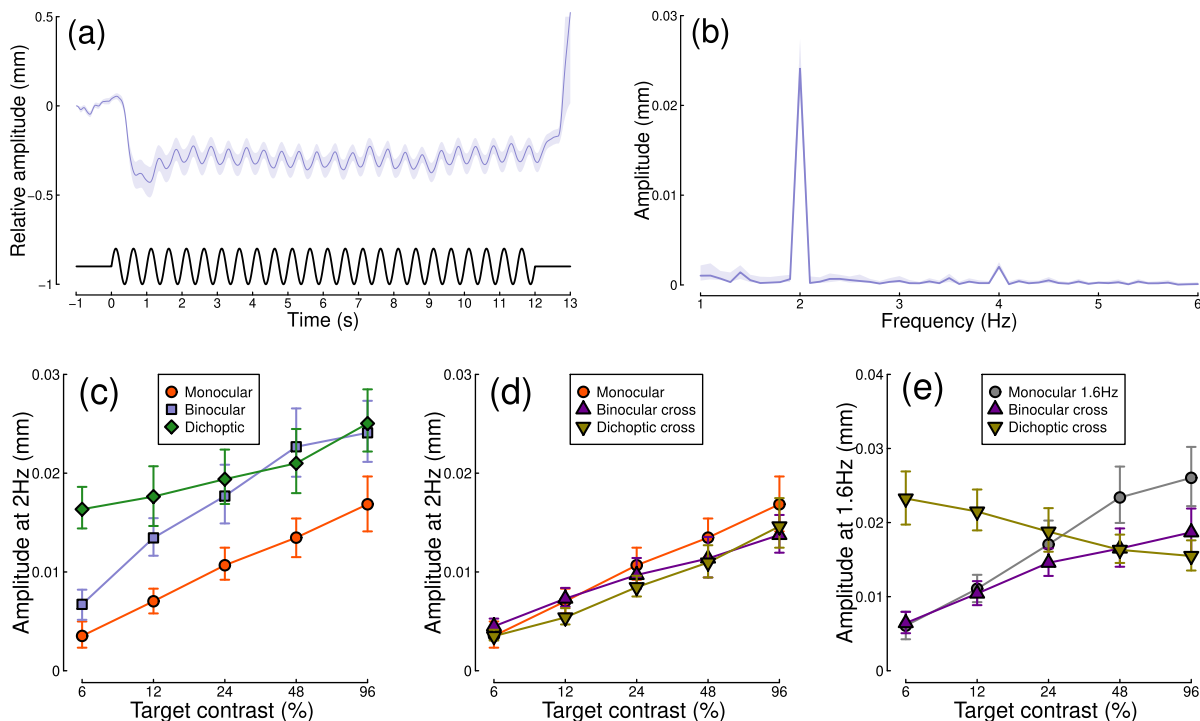


Figure A1.1: Summary of pupillometry results for N=12 participants, for peripheral stimulation at 2 Hz. See Figure 2.1 for a description of each panel.

The pupillometry results for experiment 9 are shown in Figure A1.1 and correspond closely to those from the main experiment (Figure 2.1). The ratio of binocular to monocular responses in Figure A1.1c is similar, and suppression is evident in Figure A1.1d,e. Of particular interest is the existence of a slight response at the second harmonic (4Hz, Figure A1.1b), which was not present in our original data. This may

be because the driving signal is stronger when stimulating the periphery (note the clear waveform in Figure A1.1a), or more robust to eye movements, or it might indicate additional nonlinearities not present at the fovea.
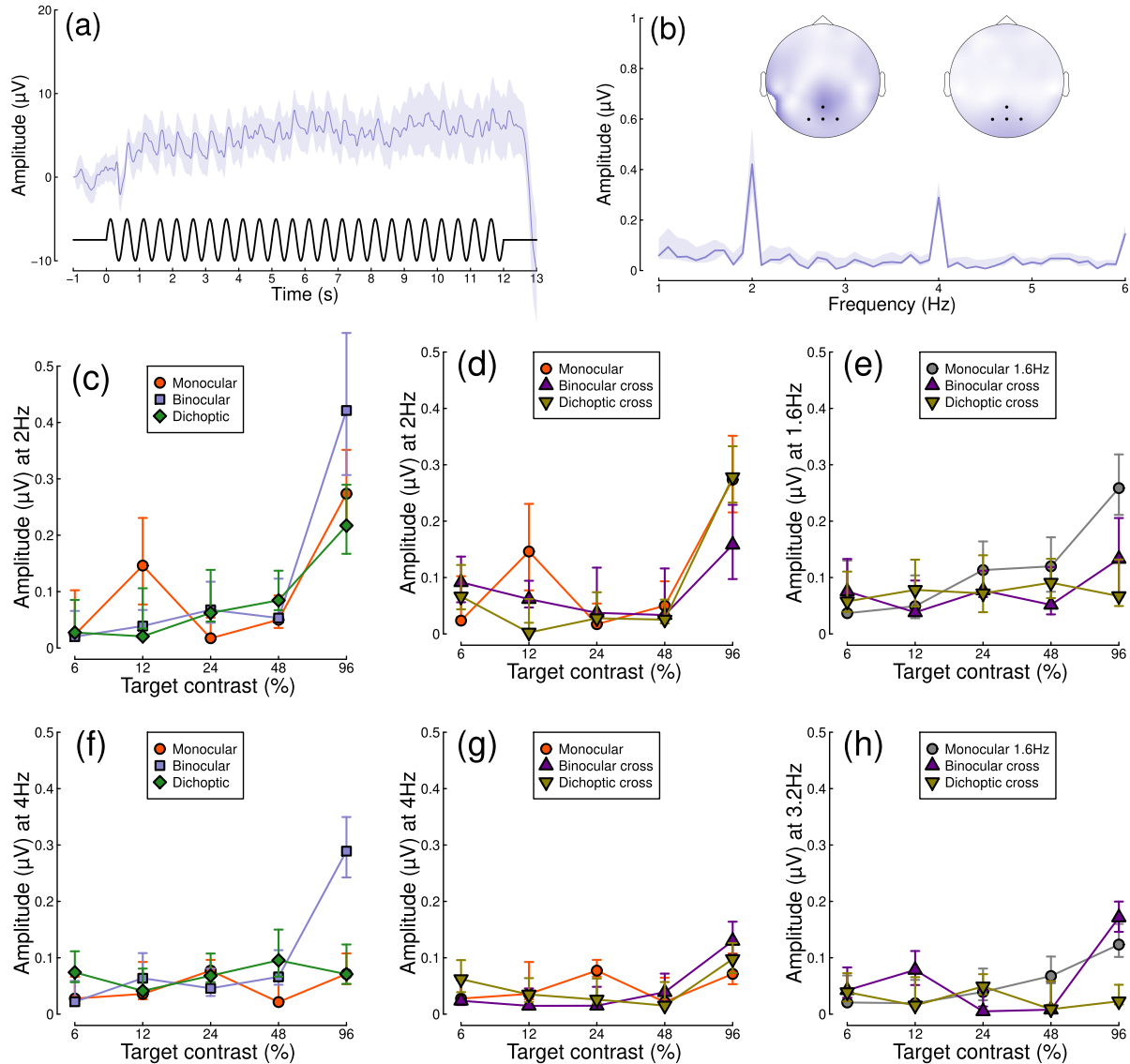


Figure A1.2: Summary of steady-state EEG results for N=12 participants, for peripheral stimulation at 2 Hz. See Figure 2.2 for a description of each panel.

The EEG results for experiment 9 are shown in Figure A1.2. These still show a strong binocular facilitation effect at the highest contrast levels (Figure A1.2c,f), but the contrast response function is less clear at both the first and second harmonics. We suspect that this is because the cortical representation of

the peripheral visual field is primarily along the calcarine sulcus, which results in some cancellation of the steady-state signal. This results in weaker signals than we obtained for foveal stimulation (represented at the occipital pole) in the main experiment (see Figure 2.2).
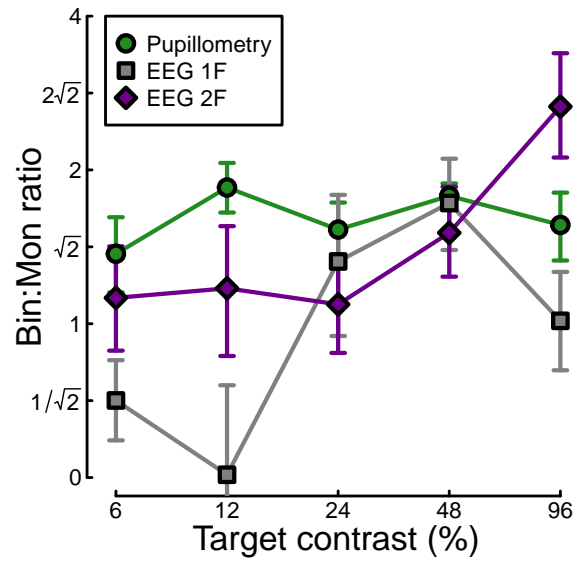


Figure A1.3: Ratio of binocular to monocular response for three data types. These were calculated using the same method as for the ratios displayed in Figure 2.3

Finally, we calculated the ratio of binocular to monocular responses across the three data types from Experiment 9 (Figure A1.3).

# Appendix 2: Pupillometry and EEG recordings for targeted ipRGCs, L cones, M cones and S cones at 2 Hz

Following the results shown in Figures A1.1 and A1.2, we initially developed four new experiments testing four photoreceptor classes using discs flickering at 2 Hz. The four experiments tested the melanospin-containing retinal ganglion cells, the L cones, the M cones and the S cones. The procedure used for these experiments is the same as the one described in chapter 4, but, in addition to pupillometry, we also recorded EEG signals. The data were analysed with the same methodology described in chapter 2. For EEG, the repetitions were averaged across only one electrode ($POz$).



Figure A2.1: Summary of pupillometry results for N=7 participants for the melanopsin condition. Panel (a) shows a group average waveform for binocular presentation (low pass filtered at 5Hz), with the driving signal plotted at the foot. Panel (b) shows the average Fourier spectrum (absolute amplitude values). Panels (c,d) show contrast response functions for pupil diameter at 2Hz for different conditions (illustrated in Figure 2.8). Panel (e) shows contrast response functions at 1.6Hz for three conditions. Shaded regions and error bars indicate bootstrapped standard errors.

# Electroencephalography



Figure A2.2: Summary of EEG results for N=7 participants for the melanopsin condition. Panel (a) shows a group average waveform for binocular presentation (low pass filtered at 5Hz), with the driving signal plotted at the foot. Panel (b) shows the average Fourier spectrum (absolute amplitude values). Panels (c,d) show contrast response functions at 2Hz for different conditions (illustrated in Figure 2.8). Panel (e) shows contrast response functions at 1.6Hz for three conditions. Panels (f-h) show the same results but for second harmonic responses. Shaded regions and error bars indicate bootstrapped standard errors.

The results for the melanopsin experiment are shown in Figure A2.1 for pupillometry and in Figure A2.2 for EEG. Figures A2.1a and A2.2a show the group average waveform for pupillometry and EEG respectively. The pupillometry waveform shows a small initial constriction of the pupil and an entrainment of the pupil response. The EEG waveform shows a rather noisy response. This is also reflected in the pupillometry

(Figure A2.1b) and the EEG (Figure A2.2b) Fourier spectra, which show a noisy signal, with no clear signals at 2 Hz, suggesting that there was no significant response from the pupils nor the visual cortex.

# Pupillometry



Figure A2.3: Summary of pupillometry results for N=8 participants for the L cones condition. Panel (a) shows a group average waveform for binocular presentation (low pass filtered at 5Hz), with the driving signal plotted at the foot. Panel (b) shows the average Fourier spectrum (absolute amplitude values). Panels (c,d) show contrast response functions for pupil diameter at 2Hz for different conditions (illustrated in Figure 2.8). Panel (e) shows contrast response functions at 1.6Hz for three conditions. Shaded regions and error bars indicate bootstrapped standard errors.

The results for the L cones experiment are shown in Figure A2.3 for pupillometry and in Figure A2.4 for EEG. Figure A2.3a shows the group average waveform for pupillometry: a clear substantial initial constriction of the pupil followed by visible oscillations at the flicker frequency can be observed. Figure A2.3b shows the averaged Fourier spectrum and shows a clear response at 2 Hz. The contrast response functions displayed in Figures A2.3c-e are clear and show strong suppression, similar to the results shown in Figure 4.5: in Figures A2.3d-e, the amplitudes of the binocular cross frequency responses (purple triangles) are consistently smaller than those of the monocular response at 2 Hz (red circles) and at 1.6 Hz (grey circles).

Figure A2.4a shows the EEG waveform: a rather noisy response can be observed. This is also reflected in the averaged Fourier spectrum (Figure A2.4b), which shows a noisy signal, with no clear signals at 2 Hz,

suggesting that there was no significant response from the visual cortex.

# Electroencephalography



Figure A2.4: Summary of EEG results for N=8 participants for the L cones condition. Panel (a) shows a group average waveform for binocular presentation (low pass filtered at 5Hz), with the driving signal plotted at the foot. Panel (b) shows the average Fourier spectrum (absolute amplitude values). Panels (c,d) show contrast response functions at 2Hz for different conditions (illustrated in Figure 2.8). Panel (e) shows contrast response functions at 1.6Hz for three conditions. Panels (f-h) show the same results but for second harmonic responses. Shaded regions and error bars indicate bootstrapped standard errors.

The results for the M cones experiment are shown in Figure A2.5 for pupillometry and in Figure A2.6 for EEG. Figure A2.5a shows the group average waveform for pupillometry: a clear substantial initial constriction of the pupil can be observed but no visible oscillations at the flicker frequency can be observed.

Figure A2.5b shows the averaged Fourier spectrum and shows a noisy response with no clear respsonse at 2 Hz, suggesting that there was no significant response of the pupils to the stimulation. Despite this, we can observe some clear contrast response functions in Figures A2.5c-e. In Figure A2.5c, we can observe that the amplitude of the binocular signal (blue squares) is smaller than that of the monocular signal (red circles), which is similar to what we observed in the results shown in Figure 4.5. This strong suppression of the signal is also reflected in Figures A2.5d-e, where the the amplitudes of the binocular cross frequency condition (purple triangles) are consistently smaller than those of the monocular 2 Hz condition (red circles) and the monocular 1.6 Hz condition (grey circles).
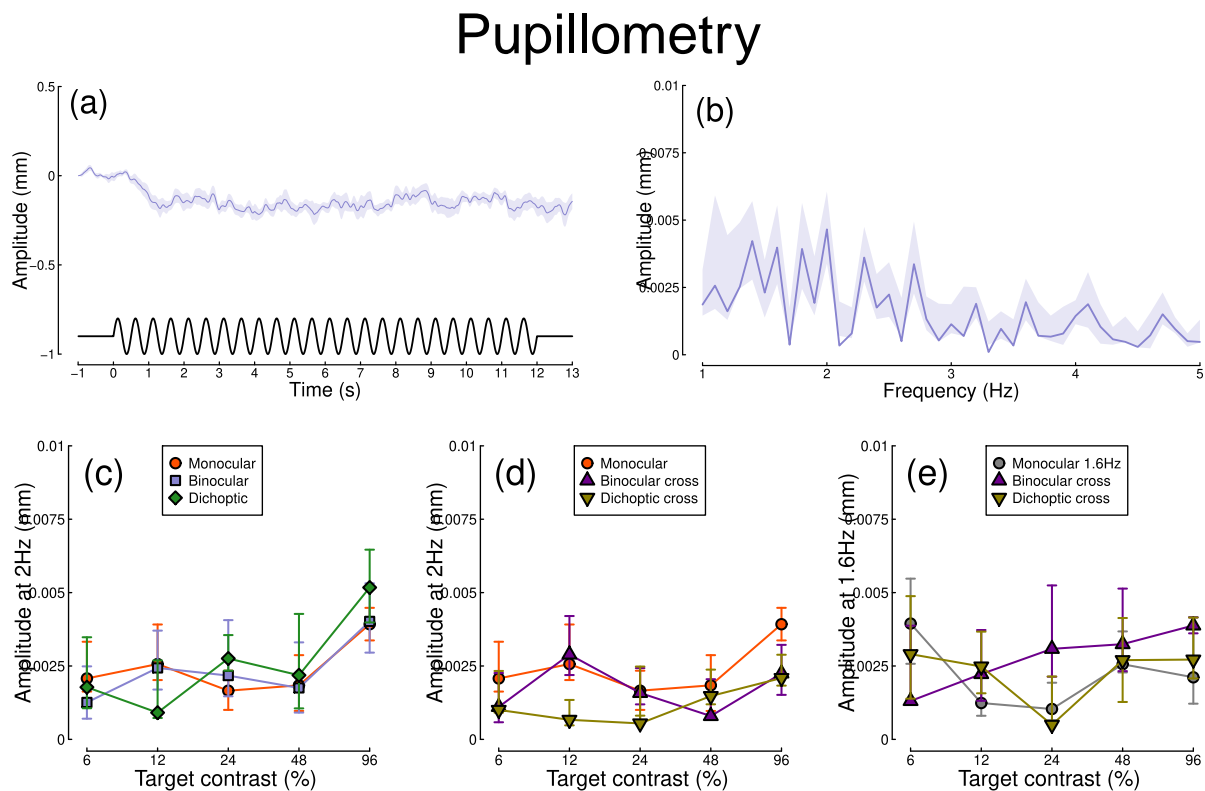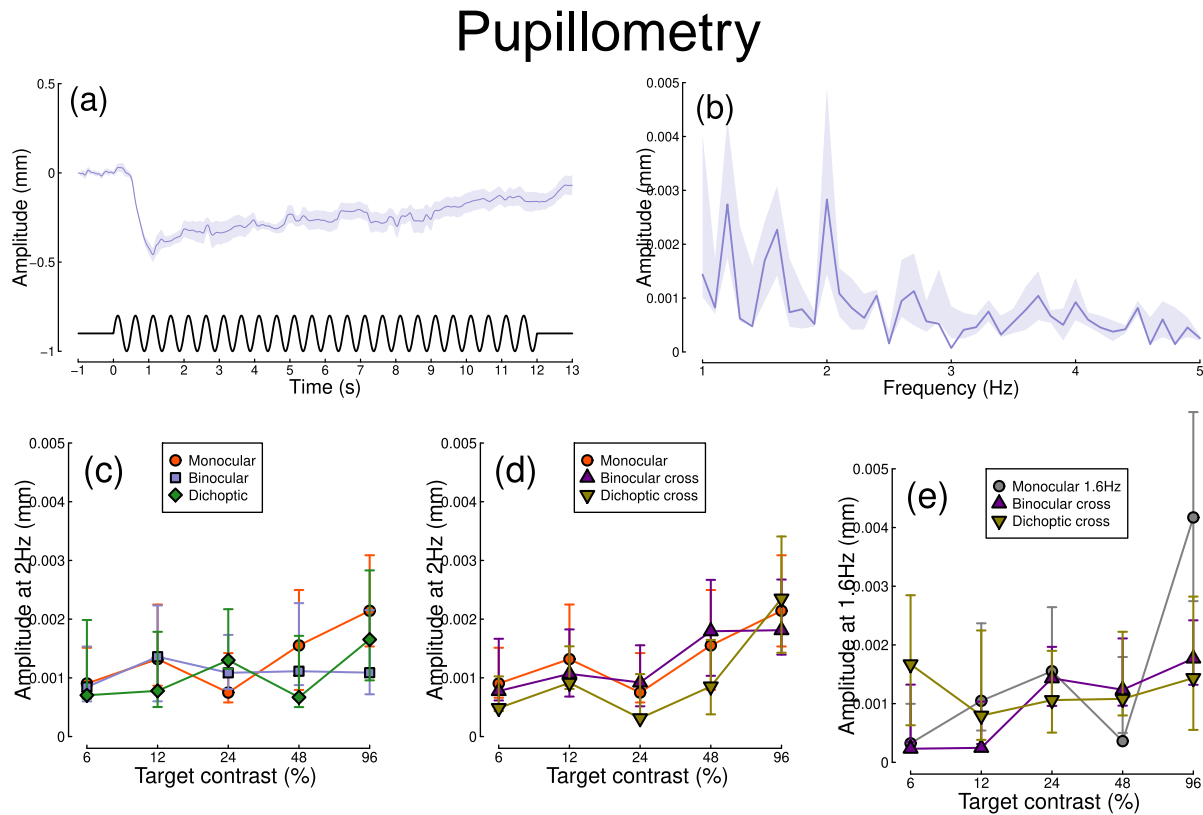


Figure A2.5: Summary of pupillometry results for N=8 participants for the M cones condition. Panel (a) shows a group average waveform for binocular presentation (low pass filtered at 5Hz), with the driving signal plotted at the foot. Panel (b) shows the average Fourier spectrum (absolute amplitude values). Panels (c,d) show contrast response functions for pupil diameter at 2Hz for different conditions (illustrated in Figure 2.8). Panel (e) shows contrast response functions at 1.6Hz for three conditions. Shaded regions and error bars indicate bootstrapped standard errors.

Figure A2.6 shows the results for the EEG: the waveform (Figure A2.6a) shows a rather noisy response. This is also reflected in the averaged Fourier spectrum (Figure A2.6b), which shows a noisy signal, with no clear signals at 2 Hz, suggesting that there was no significant response from the visual cortex.
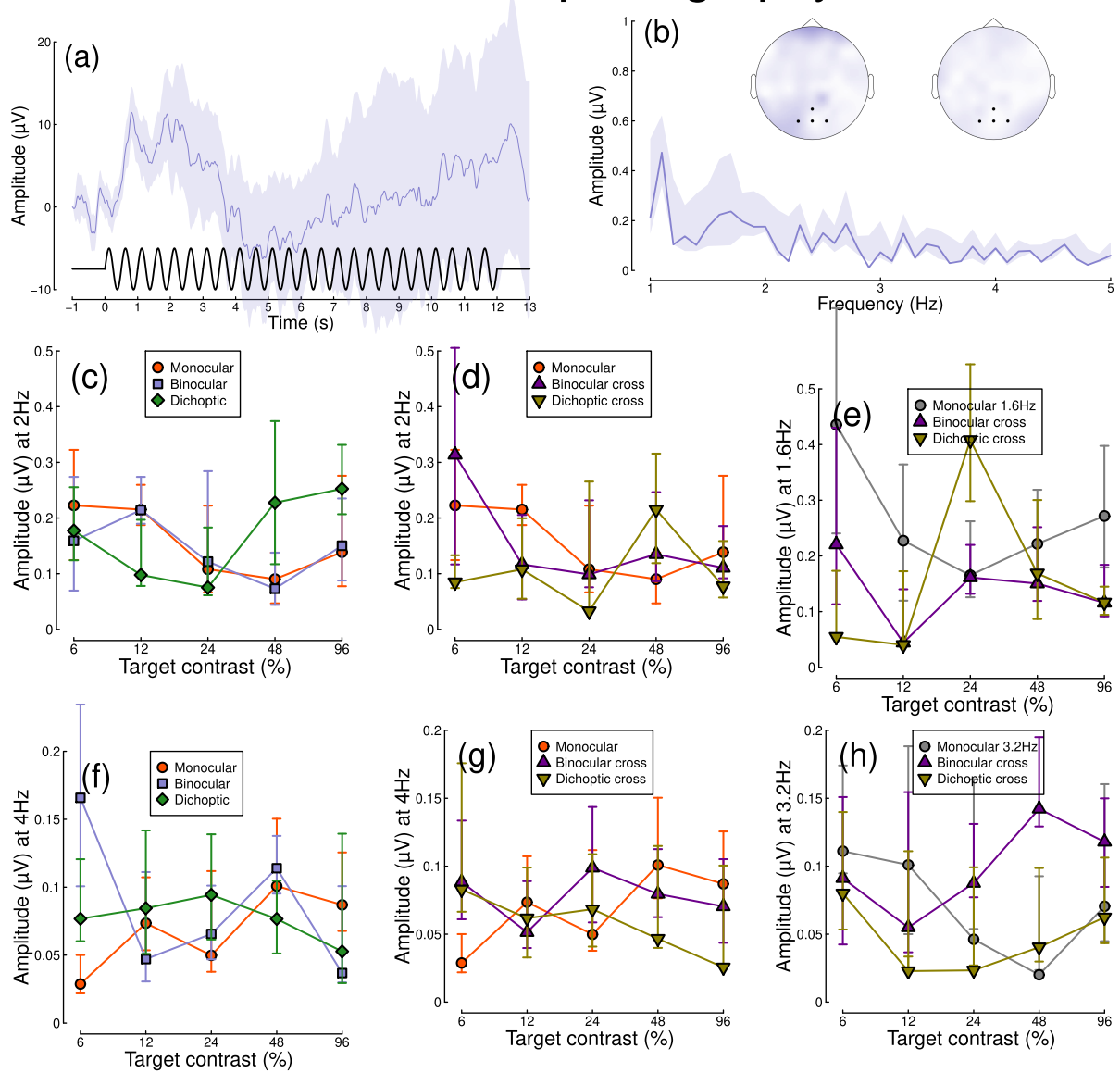
# Electroencephalography
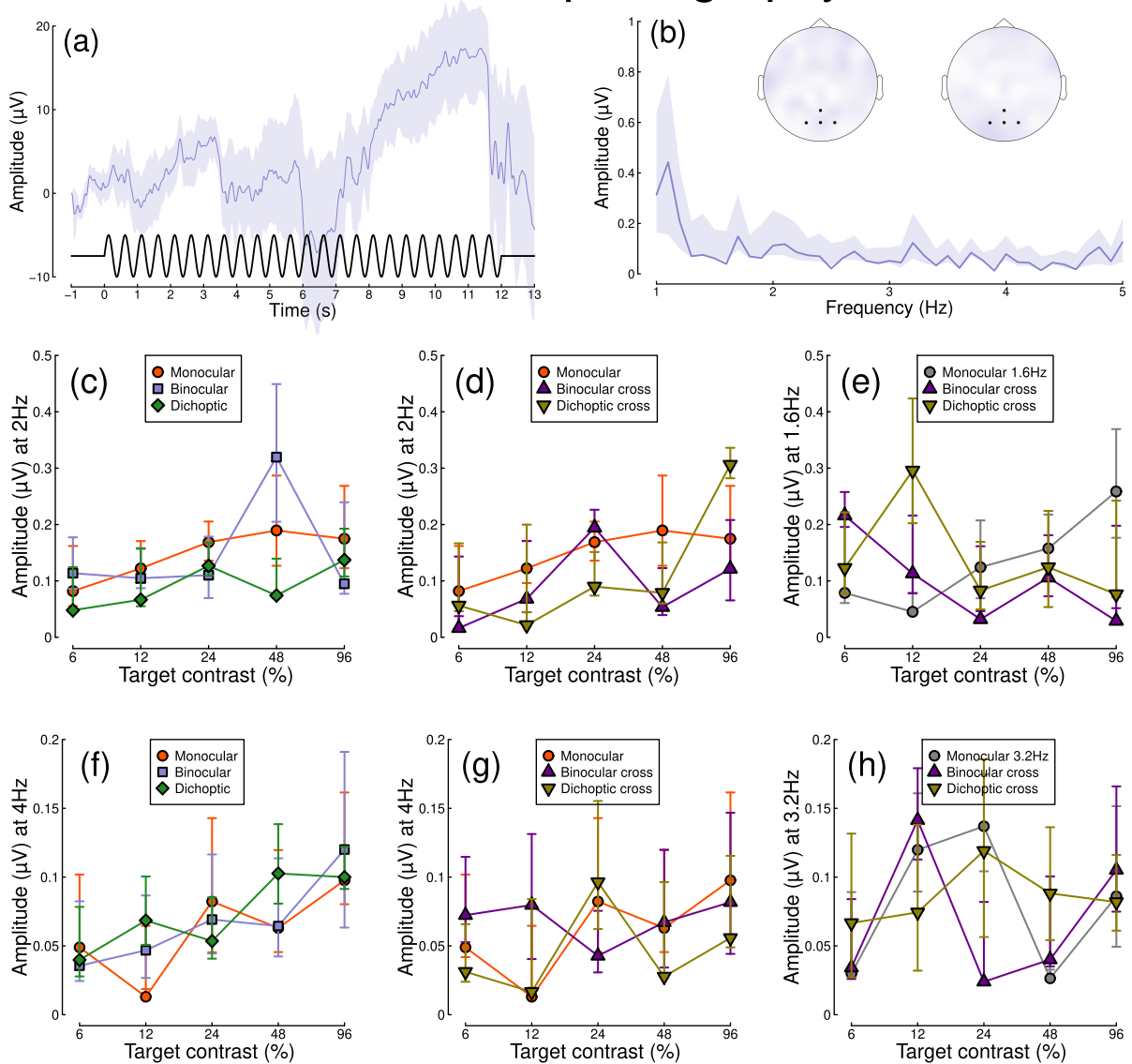


Figure A2.6: Summary of EEG results for N=8 participants for the M cones condition. Panel (a) shows a group average waveform for binocular presentation (low pass filtered at 5Hz), with the driving signal plotted at the foot. Panel (b) shows the average Fourier spectrum (absolute amplitude values). Panels (c,d) show contrast response functions at 2Hz for different conditions (illustrated in Figure 2.8). Panel (e) shows contrast response functions at 1.6Hz for three conditions. Panels (f-h) show the same results but for second harmonic responses. Shaded regions and error bars indicate bootstrapped standard errors.

Finally, the results for the S cones experiment are shown in Figure A2.7 for pupillometry and in Figure A2.8 for EEG. Figure A2.7a shows the group average waveform for pupillometry: a clear initial constriction of the pupil can be observed but no visible oscillations at the flicker frequency can be observed. Figure A2.7b shows the averaged Fourier spectrum and shows a noisy response with no clear respsonse at 2 Hz, suggesting

that there was no significant response of the pupils to the stimulation. The same is observed for the EEG results: the waveform (Figure A2.8a) shows a rather noisy response. This is also reflected in the averaged Fourier spectrum (Figure A2.8b), which shows a noisy signal, with no clear signals at 2 Hz, suggesting that there was no significant response from the visual cortex.
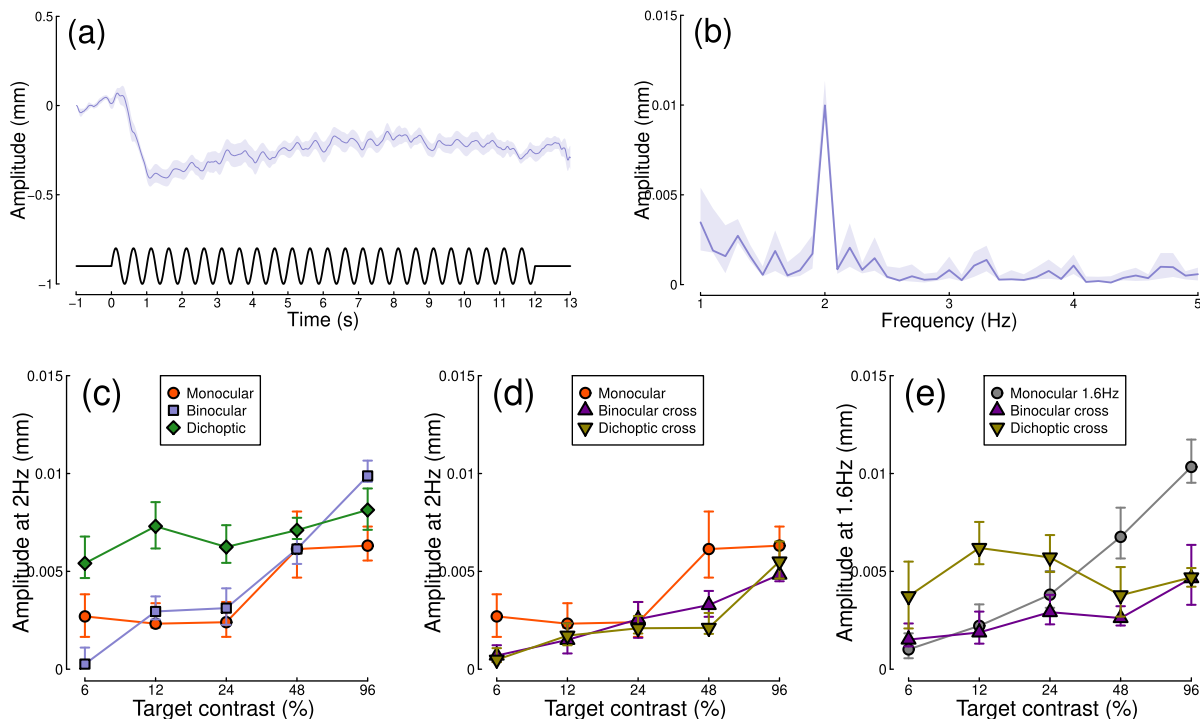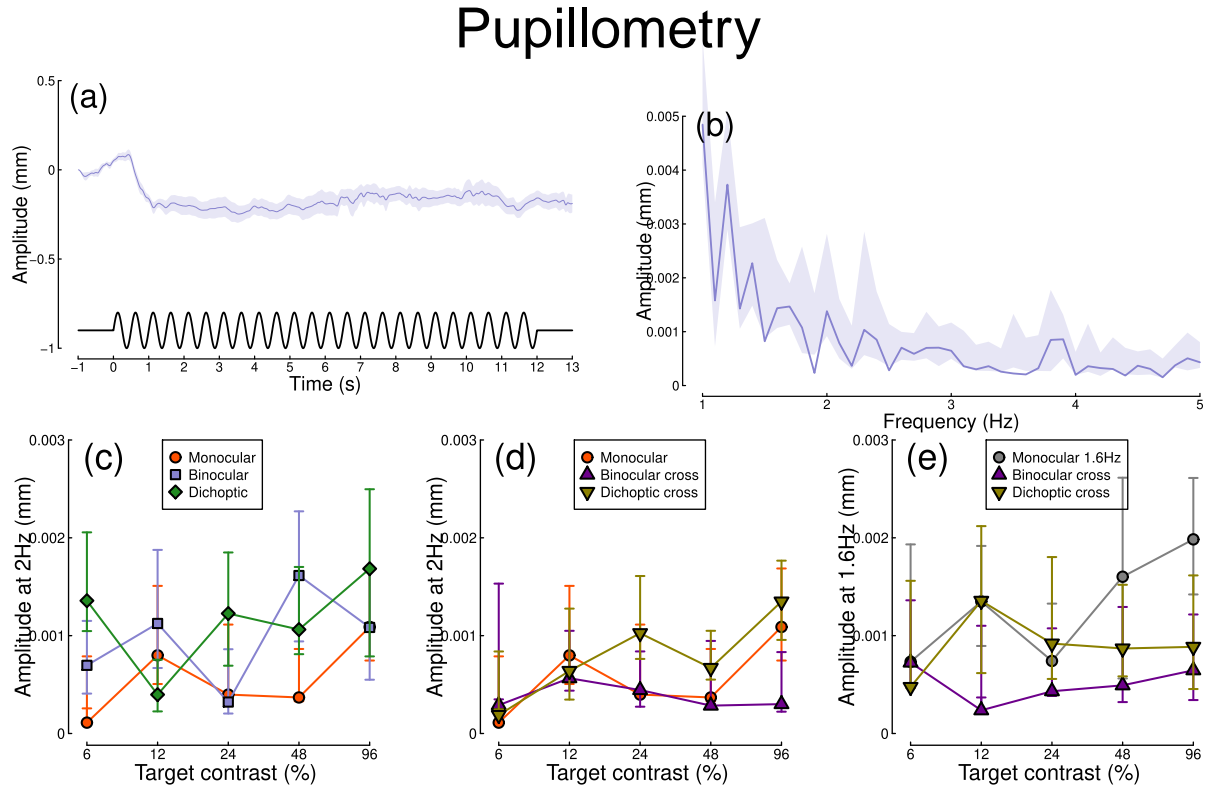
# Pupillometry



Figure A2.7: Summary of pupillometry results for N=8 participants for the S cones condition. Panel (a) shows a group average waveform for binocular presentation (low pass filtered at 5Hz), with the driving signal plotted at the foot. Panel (b) shows the average Fourier spectrum (absolute amplitude values). Panels (c,d) show contrast response functions for pupil diameter at 2Hz for different conditions (illustrated in Figure 2.8). Panel (e) shows contrast response functions at 1.6Hz for three conditions. Shaded regions and error bars indicate bootstrapped standard errors.

The lack of clear signals at 2 Hz in the pupillometry data for the melanopsin, the M cones and the S cones experiments is likely due to the fact that the amplitudes of the signals from the targeted photoreceptor modulations are about 5 (the melanopsin experiment), 8 (the M cones experiment) and 16 (the S cones experiment) times smaller than that of the luminance experiment (Figure A1.1), so the signal-to-noise ratio is too small and a much greater amount of participants would have been required to obtain clear signals. For the EEG, we suspect that the signals are generally noisy because we were stimulating the periphery of the visual cortex, which would result in some cancellation of the steady-state signal. Additionally, the

amplitudes of the signals are about 2 times smaller than that of the luminance condition (Figure A1.2), so this would result in an even smaller signal-to-noise ratio and noisier data. For these reasons we reduced the frequency to 0.5 Hz and abandoned the EEG component for the four main experiments reported in Chapter 4.
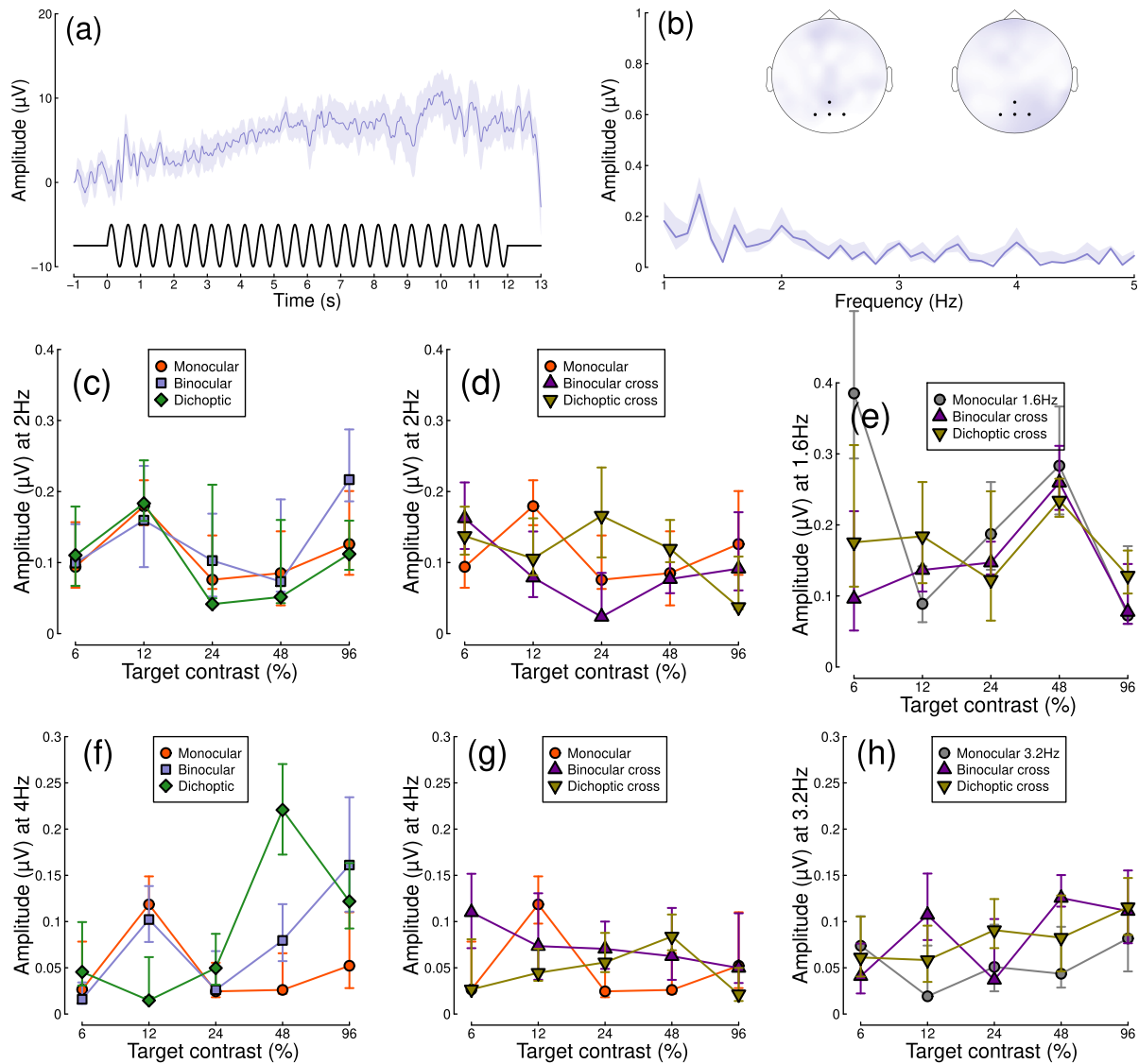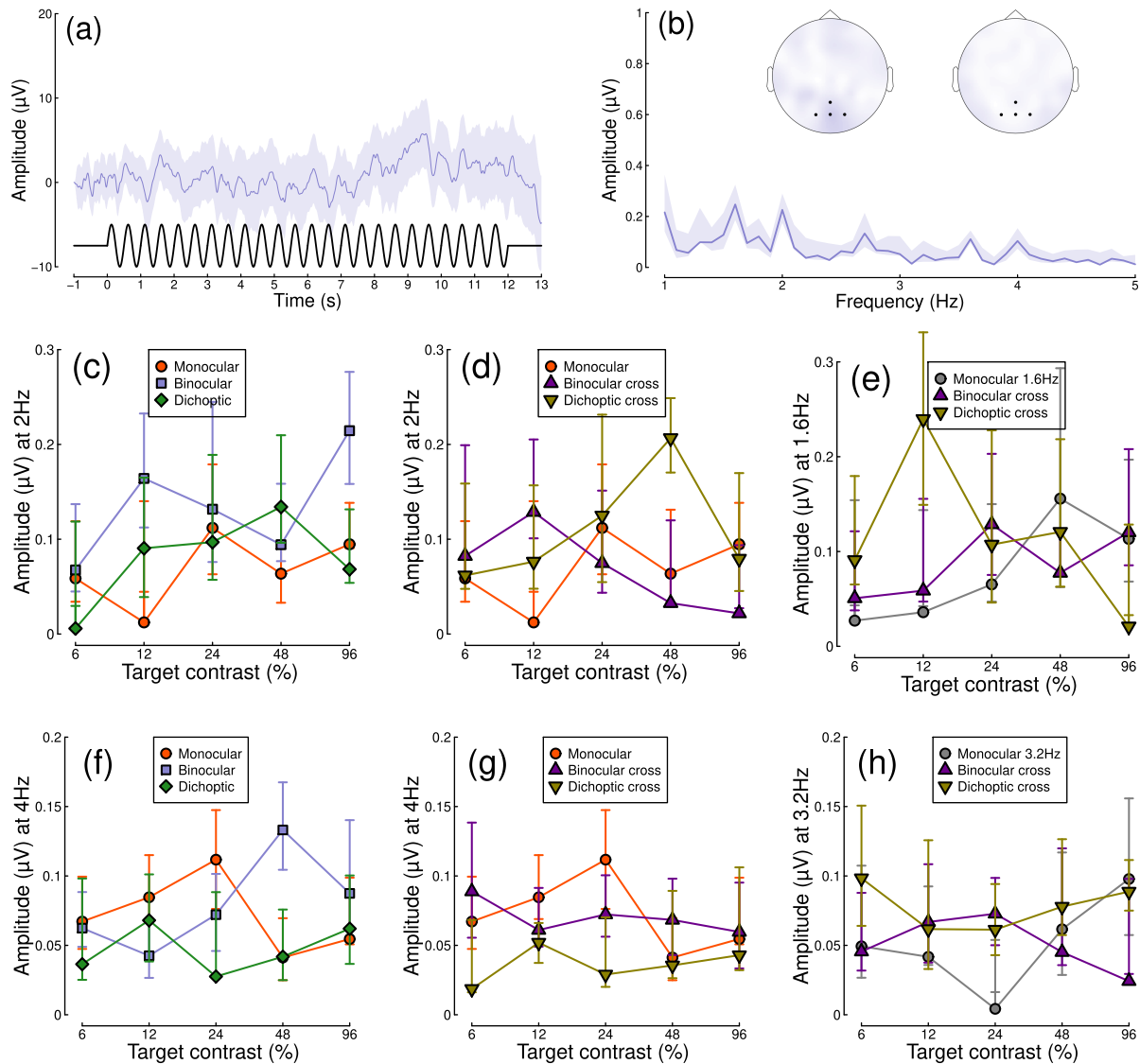


Figure A2.8: Summary of EEG results for N=8 participants for the S cones condition. Panel (a) shows a group average waveform for binocular presentation (low pass filtered at 5Hz), with the driving signal plotted at the foot. Panel (b) shows the average Fourier spectrum (absolute amplitude values). Panels (c,d) show contrast response functions at 2Hz for different conditions (illustrated in Figure 2.8). Panel (e) shows contrast response functions at 1.6Hz for three conditions. Panels (f-h) show the same results but for second harmonic responses. Shaded regions and error bars indicate bootstrapped standard errors.

# Appendix 3: Analysis of the consensual responses from Chapter 4

We ran additional analyses for the data collected in chapter 4, where we analysed the consensual responses for each experiment. For the response of the stimulated eye, we extracted the diameters recorded from the stimulated eye only and averaged them across all participants. For the consensual response, we extracted the diameters recorded from the unstimulated eye only and averaged them across all participants. The analysis was then carried out in the same manner as it is described in chapter 4.
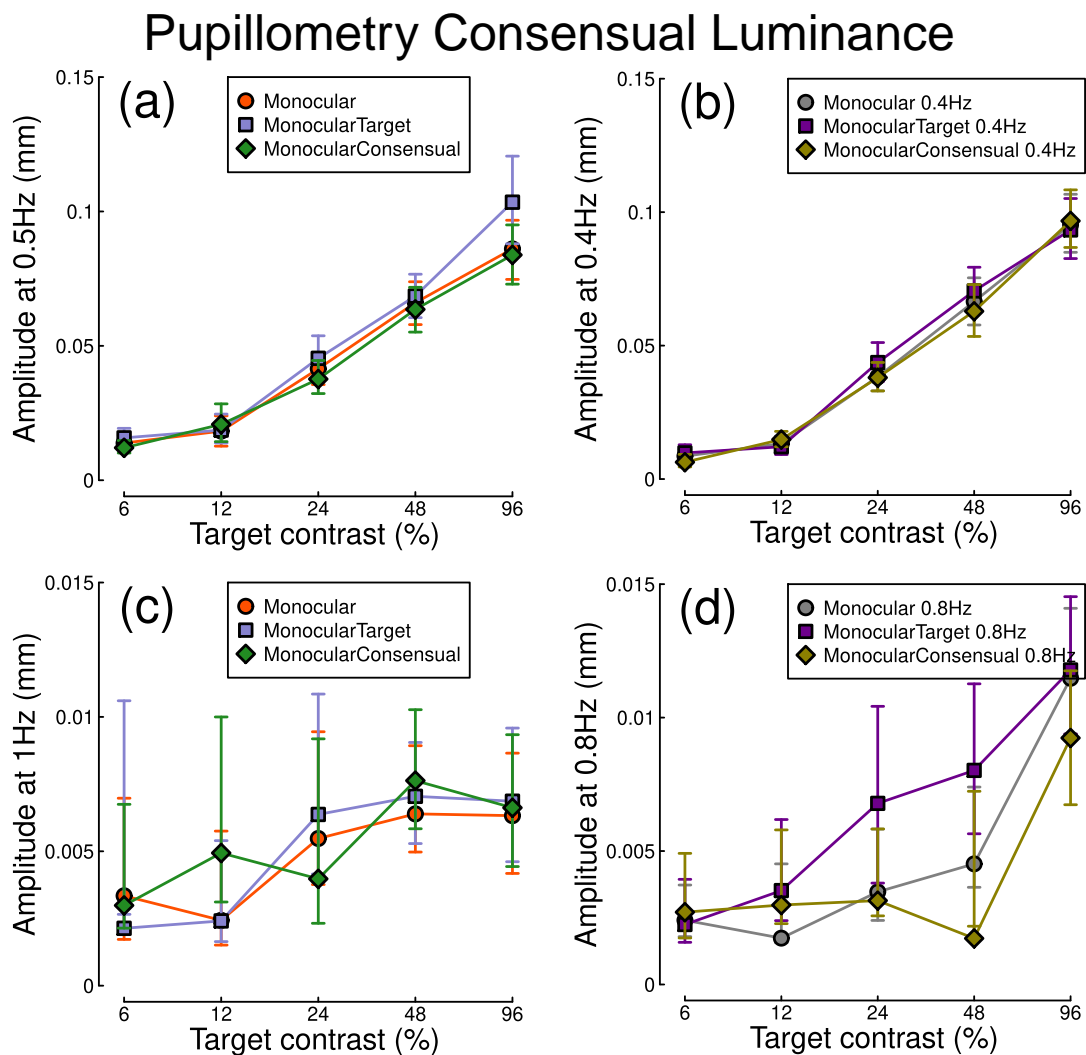


Figure A3.1: Summary of the consensual response for the luminance experiment for N=12 participants. Panel (a) and (b) show contrast response functions at 0.5 and 0.4 Hz respectively. Panels (c) and (d) are in the same format but for the second harmonic responses. Error bars indicate bootstrapped standard errors.

Figure A3.1 shows a summary of the analysis for the luminance experiment. The red and grey circles

show the monocular responses recorded from both eyes (they are the same responses displayed in red and grey in the main results in Figure 4.3). The blue and purple squares show the monocular response of the stimulated eye. The green and yellow diamonds show the monocular response of the unstimulated eye. In general, we observe that all three responses have the same pattern and are similar to each other, showing that there is a consensual response even when stimulating the periphery of the retina.
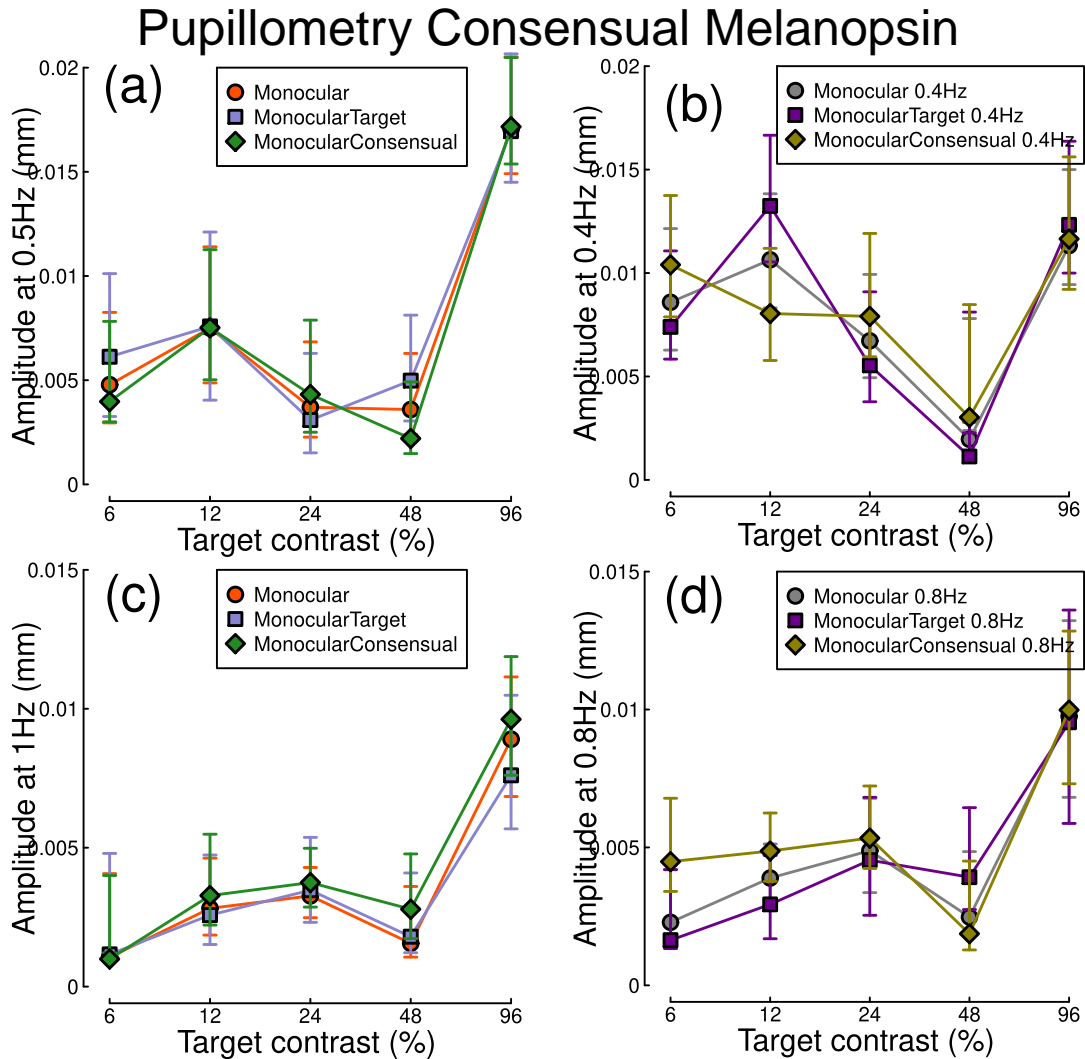


Figure A3.2: Summary of the consensual response for the melanopsin experiment for N=12 participants. Panel (a) and (b) show contrast response functions at 0.5 and 0.4 Hz respectively. Panels (c) and (d) are in the same format but for the second harmonic responses. Error bars indicate bootstrapped standard errors.

Figure A3.2 shows a summary of the analysis for the melanopsin experiment. The results are presented in the same way as in Figure A3.1. In general, we observe that all three responses have the same pattern and are similar to each other, showing that targeting the melanopsin-containing RGCs elicits a consensual
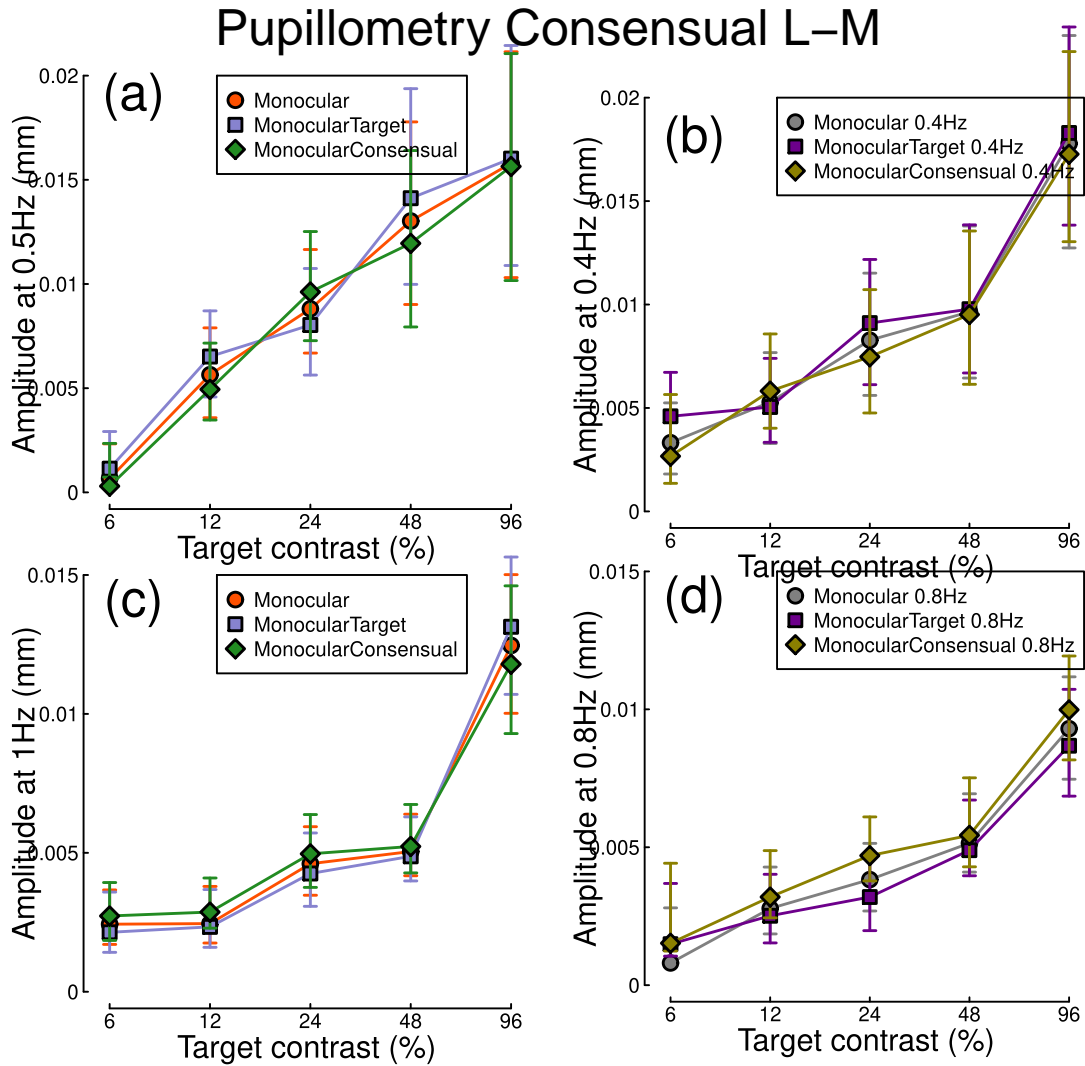
response.



Figure A3.3: Summary of the consensual response for the L-M pathway experiment for N=12 participants. Panel (a) and (b) show contrast response functions at 0.5 and 0.4 Hz respectively. Panels (c) and (d) are in the same format but for the second harmonic responses. Error bars indicate bootstrapped standard errors.

Figure A3.3 shows a summary of the analysis for the L-M pathway experiment. The results are presented in the same way as in Figure A3.1. In general, we observe that all three responses have the same pattern and are similar to each other, showing that targeting the L-M pathway elicits a consensual response.

Figure A3.4 shows a summary of the analysis for the S-(L+M) pathway experiment.The results are presented in the same way as in Figure A3.1. In general, we observe that all three responses have the same pattern and are similar to each other, showing that targeting the S-(L+M) pathway elicits a consensual
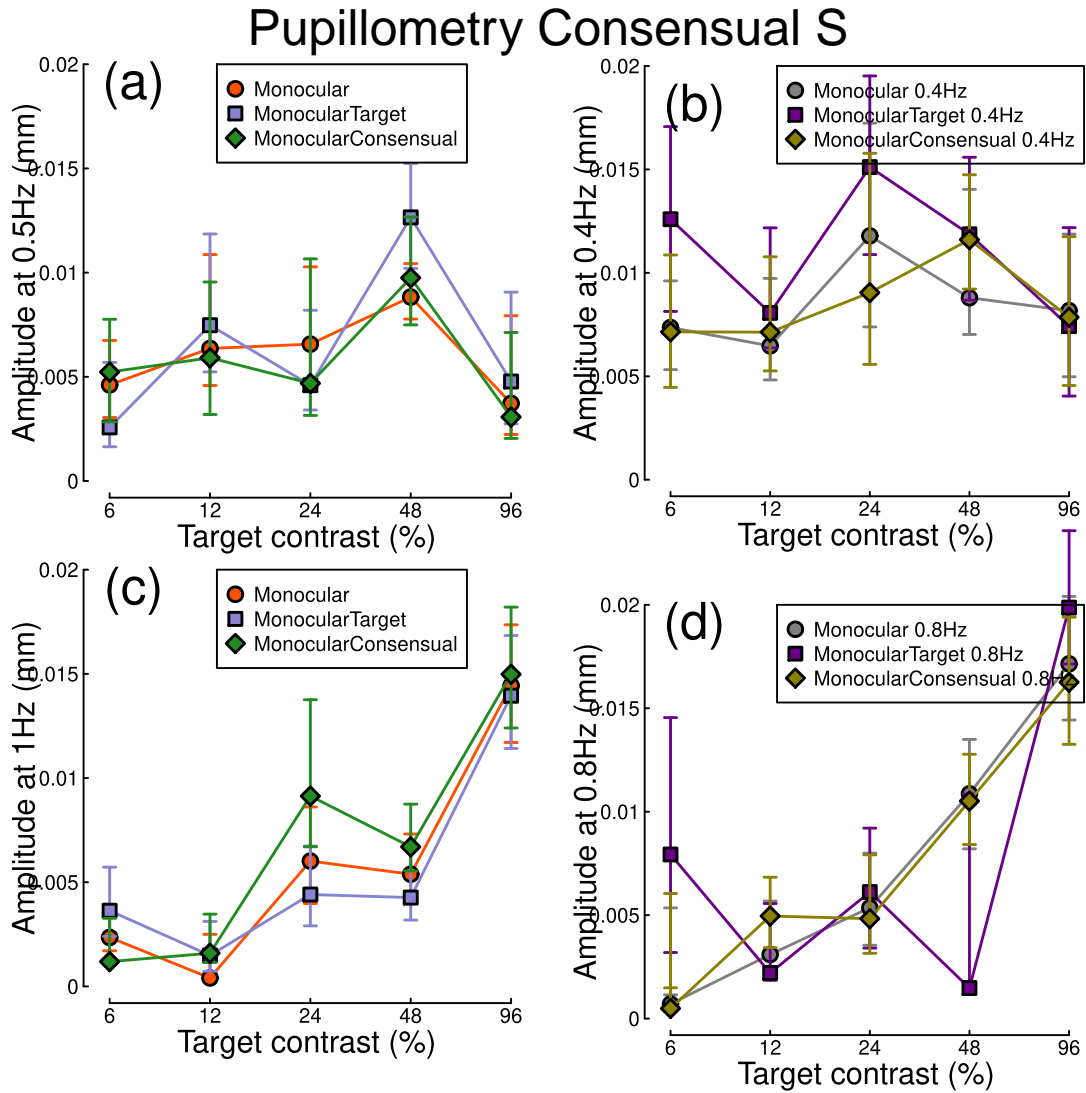
response.



Figure A3.4: Summary of the consensual response for the S-(L+M) pathway experiment for N=12 participants. Panel (a) and (b) show contrast response functions at 0.5 and 0.4 Hz respectively. Panels (c) and (d) are in the same format but for the second harmonic responses. Error bars indicate bootstrapped standard errors.

# Appendix 4: Summary tables of statistical results for Chapter 4

Tables A4.1, A4.2, A4.3, A4.4, A4.5 and A4.6 are summaries of the statistical results for the first harmonic results of the luminance condition presented in Figure 4.3.

Table A4.1: Summary of the statistical results for the monocular, binocular and dichoptic conditions for the luminance experiment results shown in Figure 4.3d.

| Effect | df | F | p value |
| --- | --- | --- | --- |
| Target contrast | 8, 220 | 80.82 | < 0.001 |
| Condition | 2, 220 | 52.88 | < 0.001 |
| Interaction | 8, 220 | 32.69 | < 0.001 |
| Target contrast (dich) | 8, 88 | 23.07 | < 0.001 |

Table A4.2: Summary of the statistical results for the monocular and dichoptic conditions for the luminance experiment results shown in Figure 4.3d.

| Effect | df | F | p value |
| --- | --- | --- | --- |
| Target contrast | 8, 220 | 18.38 | < 0.001 |
| Condition | 2, 220 | 76.13 | < 0.001 |
| Interaction | 8, 220 | 11.93 | < 0.001 |

Table A4.3: Summary of the statistical results for the monocular and binocular cross conditions for the luminance experiment results shown in Figure 4.3e.

| Effect | df | F | p value |
| --- | --- | --- | --- |
| Target contrast | 8, 220 | 75.06 | < 0.001 |
| Condition | 2, 220 | 6.89 | 0.001 |
| Interaction | 8, 220 | 29.51 | < 0.001 |

Table A4.4: Summary of the statistical results for the monocular and dichoptic cross conditions for the luminance experiment results shown in Figure 4.3e.

| Effect | df | F | p value |
| --- | --- | --- | --- |
| Target contrast | 8, 220 | 76.68 | < 0.001 |
| Condition | 2, 220 | 10.76 | < 0.001 |
| Interaction | 8, 220 | 27.52 | < 0.001 |

Table A4.5: Summary of the statistical results for the monocular cross and binocular cross conditions for the luminance experiment results shown in Figure 4.3f.

| Effect | df | F | p value |
|---|---|---|---|
| Target contrast | 8, 220 | 105.85 | < 0.001 |
| Condition | 2, 220 | 4.00 | 0.02 |
| Interaction | 8, 220 | 36.18 | < 0.001 |

Table A4.6: Summary of the statistical results for the monocular cross and dichoptic cross conditions for the luminance experiment results shown in Figure 4.3f.

| Effect | df | F | p value |
|---|---|---|---|
| Target contrast | 8, 220 | 10.09 | < 0.001 |
| Condition | 2, 220 | 15.08 | < 0.001 |
| Interaction | 8, 220 | 35.13 | < 0.001 |

Tables A4.7, A4.8, A4.9, A4.10, A4.11 and A4.12 are summaries of the statistical results for the second harmonic results of the luminance condition presented in Figure 4.3.

Table A4.7: Summary of the statistical results for the monocular, binocular and dichoptic conditions for the luminance experiment results shown in Figure 4.3g.

| Effect | df | F | p value |
|---|---|---|---|
| Target contrast | 8, 220 | 4.42 | < 0.001 |
| Condition | 2, 220 | 4.46 | 0.013 |
| Interaction | 8, 220 | 23.95 | < 0.001 |
| Target contrast (dich) | 8, 88 | 0.70 | 0.694 |

Table A4.8: Summary of the statistical results for the monocular and dichoptic conditions for the luminance experiment results shown in Figure 4.3g.

| Effect | df | F | p value |
|---|---|---|---|
| Target contrast | 8, 220 | 5.16 | < 0.001 |
| Condition | 2, 220 | 290.52 | < 0.001 |
| Interaction | 8, 220 | 23.00 | < 0.001 |

Table A4.9: Summary of the statistical results for the monocular and binocular cross conditions for the luminance experiment results shown in Figure 4.3h.

| Effect | df | F | p value |
|---|---|---|---|
| Target contrast | 8, 220 | 2.04 | 0.043 |
| Condition | 2, 220 | 0.03 | 0.972 |
| Interaction | 8, 220 | 19.54 | < 0.001 |

Table A4.10: Summary of the statistical results for the monocular and dichoptic cross conditions for the luminance experiment results shown in Figure 4.3h.

| Effect | df | F | p value |
|---|---|---|---|
| Target contrast | 8, 220 | 3.21 | 0.002 |
| Condition | 2, 220 | 0.08 | 0.925 |
| Interaction | 8, 220 | 22.10 | < 0.001 |

Table A4.11: Summary of the statistical results for the monocular cross and binocular cross conditions for the luminance experiment results shown in Figure 4.3i.

| Effect | df | F | p value |
|---|---|---|---|
| Target contrast | 8, 220 | 2.78 | 0.006 |
| Condition | 2, 220 | 1.97 | 0.141 |
| Interaction | 8, 220 | 27.69 | < 0.001 |

Table A4.12: Summary of the statistical results for the monocular cross and dichoptic cross conditions for the luminance experiment results shown in Figure 4.3i.

| Effect | df | F | p value |
|---|---|---|---|
| Target contrast | 8, 220 | 1.94 | 0.055 |
| Condition | 2, 220 | 0.30 | 0.744 |
| Interaction | 8, 220 | 28.29 | < 0.001 |

Tables A4.13, A4.14, A4.15, A4.16, A4.17 and A4.18 are summaries of the statistical results for the first harmonic results of the melanopson condition presented in Figure 4.4.

Table A4.13: Summary of the statistical results for the monocular, binocular and dichoptic conditions for the melanopsin experiment results shown in Figure 4.4d.

| Effect | df | F | p value |
|---|---|---|---|
| Target contrast | 8, 220 | 6.35 | < 0.001 |
| Condition | 2, 220 | 1.32 | 0.269 |
| Interaction | 8, 220 | 28.36 | < 0.001 |
| Target contrast (dich) | 8, 88 | 1.04 | 0.41 |

Table A4.14: Summary of the statistical results for the monocular and dichoptic conditions for the melanopsin experiment results shown in Figure 4.4d.

| Effect | df | F | p value |
|---|---|---|---|
| Target contrast | 8, 220 | 3.72 | < 0.001 |
| Condition | 2, 220 | 2.35 | 0.098 |
| Interaction | 8, 220 | 21.41 | < 0.001 |

Table A4.15: Summary of the statistical results for the monocular and binocular cross conditions for the melanopsin experiment results shown in Figure 4.4e.

| Effect | df | F | p value |
|---|---|---|---|
| Target contrast | 8, 220 | 7.74 | < 0.001 |
| Condition | 2, 220 | 0.35 | 0.706 |
| Interaction | 8, 220 | 26.09 | < 0.001 |

Table A4.16: Summary of the statistical results for the monocular and dichoptic cross conditions for the melanopsin experiment results shown in Figure 4.4e.

| Effect | df | F | p value |
|---|---|---|---|
| Target contrast | 8, 220 | 5.64 | < 0.001 |
| Condition | 2, 220 | 0.04 | 0.963 |
| Interaction | 8, 220 | 28.97 | < 0.001 |

Table A4.17: Summary of the statistical results for the monocular cross and binocular cross conditions for the melanopsin experiment results shown in Figure 4.4f.

| Effect | df | F | p value |
|---|---|---|---|
| Target contrast | 8, 220 | 105.85 | < 0.001 |
| Condition | 2, 220 | 4.00 | 0.02 |
| Interaction | 8, 220 | 36.18 | < 0.001 |

Table A4.18: Summary of the statistical results for the monocular cross and dichoptic cross conditions for the melanopsin experiment results shown in Figure 4.4f.

| Effect | df | F | p value |
|---|---|---|---|
| Target contrast | 8, 220 | 10.09 | < 0.001 |
| Condition | 2, 220 | 15.08 | < 0.001 |
| Interaction | 8, 220 | 35.13 | < 0.001 |

Tables A4.19, A4.20, A4.21, A4.22, A4.23 and A4.24 are summaries of the statistical results for the second harmonic results of the melanopsin condition presented in Figure 4.4.

Table A4.19: Summary of the statistical results for the monocular, binocular and dichoptic conditions for the melanopsin experiment results shown in Figure 4.4g.

| Effect | df | F | p value |
|---|---|---|---|
| Target contrast | 8, 220 | 4.97 | < 0.001 |
| Condition | 2, 220 | 6.86 | 0.001 |
| Interaction | 8, 220 | 23.70 | < 0.001 |
| Target contrast (dich) | 8, 88 | 1.62 | 0.132 |

Table A4.20: Summary of the statistical results for the monocular and dichoptic conditions for the melanopsin experiment results shown in Figure 4.4g.

| Effect | df | F | p value |
|---|---|---|---|
| Target contrast | 8, 220 | 1.52 | 0.153 |
| Condition | 2, 220 | 8.77 | < 0.001 |
| Interaction | 8, 220 | 22.84 | < 0.001 |

Table A4.21: Summary of the statistical results for the monocular and binocular cross conditions for the melanopsin experiment results shown in Figure 4.4h.

| Effect | df | F | p value |
|---|---|---|---|
| Target contrast | 8, 220 | 3.36 | 0.001 |
| Condition | 2, 220 | 4.71 | 0.01 |
| Interaction | 8, 220 | 24.34 | < 0.001 |

Table A4.22: Summary of the statistical results for the monocular and dichoptic cross conditions for the melanopsin experiment results shown in Figure 4.4h.

| Effect | df | F | p value |
|---|---|---|---|
| Target contrast | 8, 220 | 2.96 | 0.004 |
| Condition | 2, 220 | 1.80 | 0.168 |
| Interaction | 8, 220 | 20.88 | < 0.001 |

Table A4.23: Summary of the statistical results for the monocular cross and binocular cross conditions for the melanopsin experiment results shown in Figure 4.4i.

| Effect | df | F | p value |
|---|---|---|---|
| Target contrast | 8, 220 | 3.14 | 0.002 |
| Condition | 2, 220 | 6.88 | 0.001 |
| Interaction | 8, 220 | 28.50 | < 0.001 |

Table A4.24: Summary of the statistical results for the monocular cross and dichoptic cross conditions for the melanopsin experiment results shown in Figure 4.4i.

| Effect | df | F | p value |
|---|---|---|---|
| Target contrast | 8, 220 | 1.56 | 0.139 |
| Condition | 2, 220 | 2.11 | 0.124 |
| Interaction | 8, 220 | 29.19 | < 0.001 |

Tables A4.25, A4.26, A4.27, A4.28, A4.29 and A4.30 are summaries of the statistical results for the first harmonic results of the L-M pathway condition presented in Figure 4.5.

Table A4.25: Summary of the statistical results for the monocular, binocular and dichoptic conditions for the L-M pathway experiment results shown in Figure 4.5d.

| Effect | df | F | p value |
|---|---|---|---|
| Target contrast | 8, 220 | 7.66 | < 0.001 |
| Condition | 2, 220 | 6.13 | 0.003 |
| Interaction | 8, 220 | 43.36 | < 0.001 |
| Target contrast (dich) | 8, 88 | 0.64 | 0.744 |

Table A4.26: Summary of the statistical results for the monocular and dichoptic conditions for the L-M pathway experiment results shown in Figure 4.5d.

| Effect | df | F | p value |
|---|---|---|---|
| Target contrast | 8, 220 | 2.24 | 0.026 |
| Condition | 2, 220 | 2.30 | 0.102 |
| Interaction | 8, 220 | 22.15 | < 0.001 |

Table A4.27: Summary of the statistical results for the monocular and binocular cross conditions for the L-M pathway experiment results shown in Figure 4.5e.

| Effect | df | F | p value |
|---|---|---|---|
| Target contrast | 8, 220 | 4.07 | < 0.001 |
| Condition | 2, 220 | 8.51 | < 0.001 |
| Interaction | 8, 220 | 33.34 | < 0.001 |

Table A4.28: Summary of the statistical results for the monocular and dichoptic cross conditions for the L-M pathway experiment results shown in Figure 4.5e.

| Effect | df | F | p value |
|---|---|---|---|
| Target contrast | 8, 220 | 7.24 | < 0.001 |
| Condition | 2, 220 | 9.15 | < 0.001 |
| Interaction | 8, 220 | 36.54 | < 0.001 |

Table A4.29: Summary of the statistical results for the monocular cross and binocular cross conditions for the L-M pathway experiment results shown in Figure 4.5f.

| Effect | df | F | p value |
|---|---|---|---|
| Target contrast | 8, 220 | 105.85 | < 0.001 |
| Condition | 2, 220 | 4.00 | 0.02 |
| Interaction | 8, 220 | 36.18 | < 0.001 |

Table A4.30: Summary of the statistical results for the monocular cross and dichoptic cross conditions for the L-M pathway experiment results shown in Figure 4.5f.

| Effect | df | F | p value |
|---|---|---|---|
| Target contrast | 8, 220 | 10.09 | < 0.001 |
| Condition | 2, 220 | 15.08 | < 0.001 |
| Interaction | 8, 220 | 35.13 | < 0.001 |

Tables A4.31, A4.32, A4.33, A4.34, A4.35 and A4.36 are summaries of the statistical results for the second harmonic results of the L-M pathway condition presented in Figure 4.5.

Table A4.31: Summary of the statistical results for the monocular, binocular and dichoptic conditions for the L-M pathway experiment results shown in Figure 4.5g.

| Effect | df | F | p value |
|---|---|---|---|
| Target contrast | 8, 220 | 18.66 | < 0.001 |
| Condition | 2, 220 | 9.76 | < 0.001 |
| Interaction | 8, 220 | 38.76 | < 0.001 |
| Target contrast (dich) | 8, 88 | 5.15 | < 0.001 |

Table A4.32: Summary of the statistical results for the monocular and dichoptic conditions for the L-M pathway experiment results shown in Figure 4.5g.

| Effect | df | F | p value |
|---|---|---|---|
| Target contrast | 8, 220 | 1.35 | 0.219 |
| Condition | 2, 220 | 10.09 | < 0.001 |
| Interaction | 8, 220 | 22.70 | < 0.001 |

Table A4.33: Summary of the statistical results for the monocular and binocular cross conditions for the L-M pathway experiment results shown in Figure 4.5h.

| Effect | df | F | p value |
|---|---|---|---|
| Target contrast | 8, 220 | 12.09 | < 0.001 |
| Condition | 2, 220 | 2.51 | 0.084 |
| Interaction | 8, 220 | 29.13 | < 0.001 |

Table A4.34: Summary of the statistical results for the monocular and dichoptic cross conditions for the L-M pathway experiment results shown in Figure 4.5h.

| Effect | df | F | p value |
|---|---|---|---|
| Target contrast | 8, 220 | 18.86 | < 0.001 |
| Condition | 2, 220 | 2.02 | 0.135 |
| Interaction | 8, 220 | 42.77 | < 0.001 |

Table A4.35: Summary of the statistical results for the monocular cross and binocular cross conditions for the L-M pathway experiment results shown in Figure 4.5i.

| Effect | df | F | p value |
|---|---|---|---|
| Target contrast | 8, 220 | 5.10 | < 0.001 |
| Condition | 2, 220 | 3.42 | 0.035 |
| Interaction | 8, 220 | 25.72 | < 0.001 |

Table A4.36: Summary of the statistical results for the monocular cross and dichoptic cross conditions for the L-M pathway experiment results shown in Figure 4.5i.

| Effect | df | F | p value |
|---|---|---|---|
| Target contrast | 8, 220 | 0.51 | 0.851 |
| Condition | 2, 220 | 0.65 | 0.522 |
| Interaction | 8, 220 | 18.95 | < 0.001 |

Tables A4.37, A4.38, A4.39, A4.40, A4.41 and A4.42 are summaries of the statistical results for the first harmonic results of the S-(L+M) pathway condition presented in Figure 4.6.

Table A4.37: Summary of the statistical results for the monocular, binocular and dichoptic conditions for the S-(L+M) pathway experiment results shown in Figure 4.6d.

| Effect | df | F | p value |
|---|---|---|---|
| Target contrast | 8, 220 | 2.03 | 0.044 |
| Condition | 2, 220 | 0.87 | 0.42 |
| Interaction | 8, 220 | 19.21 | < 0.001 |
| Target contrast (dich) | 8, 88 | 1.73 | 0.102 |

Table A4.38: Summary of the statistical results for the monocular and dichoptic conditions for the S-(L+M) pathway experiment results shown in Figure 4.6d.

| Effect | df | F | p value |
|---|---|---|---|
| Target contrast | 8, 220 | 1.27 | 0.26 |
| Condition | 2, 220 | 5.50 | 0.005 |
| Interaction | 8, 220 | 15.62 | < 0.001 |

Table A4.39: Summary of the statistical results for the monocular and binocular cross conditions for the S-(L+M) pathway experiment results shown in Figure 4.6e.

| Effect | df | F | p value |
|---|---|---|---|
| Target contrast | 8, 220 | 0.45 | 0.89 |
| Condition | 2, 220 | 0.12 | 0.886 |
| Interaction | 8, 220 | 20.28 | < 0.001 |

Table A4.40: Summary of the statistical results for the monocular and dichoptic cross conditions for the S-(L+M) pathway experiment results shown in Figure 4.6e.

| Effect | df | F | p value |
|---|---|---|---|
| Target contrast | 8, 220 | 2.92 | 0.004 |
| Condition | 2, 220 | 2.54 | 0.081 |
| Interaction | 8, 220 | 19.79 | < 0.001 |

Table A4.41: Summary of the statistical results for the monocular cross and binocular cross conditions for the S-(L+M) pathway experiment results shown in Figure 4.6f.

| Effect | df | F | p value |
|---|---|---|---|
| Target contrast | 8, 220 | 105.85 | < 0.001 |
| Condition | 2, 220 | 4.00 | 0.02 |
| Interaction | 8, 220 | 36.18 | < 0.001 |

Table A4.42: Summary of the statistical results for the monocular cross and dichoptic cross conditions for the S-(L+M) pathway experiment results shown in Figure 4.6f.

| Effect | df | F | p value |
|---|---|---|---|
| Target contrast | 8, 220 | 10.09 | < 0.001 |
| Condition | 2, 220 | 15.08 | < 0.001 |
| Interaction | 8, 220 | 35.13 | < 0.001 |

Tables A4.43, A4.44, A4.45, A4.46, A4.47 and A4.48 are summaries of the statistical results for the second harmonic results of the S-(L+M) pathway condition presented in Figure 4.6.

Table A4.43: Summary of the statistical results for the monocular, binocular and dichoptic conditions for the S-(L+M) pathway experiment results shown in Figure 4.6g.

| Effect | df | F | p value |
|---|---|---|---|
| Target contrast | 8, 220 | 10.81 | < 0.001 |
| Condition | 2, 220 | 3.89 | 0.022 |
| Interaction | 8, 220 | 27.36 | < 0.001 |
| Target contrast (dich) | 8, 88 | 1.17 | 0.324 |

Table A4.44: Summary of the statistical results for the monocular and dichoptic conditions for the S-(L+M) pathway experiment results shown in Figure 4.6g.

| Effect | df | F | p value |
|---|---|---|---|
| Target contrast | 8, 220 | 2.64 | 0.009 |
| Condition | 2, 220 | 64.64 | < 0.001 |
| Interaction | 8, 220 | 27.96 | < 0.001 |

Table A4.45: Summary of the statistical results for the monocular and binocular cross conditions for the S-(L+M) pathway experiment results shown in Figure 4.6h.

| Effect | df | F | p value |
| --- | --- | --- | --- |
| Target contrast | 8, 220 | 7.01 | < 0.001 |
| Condition | 2, 220 | 1.89 | 0.154 |
| Interaction | 8, 220 | 30.28 | < 0.001 |

Table A4.46: Summary of the statistical results for the monocular and dichoptic cross conditions for the S-(L+M) pathway experiment results shown in Figure 4.6h.

| Effect | df | F | p value |
| --- | --- | --- | --- |
| Target contrast | 8, 220 | 10.11 | < 0.001 |
| Condition | 2, 220 | 2.34 | 0.099 |
| Interaction | 8, 220 | 34.59 | < 0.001 |

Table A4.47: Summary of the statistical results for the monocular cross and binocular cross conditions for the S-(L+M) pathway experiment results shown in Figure 4.6i.

| Effect | df | F | p value |
| --- | --- | --- | --- |
| Target contrast | 8, 220 | 5.68 | < 0.001 |
| Condition | 2, 220 | 3.09 | 0.048 |
| Interaction | 8, 220 | 18.97 | < 0.001 |

Table A4.48: Summary of the statistical results for the monocular cross and dichoptic cross conditions for the S-(L+M) pathway experiment results shown in Figure 4.6i.

| Effect | df | F | p value |
| --- | --- | --- | --- |
| Target contrast | 8, 220 | 1.07 | 0.383 |
| Condition | 2, 220 | 2.19 | 0.114 |
| Interaction | 8, 220 | 28.97 | < 0.001 |

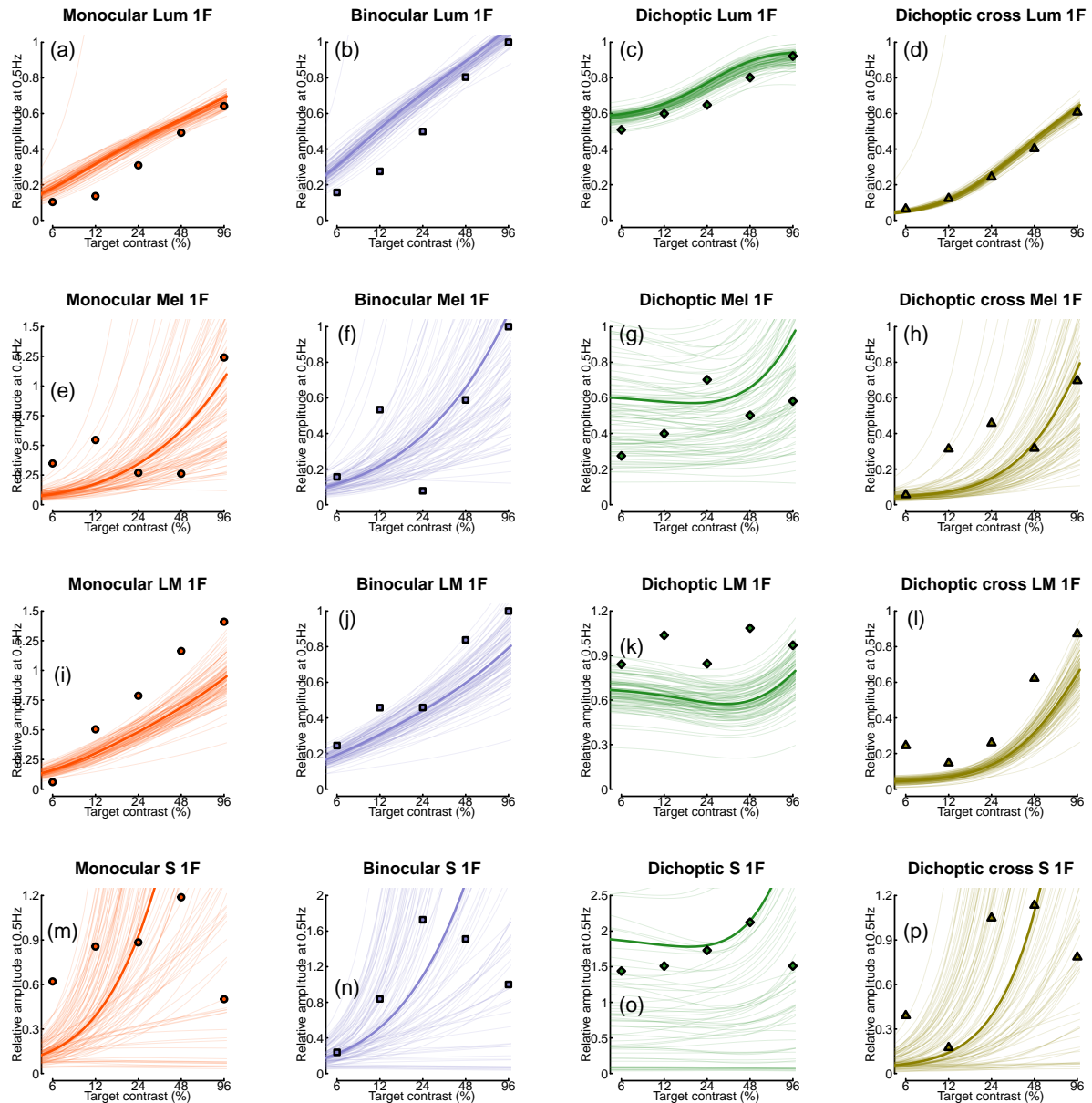# Appendix 5: Fit examples using computational model from Chapter 4



Figure A5.1: Summary of fit examples for the results at the first harmonic frequency. Panels (a-d) show empirical data for the luminance experiment for the monocular, binocular, dichoptic and cross-frequency dichoptic configuration respectively. Panels (e-h) show empirical data for the melanopsin experiment for the monocular, binocular, dichoptic and cross-frequency dichoptic configuration respectively. Panels (i-l) show empirical data for the L-M pathway experiment for the monocular, binocular, dichoptic and cross-frequency dichoptic configuration respectively. Panels (m-p) show empirical data for the S-(L+M) pathway experiment for the monocular, binocular, dichoptic and cross-frequency dichoptic configuration respectively. The bold curves show model behaviour generated using the median group-level parameter values and are the same as the ones in Figures 4.7a-d. The shaded lines show the model behaviour for other 100 instances.
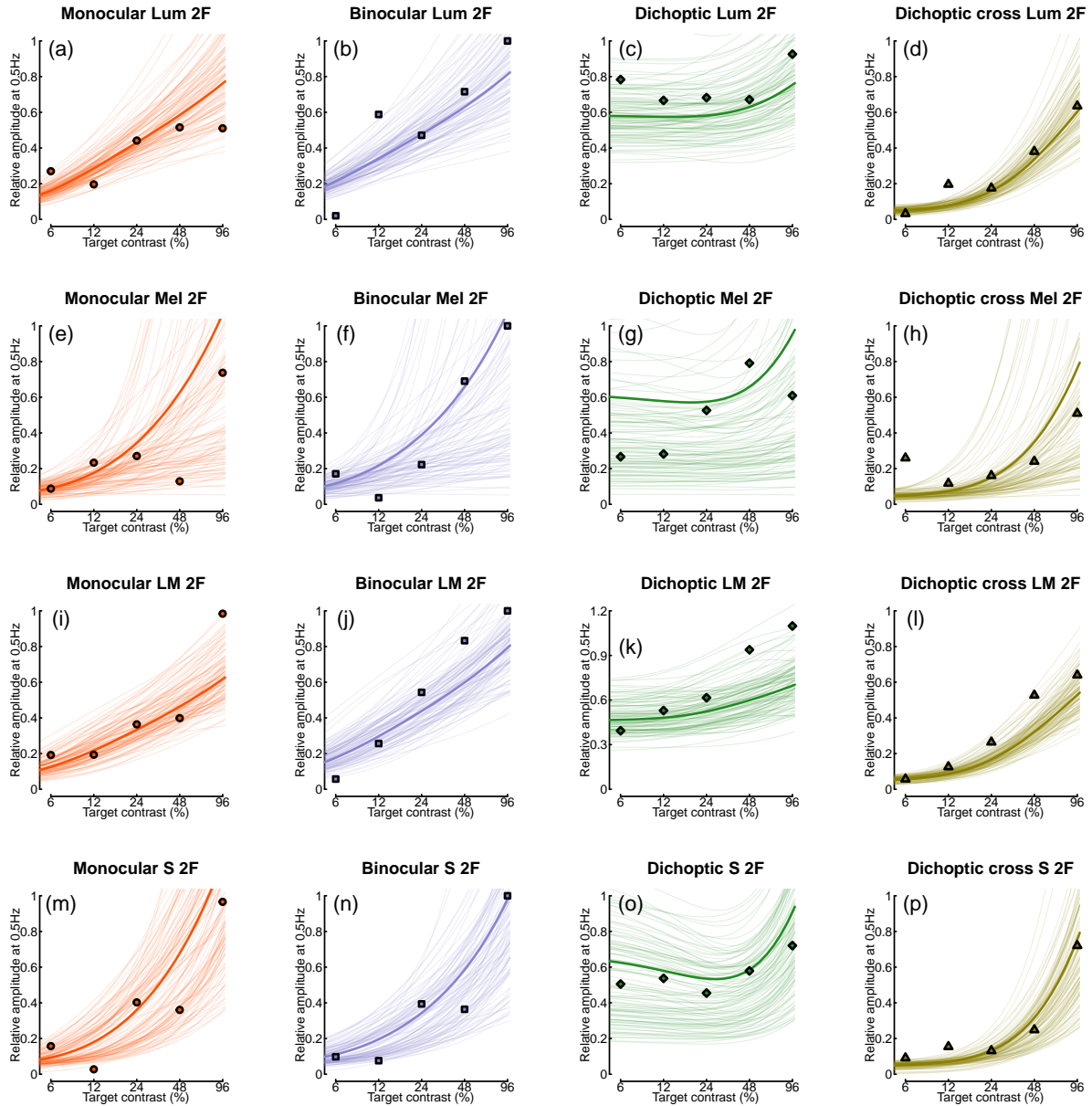
Figure A5.2: Summary of fit examples for the results at the second harmonic frequency. Panels (a-d) show empirical data for the luminance experiment for the monocular, binocular, dichoptic and cross-frequency dichoptic configuration respectively. Panels (e-h) show empirical data for the melanopsin experiment for the monocular, binocular, dichoptic and cross-frequency dichoptic configuration respectively. Panels (i-l) show empirical data for the L-M pathway experiment for the monocular, binocular, dichoptic and cross-frequency dichoptic configuration respectively. Panels (m-p) show empirical data for the S-(L+M) pathway experiment for the monocular, binocular, dichoptic and cross-frequency dichoptic configuration respectively. The bold curves show model behaviour generated using the median group-level parameter values and are the same as the ones in Figures 4.7f-i. The shaded lines show the model behaviour for other 100 instances.

135

# References

Anderson PA, Movshon JA. 1989. Binocular combination of contrast signals. *Vision Res* **29**:1115–32. doi:10.1016/0042-6989(89)90060-6

Andersson JLR, Jenkinson M, Smith S. 2007a. Non-linear optimisation (FMRIB Technical Report TR07JA1).

Andersson JLR, Jenkinson M, Smith S. 2007b. Non-linear registration, aka spatial normalisation (FMRIB Technical Report TR07JA2).

Angée C, Nedelec B, Erjavec E, Rozet J-M, Fares Taie L. 2021. Congenital microcoria: Clinical features and molecular genetics. *Genes (Basel)* **12**. doi:10.3390/genes12050624

Anstis S, Ho A. 1998. Nonlinear combination of luminance excursions during flicker, simultaneous contrast, afterimages and binocular fusion. *Vision Res* **38**:523–39. doi:10.1016/s0042-6989(97)00167-3

Anstis SM, Cavanagh P. 1983. A minimum motion technique for judging equiluminance. York University.

Apkarian PA, Nakayama K, Tyler CW. 1981. Binocularity in the human visual evoked potential: Facilitation, summation and suppression. *Electroencephalogr Clin Neurophysiol* **51**:32–48. doi:10.1016/0013-4694(81)91507-8

Baitch LW, Levi DM. 1988. Evidence for nonlinear binocular interactions in human visual cortex. *Vision Res* **28**:1139–43. doi:10.1016/0042-6989(88)90140-x

Baker DH. 2021. Statistical analysis of periodic data in neuroscience. *Neurons, Behavior, Data analysis, and Theory* **5**. doi:10.51628/001c.27680

Baker DH, Lygo FA, Meese TS, Georgeson MA. 2018. Binocular summation revisited: Beyond $\sqrt{2}$. *Psychol Bull* **144**:1186–1199. doi:10.1037/bul0000163

Baker DH, Meese TS, Georgeson MA. 2007. Binocular interaction: Contrast matching and contrast discrimination are predicted by the same model. *Spat Vis* **20**:397–413. doi:10.1163/156856807781503622

Baker DH, Vilidaite G, McClarnon E, Valkova E, Bruno A, Millman RE. 2020. Binaural summation of amplitude modulation involves weak interaural suppression. *Sci Rep* **10**:3560. doi:10.1038/s41598-020-60602-5

Baker DH, Vilidaite G, Wade AR. 2021. Steady-state measures of visual suppression. *PLOS Computational Biology* **17**:e1009507. doi:10.1371/journal.pcbi.1009507

Baker DH, Wade AR. 2017. Evidence for an optimal algorithm underlying signal combination in human visual cortex. *Cereb Cortex* **27**:254–264. doi:10.1093/cercor/bhw395

Baker DH, Wallis SA, Georgeson MA, Meese TS. 2012. Nonlinearities in the binocular combination of luminance and contrast. *Vision Research* **56**:1–9. doi:10.1016/j.visres.2012.01.008

Barrionuevo PA, Cao D. 2016. Luminance and chromatic signals interact differently with melanopsin activation to control the pupil light response. *Journal of Vision* **16(11)**:29. doi:10.1167/16.11.29

Barrionuevo PA, McAnany JJ, Zele AJ, Cao D. 2018. Non-linearities in the Rod and Cone Photoreceptor Inputs to the Afferent Pupil Light Response. *Frontiers in Neurology* **9**.

Barrionuevo PA, Nicandro N, McAnany JJ, Zele AJ, Gamlin P, Cao D. 2014. Assessing rod, cone, and melanopsin contributions to human pupil flicker responses. *Investigative Ophthalmology & Visual Science* **55**:719–27. doi:10.1167/iovs.13-13252

Beckmann CF, Jenkinson M, Smith SM. 2003. General multilevel linear modeling for group analysis in fmri. *NeuroImage* **20**:1052–63. doi:10.1016/S1053-8119(03)00435-X.

Bergamin O, Kardon RH. 2003. Latency of the pupil light reflex: Sample rate, stimulus intensity, and variation in normal subjects. *Investigative Ophthalmology & Visual Science* **44**:1546–1554.

Binda P, Murray SO. 2015. Keeping a large-pupilled eye on high-level visual processing. *Trends in Cognitive Sciences* **19**:1–3.

Binda P, Pereverzeva M, Murray SO. 2013. Attention to bright surfaces enhances the pupillary light reflex. *Journal of Neuroscience* **33**:2199–2204.

Blake R, Wilson H. 2011. Binocular vision. *Vision Research* **51**:754–770.

Bradley MM, Miccoli L, Escrig MA, Lang PJ. 2008. The pupil as a measure of emotional arousal and autonomic activation. *Psychophysiology* **45**:602–7. doi:10.1111/j.1469-8986.2008.00654.x

Bruyns-Haylett M, Luo J, Kennerley AJ, Harris S, Boorman L, Milne E, Vautrelle N, Hayashi Y, Whalley BJ, Jones M, Berwick J, Riera J, Zheng Y. 2017. The neurogenesis of p1 and n1: A concurrent eeg/lfp study. *NeuroImage* **146**:575–588. doi:https://doi.org/10.1016/j.neuroimage.2016.09.034

Busse L, Wade AR, Carandini M. 2009. Representation of concurrent stimuli by population activity in visual cortex. *Neuron* **64**:931–942. doi:10.1016/j.neuron.2009.11.004

Buxton RB. 2013. The physics of functional magnetic resonance imaging (fMRI). *Reports on Progress in Physics* **76**:096601. doi:10.1088/0034-4885/76/9/096601

Campbell FW, Green DG. 1965. Monocular versus binocular visual acuity. *Nature* **208**:191–2. doi:10.1038/208191a0

Cao D, Nicandro N, Barrionuevo PA. 2015. A five-primary photostimulator suitable for studying intrinsically photosensitive retinal ganglion cell functions in humans. *Journal of Vision* **15**:27. doi:10.1167/15.1.27

Carpenter B, Gelman A, Hoffman MD, Lee D, Goodrich B, Betancourt M, Brubaker M, Guo J, Li P, Riddell A. 2017. Stan: A probabilistic programming language. *Journal of Statistical Software* **76**:1–32. doi:10.18637/jss.v076.i01

Carroll J, Neitz J, Neitz M. 2002. Estimates of L:M cone ratio from ERG flicker photometry and genetics. *Journal of Vision* **2**:1. doi:10.1167/2.8.1

Cavanagh P, MacLeod DIA, Anstis SM. 1987. Equiluminance: Spatial and temporal factors and the contribution of blue-sensitive cones. *Journal of the Optical Society of America: A* **4**:1428–38.

Czeisler CA, Shanahan TL, Klerman EB, Martens H, Brotman DJ, Emens JS, Klein T, Rizzo JF. 1995. Suppression of melatonin secretion in some blind patients by exposure to bright light. *New England Journal of Medicine* **332**:6–11. doi:10.1056/nejm199501053320102

Dacey DM, Liao H-W, Peterson BB, Robinson FR, Smith VC, Pokorny J, Yau K-W, Gamlin PD. 2005. Melanopsin-expressing ganglion cells in primate retina signal colour and irradiance and project to the LGN. *Nature* **433**:749–754. doi:10.1038/nature03387

Dacey DM, Peterson BB, Robinson FR, Gamlin PD. 2003. Fireworks in the primate retina: In vitro photodynamics reveals diverse lgn-projecting ganglion cell types. *Neuron* **37**:15–27. doi:https://doi.org/10.1016/S0896-6273(02)01143-1

Delorme A, Makeig S. 2004. EEGLAB: An open source toolbox for analysis of single-trial EEG dynamics including independent component analysis. *J Neurosci Methods* **134**:9–21. doi:10.1016/j.jneumeth.2003.10.009

Denny N, Frumkes TE, Barris MC, Eysteinsson T. 1991. Tonic interocular suppression and binocular summation in human vision. *The Journal of Physiology* **437**:449–460.

Ding J, Sperling G. 2006. A gain-control theory of binocular combination. *Proc Natl Acad Sci U S A* **103**:1141–6. doi:10.1073/pnas.0509629103

Doesschate J ten, Alpern M. 1967. Effect of photoexcitation of the two retinas on pupil size. *Journal of Neurophysiology* **30**:562–76. doi:10.1152/jn.1967.30.3.562

Dougherty K, Cox MA, Westerberg JA, Maier A. 2019. Binocular modulation of monocular v1 neurons. *Curr Biol* **29**:381–391.e4. doi:10.1016/j.cub.2018.12.004

Economides JR, Sincich LC, Adams DL, Horton JC. 2011. Orientation tuning of cytochrome oxidase patches in macaque primary visual cortex. *Nat Neurosci* **14**:1574–80. doi:10.1038/nn.2958

Edwards DP, Purpura KP, Kaplan E. 1995. Contrast sensitivity and spatial frequency response of primate cortical neurons in and around the cytochrome oxidase blobs. *Vision Res* **35**:1501–23. doi:10.1016/0042-6989(94)00253-i

Ellis CJ. 1981. The pupillary light reflex in normal subjects. *British Journal of Ophthalmology* **65**:754–759.

Ernst MO, Banks MS. 2002. Humans integrate visual and haptic information in a statistically optimal fashion. *Nature* **415**:429–33. doi:10.1038/415429a

Estévez O, Spekreijse H. 1982. The "silent substitution" method in visual research. *Vision Research* **22**:681–691. doi:10.1016/0042-6989(82)90104-3

Fabius JH, Mathôt S, Schut MJ, Nijboer TCW, Stigchel SV. 2017. Focus of spatial attention during spatial working memory maintenance: Evidence from pupillary light response. *Visual Cognition* **25**:10–20.

Figueira JSB, Kutlu E, Scott LS, Keil A. 2022. The freqtag toolbox: A principled approach to analyzing electrophysiological time series in frequency tagging paradigms. *Dev Cogn Neurosci* **54**:101066. doi:10.1016/j.dcn.2022.101066

Flitcroft DI, Judge SJ, Morley JW. 1992. Binocular interactions in accommodation control: Effects of anisometropic stimuli. *J Neurosci* **12**:188–203. doi:10.1523/JNEUROSCI.12-01-00188.1992

Freedman MS, Lucas RJ, Soni B, Schantz M von, Muñoz M, David-Gray Z, Foster R. 1999. Regulation of mammalian circadian behavior by non-rod, non-cone, ocular photoreceptors. *Science* **284**:502–504. doi:10.1126/science.284.5413.502

Fu Z, Hong H, Su Z, Lou B, Pan C-W, Liu H. 2020. Global prevalence of amblyopia and disease burden projections through 2040: A systematic review and meta-analysis. *British Journal of Ophthalmology* **104**:1164–1170. doi:10.1136/bjophthalmol-2019-314759

Gamlin PDR, McDougal DH, Pokorny J, Smith VC, Yau K-W, Dacey DM. 2007. Human and macaque pupil responses driven by melanopsin-containing retinal ganglion cells. *Vision Research* **47**:946–954. doi:10.1016/j.visres.2006.12.015

Gheiratmand M, Meese TS, Mullen KT. 2013. Blobs versus bars: Psychophysical evidence supports two types of orientation response in human color vision. *Journal of Vision* **13(1)**:2. doi:10.1167/13.1.2

Glover GH. 2011. Overview of functional magnetic resonance imaging. *Neurosurgery Clinics of North America* **22**:133–139. doi:https://doi.org/10.1016/j.nec.2010.11.001

Greve DN, Fischl B. 2009. Accurate and robust brain image alignment using boundary-based registration. *NeuroImage* **48**:63–72. doi:10.1016/j.neuroimage.2009.06.060.

Heeger DJ. 1992. Normalization of cell responses in cat striate cortex. *Visual Neuroscience* **9**:181–197.

Hess EH, Polt JM. 1964. Pupil size in relation to mental activity during simple problem-solving. *Science* **143**:1190–1192. doi:10.1126/science.143.3611.1190

Hess EH, Polt JM. 1960. Pupil size as related to interest value of visual stimuli. *Science* **132**:349–350. doi:10.1126/science.132.3423.349

Hess RF, Mansouri B, Thompson B. 2010. A new binocular approach to the treatment of amblyopia in adults well beyond the critical period of visual development. *Restorative neurology and neuroscience* **28**:793–802. doi:10.3233/RNN-2010-0550

Hofer H, Carroll J, Neitz J, Neitz M, Williams DR. 2005. Organization of the human trichromatic cone mosaic. *The Journal of Neuroscience* **25**:9669–9679. doi:10.1523/jneurosci.2414-05.2005

Horton JC, Hubel DH. 1981. Regular patchy distribution of cytochrome oxidase staining in primary visual cortex of macaque monkey. *Nature* **292**:762–4. doi:10.1038/292762a0

Hubel DH, Wiesel TN. 1962. Receptive fields, binocular interaction and functional architecture in the cat's visual cortex. *J Physiol* **160**:106–54. doi:10.1113/jphysiol.1962.sp006837

Jenkinson M. 2003. Fast, automated, n-dimensional phase-unwrapping algorithm. *Magnetic Resonance in Medicine* **49**:193–97. doi:10.1002/mrm.10354.

Jenkinson M. 2001. Improved unwarping of epi images using regularised b0 maps. *NeuroImage* **13**. doi:10.1016/s1053-8119(01)91508-3.

Jenkinson M, Bannister P, Brady M, Smith S. 2002. Improved optimization for the robust and accurate linear registration and motion correction of brain images. *NeuroImage* **17**:825–41. doi:10.1006/nimg.2002.1132.

Jenkinson M, Beckmann CF, Behrens TEJ, Woolrich MW, Smith SM. 2012. FSL. *NeuroImage* **62**:782–90. doi:10.1016/j.neuroimage.2011.09.015

Jenkinson M, Smith S. 2001. A global optimisation method for robust affine registration of brain images. *Medical Image Analysis* **5**:143–56. doi:10.1016/S1361-8415(01)00036-6.

Jezzard P, Balaban RS. 1995. Correction for geometric distortion in echo planar images from b0 field variations. *Magnetic Resonance in Medicine* **34**:65–73. doi:10.1002/mrm.1910340111.

Kahneman D, Beatty J. 1966. Pupil diameter and load on memory. *Science* **154**:1583–1585. doi:10.1126/science.154.3756.1583

Kassner M, Patera W, Bulling A. 2014. Pupil: An open source platform for pervasive eye tracking and mobile gaze-based interaction.Proceedings of the 2014 ACM International Joint Conference on Pervasive and Ubiquitous Computing: Adjunct Publication. UbiComp '14 Adjunct; ACM. pp. 1151–1160. doi:10.1145/2638728.2641695

Kim S-G, Richter W, U??urbil K. 1997. Limitations of temporal resolution in functional MRI. *Magnetic Resonance in Medicine* **37**:631–636. doi:10.1002/mrm.1910370427

Kingdom FAA, Libenson L. 2015. Dichoptic color saturation mixture: Binocular luminance contrast promotes perceptual averaging. *J Vis* **15(5)**:2. doi:10.1167/15.5.2

Koss MC. 1986. Pupillary dilation as an index of central nervous system $\alpha$2-adrenoceptor activation. *Journal of Pharmacological Methods* **15**:1–19.

Laeng B, Sirois S, Gredebäck G. 2012. Pupillometry: A window to the preconscious? *Perspectives on Psychological Science* **7**:18–27. doi:10.1177/1745691611427305

Legge GE. 1984. Binocular contrast summation–ii. Quadratic summation. *Vision Res* **24**:385–94. doi:10.1016/0042-6989(84)90064-6

Legge GE, Rubin GS. 1981. Binocular interactions in suprathreshold contrast perception. *Percept Psychophys* **30**:49–61. doi:10.3758/bf03206136

Levelt WJ. 1965. Binocular brightness averaging and contour information. *Br J Psychol* **56**:1–13. doi:10.1111/j.2044-8295.1965.tb00939.x

Li Z, Atick JJ. 1994. Efficient stereo coding in the multiscale representation. *Network: Computation in Neural Systems* **5**:157–174. doi:10.1088/0954-898X_5_2_003

Livingstone MS, Hubel DH. 1984. Anatomy and physiology of a color system in the primate visual cortex. *J Neurosci* **4**:309–56. doi:10.1523/JNEUROSCI.04-01-00309.1984

Lockley SW, Skene DJ, Arendt J, Tabandeh H, Bird AC, Defrance R. 1997. Relationship between melatonin rhythms and visual loss in the blind. *The Journal of Clinical Endocrinology & Metabolism* **82**:3763–3770. doi:10.1210/jcem.82.11.4355

Lucas RJ, Hattar S, Takao M, Berson DM, Foster RG, Yau K-W. 2003. Diminished pupillary light reflex at high irradiances in melanopsin-knockout mice. *Science* **299**:245–247. doi:10.1126/science.1077293

Lygo FA, Richard B, Wade AR, Morland AB, Baker DH. 2021. Neural markers of suppression in impaired binocular vision. *NeuroImage* **230**:117780. doi:10.1016/j.neuroimage.2021.117780

Markwell EL, Feigl B, Zele AJ. 2010. Intrinsically photosensitive melanopsin retinal ganglion cell contributions to the pupillary light reflex and circadian rhythm. *Clinical and Experimental Optometry* **93**:137–149. doi:10.1111/j.1444-0938.2010.00479.x

Martin JT, Boynton GM, Baker DH, Wade AR, Spitschan M. 2023. PySilSub: An open-source python toolbox for implementing the method of silent substitution in vision and nonvisual photoreception research. *Journal of Vision* **23**:10. doi:10.1167/jov.23.7.10

Martin JT, Pinto J, Bulte D, Spitschan M. 2022. PyPlr: A versatile, integrated system of hardware and software for researching the human pupillary light reflex. *Behavior Research Methods* **54**:2720–2739. doi:10.3758/s13428-021-01759-3

Mathôt S. 2018. Pupillometry: Psychology, physiology, and function. *Journal of Cognition* **1**:16. doi:10.5334/joc.18

Mathôt S, Grainger J, Strijkers K. 2017. Pupillary responses to words that convey a sense of brightness or darkness. *Psychological Science* **28**:1116–1124.

May K, Zhaoping L. 2022. Li and Atick's theory of efficient binocular coding: A tutorial and mini-review. *Vision Res* **201**:107950. doi:10.1016/j.visres.2021.08.005

Mazziotta J, Toga A, Evans A, Fox P, Lancaster J, Zilles K, Woods R, Paus T, Simpson G, Pike B, Holmes C, Collins L, Thompson P, MacDonald D, Iacoboni M, Schormann T, Amunts K, Palomero-Gallagher N, Geyer S, Parsons L, Narr K, Kabani N, Goualher G, Boomsma D, Cannon T, Kawashima R, Mazoyer B. 2001. A probabilistic atlas and reference system for the human brain: International consortium for brain mapping (icbm. *Philosophical Transactions of the Royal Society B: Biological Sciences* **356**:1293–1322. doi:10.1098/rstb.2001.0915.

McDougal DH, Gamlin PD. 2015. Autonomic control of the eye. *Comprehensive Physiology* **5**:439–473. doi:10.1002/cphy.c140014

McDougal DH, Gamlin PD. 2010. The influence of intrinsically-photosensitive retinal ganglion cells on the spectral sensitivity and response dynamics of the human pupillary light reflex. *Vision Research* **50**:72–87. doi:10.1016/j.visres.2009.10.012

McDougal DH, Gamlin PD. 2008. Pupillary control pathways In: Masland RH, Albright TD, Albright TD, Masland RH, Dallos P, Oertel D, Gardner EP, editors. The Senses: A Comprehensive Reference. New York: Academic Press. pp. 521–536.

Meese TS, Baker DH. 2011. A reevaluation of achromatic spatio-temporal vision: Nonoriented filters are monocular, they adapt, and can be used for decision making at high flicker speeds. *iPerception* **2**:159–82. doi:10.1068/i0416

Meese TS, Georgeson MA, Baker DH. 2006. Binocular contrast vision at and above threshold. *Journal of Vision* **6**:1224–43. doi:10.1167/6.11.7

Meese TS, Summers RJ. 2007. Area summation in human vision at and above detection threshold. *Proc Biol Sci* **274**:2891–900. doi:10.1098/rspb.2007.0957

Moradi F, Heeger DJ. 2009. Inter-ocular contrast normalization in human visual cortex. *Journal of Vision* **9**:13–13. doi:10.1167/9.3.13

Murray IJ, Kremers J, McKeefry D, Parry NRA. 2018. Paradoxical pupil responses to isolated M-cone increments. *Journal of the Optical Society of America A* **35**:B66–B71. doi:10.1364/JOSAA.35.000B66

Norcia AM, Appelbaum LG, Ales JM, Cottereau BR, Rossion B. 2015. The steady-state visual evoked potential in vision research: A review. *Journal of Vision* **15(6)**:4. doi:10.1167/15.6.4

Ogawa S, Lee TM, Kay AR, Tank DW. 1990. Brain magnetic resonance imaging with contrast dependent on blood oxygenation. *Proceedings of the National Academy of Sciences* **87**:9868–72. doi:10.1073/pnas.87.24.9868.

Panda S, Sato TK, Castrucci AM, Rollag MD, DeGrip WJ, Hogenesch JB, Provencio I, Kay SA. 2002. Melanopsin (opn4) requirement for normal light-induced circadian phase shifting. *Science* **298**:2213–2216. doi:10.1126/science.1076848

Pirenne MH. 1943. Binocular and uniocular threshold of vision. *Nature* **152**:698–699.

Privitera CM, Stark LW. 2006. A binocular pupil model for simulation of relative afferent pupil defects and the swinging flashlight test. *Biol Cybern* **94**:215–24. doi:10.1007/s00422-005-0042-8

Provencio I, Rodriguez IR, Jiang G, Hayes WP, Moreira EF, Rollag MD. 2000. A Novel Human Opsin in the Inner Retina. *Journal of Neuroscience* **20**:600–605. doi:10.1523/JNEUROSCI.20-02-00600.2000

Purves D, Brannon EM, Cabeza R, LaBar KS, Huettel SA, Platt ML, Woldorff MG. 2008. Principles of cognitive neuroscience. Oxford University Press, Incorporated.

Quaia C, Optican LM, Cumming BG. 2018. Binocular summation for reflexive eye movements. *J Vis* **18(4)**:7. doi:10.1167/18.4.7

Reeves P. 1918. Rate of pupillary dilation and contraction. *Psychological Review* **25**:330. doi:10.1037/h0075293

Regan D. 1966. Some characteristics of average steady-state and transient responses evoked by modulated light. *Electroencephalogr Clin Neurophysiol* **20**:238–48. doi:10.1016/0013-4694(66)90088-5

Regan MP, Regan D. 1988. A frequency domain technique for characterizing nonlinearities in biological systems. *Journal of Theoretical Biology* **133**:293–317. doi:https://doi.org/10.1016/S0022-5193(88)80323-0

Repka MX, Beck RW, Holmes JM, Birch EE, Chandler DL, Cotter SA, Hertle RW, Kraker RT, Moke PS, Quinn GE, Scheiman MM, Group PEDI. 2003. A randomized trial of patching regimens for treatment of moderate amblyopia in children. *Archives of Ophthalmology (Chicago, Ill: 1960)* **121**:603–611. doi:10.1001/archopht.121.5.603

Repka MX, Cotter SA, Beck RW, Kraker RT, Birch EE, Everett DF, Hertle RW, Holmes JM, Quinn GE, Sala NA, Scheiman MM, Stager DR, Wallace DK, Group PEDI. 2004. A randomized trial of atropine regimens for treatment of moderate amblyopia in children. *Ophthalmology* **111**:2076–2085. doi:10.1016/j.ophtha.2004.04.032

Repka MX, Wallace DK, Beck RW, Kraker RT, Birch EE, Cotter SA, Donahue S, Everett DF, Hertle RW, Holmes JM, Quinn GE, Scheiman MM, Weakley DR, Group PEDI. 2005. Two-year follow-up of a 6-month randomized trial of atropine vs patching for treatment of moderate amblyopia in children. *Archives of Ophthalmology (Chicago, Ill: 1960)* **123**:149–157. doi:10.1001/archopht.123.2.149

Ruby NF, Brennan TJ, Xie X, Cao V, Franken P, Heller HC, O'Hara BF. 2002. Role of melanopsin in circadian responses to light. *Science* **298**:2211–2213. doi:10.1126/science.1076701

Schrödinger E. 1926. Die gesichtsempfindungen.Mueller-Pouillets Lehrbuch Der Physik (11th Ed.). Vieweg: Braunschweig. pp. 456–560.

Segala FG, Bruno A, Martin JT, Aung MT, Wade AR, Baker DH. 2023a. Different rules for binocular combination of luminance flicker in cortical and subcortical pathways (code). Github. Https://github.com/bakerdh/pupillometryeeg/. 7ecf7ff.

Segala FG, Bruno A, Martin JT, Aung MT, Wade AR, Baker DH. 2023b. Different rules for binocular combination of luminance flicker in cortical and subcortical pathways. *eLife* **12**. doi:10.7554/elife.87048

Segala FG, Bruno A, Wade AR, Baker DH. 2022. Binocular response to light: Contrast matching of luminance flicker. *Perception* **51**:1–207. doi:10.1177/03010066221141167

Segala FG, Bruno A, Wade AR, Baker DH. 2021. Binocular response to light: A novel pupillometric and electrophysiological approach. *Perception* **50**:1–244. doi:10.1177/03010066211059887

Shapiro AG, Pokorny J, Smith VC. 1996. Conerod receptor spaces with illustrations that use CRT phosphor and light-emitting-diode spectra. *Journal of the Optical Society of America A* **13**:2319. doi:10.1364/josaa.13.002319

Sirois S, Brisson J. 2014. Pupillometry. *WIREs Cognitive Science* **5**:679–692. doi:10.1002/wcs.1323

Smith SM. 2002. Fast robust automated brain extraction. *Human Brain Mapping* **17**:143–55. doi:10.1002/hbm.10062.

Smith SM, Brady JM. 1997. SUSAN - a new approach to low level image processing. *International Journal of Computer Vision* **23**:45–78. doi:10.1023/A:1007963824710.

Smith VC, Pokorny J. 1975. Spectral sensitivity of the foveal cone photopigments between 400 and 500 nm. *Vision Research* **15**:161–71. doi:10.1016/0042-6989(75)90203-5.

Spector RH. 1990. The pupils In: Walker HK, Hall WD, Hurst JW, editors. Clinical Methods: The History, Physical, and Laboratory Examinations. Boston: Butterworths.

Spitschan M. 2019. Photoreceptor inputs to pupil control. *Journal of Vision* **19**:5. doi:10.1167/19.9.5

Spitschan M, Cajochen C. 2019. Binocular facilitation in light-mediated melatonin suppression? *J Pineal Res* **67**:e12602. doi:10.1111/jpi.12602

Spitschan M, Jain S, Brainard DH, Aguirre GK. 2014. Opponent melanopsin and s-cone signals in the human pupillary light response. *Proceedings of the National Academy of Sciences* **111**:15568–15572. doi:10.1073/pnas.1400942111

Spitschan M, Woelders T. 2018. The Method of Silent Substitution for Examining Melanopsin Contributions to Pupil Control. *Frontiers in Neurology* **9**.

Srinivasan R, Nunez PL, Tucker DM, Silberstein RB, Cadusch PJ. 1996. Spatial sampling and filtering of EEG with spline laplacians to estimate cortical potentials. *Brain Topography* **8**:355–366. doi:10.1007/bf01186911

Stark L, Sherman PM. 1957. A SERVOANALYTIC STUDY OF CONSENSUAL PUPIL REFLEX TO LIGHT. *Journal of Neurophysiology* **20**:17–26. doi:10.1152/jn.1957.20.1.17

Stockman A, Sharpe LT. 2000. The spectral sensitivities of the middle- and long-wavelength-sensitive cones derived from measurements in observers of known genotype. *Vision Res* **40**:1711–37. doi:10.1016/s0042-6989(00)00021-3

Thomson LC. 1947. Binocular summation within the nervous pathways of the pupillary light reflex. *The Journal of Physiology* **106**:59–65. doi:10.1113/jphysiol.1947.sp004192

Tootell RB, Silverman MS, Hamilton SL, Switkes E, De Valois RL. 1988. Functional anatomy of macaque striate cortex. V. Spatial frequency. *Journal of Neuroscience* **8**:1610–24. doi:10.1523/JNEUROSCI.08-05-01610.1988

Tsai JJ, Wade AR, Norcia AM. 2012. Dynamics of normalization underlying masking in human visual cortex. *J Neurosci* **32**:2783–9. doi:10.1523/JNEUROSCI.4485-11.2012

Tychsen L, Wong AM-F, Burkhalter A. 2004. Paucity of horizontal connections for binocular vision in v1 of naturally strabismic macaques: Cytochrome oxidase compartment specificity. *The Journal of Comparative Neurology* **474**:261–275. doi:10.1002/cne.20113

Verdon W, Howarth PA. 1988. The pupil's response to short wavelength cone stimulation. *Vision research* **28**:1119–1128. doi:10.1016/0042-6989(88)90138-1

Victor JD, Mast J. 1991. A new statistic for steady-state evoked potentials. *Electroencephalogr Clin Neurophysiol* **78**:378–88. doi:10.1016/0013-4694(91)90099-p

Wang C-A, Munoz DP. 2015. A circuit for pupil orienting responses: Implications for cognitive modulation of pupil size. *Current Opinion in Neurobiology* **33**:134–40. doi:10.1016/j.conb.2015.03.018

Woelders T, Leenheers T, Gordijn MCM, Hut RA, Beersma DGM, Wams EJ. 2018. Melanopsin- and L-cone–induced pupil constriction is inhibited by S- and M-cones in humans. *Proceedings of the National Academy of Sciences* **115**:792–797. doi:10.1073/pnas.1716281115

Woolrich M. 2008. Robust group analysis using outlier inference. *NeuroImage* **41**:286–301.

Woolrich MW, Behrens TEJ, Beckmann CF, Jenkinson M, Smith SM. 2004. Multilevel linear modelling for fmri group analysis using bayesian inference. *NeuroImage* **21**:1732–47.

Woolrich MW, Ripley BD, Brady M, Smith SM. 2001. Temporal autocorrelation in univariate linear modeling of fmri data. *NeuroImage* **14**:1370–86. doi:10.1006/nimg.2001.0931.

Worsley KJ. 2001. Statistical analysis of activation images In: Jezzard P, Matthews PM, Smith SM, editors. Functional Mri: An Introduction to Methods. Oxford: Oxford University Press. pp. 251–70.

Wyatt HJ, Musselman JF. 1981. Pupillary light reflex in humans: Evidence for an unbalanced pathway from nasal retina, and for signal cancellation in brainstem. *Vision Research* **21**:513–25. doi:10.1016/0042-6989(81)90097-3

Yoshimura T, Ebihara S. 1996. Spectral sensitivity of photoreceptors mediating phase-shifts of circadian rhythms in retinally degenerate CBA/j (rd/rd) and normal CBA/n (+/+) mice. *Journal of Comparative Physiology A* **178**. doi:10.1007/bf00225828

Zele AJ, Feigl B, Adhikari P, Maynard ML, Cao D. 2018. Melanopsin photoreception contributes to human visual detection, temporal and colour processing. *Scientific Reports* **8**. doi:10.1038/s41598-018-22197-w